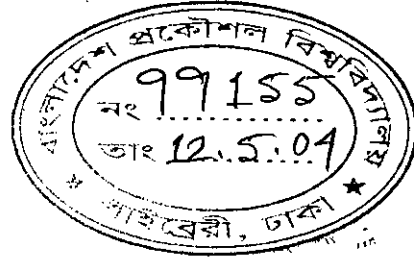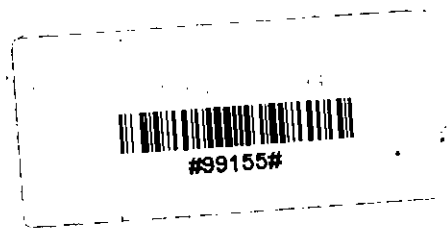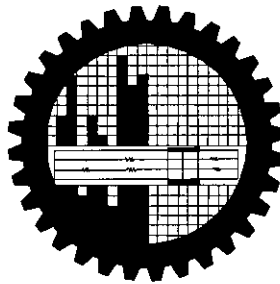# Analysis of Self-Phase Modulation Effect on Optical WDM System with Dispersion Compensation

by

Muhammad Anisuzzaman Talukder

A thesis submitted to the Department of Electrical and Electronic Engineering of
Bangladesh University of Engineering and Technology
in partial fulfillment of the requirements for the degree of
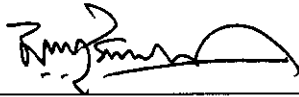MASTER OF SCIENCE IN ELECTRICAL AND ELECTRONIC
ENGINEERING

Department of Electrical and Electronic Engineering
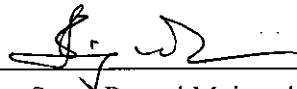BANGLADESH UNIVERSITY OF ENGINEERING AND TECHNOLOGY
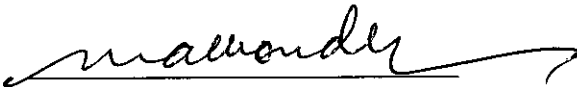
2004

APPROVAL CERTIFICATE

The thesis titled *"Analysis of Self-Phase Modulation Effect on Optical WDM System with Dispersion Compensation"* submitted by Muhammad Anisuzzaman Talukder, Roll No.: 100106259P, Session: October 2001, has been accepted as satisfactory in partial fulfillment of the requirement for the degree of Master of Science in Electrical and Electronic Engineering on May 01, 2004.

BOARD OF EXAMINERS

1. _____   Chairman
   Dr. M. Nazrul Islam
   Associate Professor
   Department of Electrical and Electronic Engineering
   BUET, Dhaka-1000, Bangladesh

2. _____   Member
   Dr. Satya Prasad Majumder
   Professor
   Department of Electrical and Electronic Engineering
   BUET, Dhaka-1000, Bangladesh

3. _____   Member
   Dr. Md. Saifur Rahman
   Professor
   Department of Electrical and Electronic Engineering
   BUET, Dhaka-1000, Bangladesh

4. _____   Member
   Dr. Mohammad Ali Choudhury   (Ex-fficio)
   Professor & Head
   Department of Electrical and Electronic Engineering
   BUET, Dhaka-1000, Bangladesh

5. _____   Member
   Dr. Farruk Ahmed   (External)
   Professor (on leave)
   Department of Applied Physics and Electronics
   University of Dhaka
   Professor
   North South University, Dhaka, Bangladesh

DECLARATION

It is hereby declared that this thesis or any part of it has not been submitted elsewhere for the award of any degree or diploma.

Signature of the Candidate

(Muhammad Anisuzzaman Talukder)

DEDICATED TO MY WIFE

CONTENTS

Chapter 3: Numerical Analysis Technique

Chapter 4: Performance Analysis of Post-Compensation Configuration

Chapter 5: Performance Analysis of Pre-Compensation Configuration

Chapter 6: Performance Analysis of Bi-end Compensation Configuration

Chapter 7: Conclusion

References

List of Figures

List of Tables

List of Symbols

α	attenuation constant
A	amplitude of the pulse envelope
U	normalized pulse intensity
β_2	second-order GVD parameter
β_3	third-order GVD parameter
γ	fiber nonlinearity coefficient
ϕ_{NL}	nonlinear phase shift
z_{eff}	effective distance
P_0	peak power
$\delta\omega$	frequency chirp
T_0	pulse width at 1/e intensity point
L_D	dispersion length
L_{NL}	nonlinear length
ξ	normalized distance
τ	normalized time
N	ratio of dispersion length to nonlinear length
$\hat{D}$	dispersion operator
$\hat{N}$	nonlinear operator
h	step size
P_{in}	input power
χ	fiber nonlinear susceptibility
L	fiber length
A_{eff}	effective core area of fiber
c	speed of light
λ	wavelength
R	photodetector's responsivity
σ_T	thermal noise

σ_s	shot noise
σ	total noise
Δf	bandwidth
G	amplifier gain
$\Delta \nu$	filter bandwidth
n_{sp}	spontaneous emission factor
F_n	noise figure
P_{ISI}	interfering power
P_{sp}	ASE power
σ_{sig-sp}	signal-to-spontaneous beat noise
σ_{sp-sp}	spontaneous-to-spontaneous beat noise
T_b	bit period
I_d	dark current
$\hbar$	planck's constant

List of Abbreviations

ASE	Amplified Spontaneous Emission
BECC	Bi-end Compensation Configuration
BER	Bit Error Rate
DCF	Dispersion Compensating Fiber
DSF	Dispersion Shifted Fiber
EDFA	Erbium-doped Fiber Amplifier
FWM	Four-Wave Mixing
GVD	Group Velocity Dispersion
ISI	Inter Symbol Interference
LASER	Light Amplification by Stimulated Emission of Radiation
LED	Light Emitting Diode
NLSE	Nonlinear Schrodinger Equation
NRZ	Non-return to Zero
POCC	Post-Compensation Configuration
PRCC	Pre-Compensation Configuration
SMF	Single Mode Fiber
SNR	Signal to Noise Ratio
SPM	Self Phase Modulation
SSFT	Split-Step Fourier Transform
SSMF	Standard Single Mode Fiber
WDM	Wavelength Division Multiplexing
XPM	Cross Phase Modulation

Acknowledgement

I am highly pleased to express my sincere and profound gratitude to my supervisor Dr. M. Nazrul Islam, Associate Professor, Department of Electrical and Electronic Engineering (EEE), Bangladesh University of Engineering and Technology, Dhaka, for providing me the opportunity to conduct graduate research in optical communications. I convey my hearty thanks to him for his continuous guidance, suggestions and wholehearted help through the course of the work.

I would like to express my special thanks to Dr. Satya Prasad Majumder, Professor, Department of EEE, BUET, for his invaluable suggestions and discussions.

I would also like to thank my colleagues especially Mohammad Faisal and Md. Touhidur Rahman for their support and continuous encouragement. Since computer simulations took much time, it was very helpful for me using the resources in Robert Noyce Simulation Lab. I thank to all who were concerned in setting up this lab in EEE department, BUET.

I like to express my heartfelt thanks and gratitude to all my family members for their invaluable encouragement.

Finally, I am grateful to Almighty Allah for enabling me to complete the thesis.

Abstract

The third-generation terrestrial systems operating near 1.55 µm generally use the existing fiber-cable network installed during the 1980s and consisting of more than 50 million kilometers of the "standard" single-mode fiber with zero dispersion wavelength at 1.31 µm. Therefore the dispersion parameter in the 1.55-µm region of such fibers is very high ($\approx 17\, ps/(km-nm)$). As a result, group-velocity dispersion (GVD) severely limits the transmission performance. Nevertheless the dispersion-management technique is well adopted for constructing long-distance transmission systems. In the conventional dispersion-managed system, the nonzero anomalous GVD of single-mode fibers (SMF) is periodically compensated by the proper length of DCF's placed at the end of the compensation interval. In a WDM system, perfect dispersion compensation can be achieved only for a single channel. Supposing perfect dispersion compensation is accomplished for a particular channel of the WDM system, other wavelength channels encounter with different amount of cumulative dispersion proportional to their wavelength separations from the zero average-dispersion wavelength channel. In such a case, waveform distortion induced by the nonlinear interplay between the Self-phase modulation (SPM) and the cumulative residual GVD cannot be generally compensated by the mere pre-post compensation scheme. As a result, the transmission window of the conventional long-distance dispersion managed WDM system is severely limited by the interplay between SPM and residual dispersion rather than by the flat-gain bandwidth of cascaded EDFAs.

In this study, the impact of SPM on power margins that can be launched into a SMF transmission system with dispersion compensation is extensively investigated by computer simulation at 10-Gb/s. The pulse propagation in a dispersive and nonlinear fiber has been simulated using split-step Fourier transform method. From the output pulse shapes eye diagrams have been drawn and eye opening penalty at different length and different residual dispersion has been evaluated. Maximum threshold power that can be applied to the system has been determined at different fiber length and at different residual dispersion. Receiver performance for optical pulse transmission in presence of both GVD and SPM effects has been quantified as Q parameter and SNR. It is shown that most performing technique is the bi-end compensation configuration. And in all of the compensation techniques, positive residual dispersion generally shows better performance than negative residual dispersion. So, in case of WDM system implementation, most of the channels should be placed at the positive residual dispersion regime. Moreover, SPM effects are maximum for post-compensation configuration with zero residual dispersion. But at non-zero residual dispersion, pre-compensation suffers most. So, a design rule is proposed to perform optimal dispersion compensation in multichannel transmission in presence of SPM.

Chapter 1

Introduction
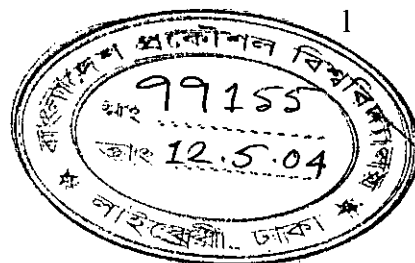
1.1 Communication Systems

A communication system transmits information from one place to another, whether separated by a few kilometers or by transoceanic distances. Information is often carried by an electromagnetic carrier wave whose frequency can vary from a few megahertz to several hundred terahertz. Optical communication systems use high carrier frequencies (~100 THz) in the visible or near-infrared region of the electromagnetic spectrum as shown in figure 1.1. They are sometimes called lightwave systems to distinguish them from microwave systems, whose carrier frequency is typically smaller by five orders of magnitude (~1 GHz). Fiber-optic communication systems are lightwave systems that employ optical fibers for information transmission. Such systems have been deployed worldwide since 1980 and have indeed revolutionized the technology behind telecommunications. Indeed, the lightwave technology, together with microelectronics, is believed to be a major factor in the advent of the "information age."

1.2 Historical Perspective

The use of light for communication purposes dates back to antiquity if we interpret optical communications in a broad sense [1]. Most civilizations have used mirrors, fire beacons, or smoke signals to convey a single piece of information (such as victory in a war). Essentially the same idea was used up to the end of the eighteenth century through signaling lamps, flags, and other semaphore devices. The idea was extended further, following a suggestion of Claude Chappe in 1792, to transmit mechanically coded messages over long distances (~100 km) by the use of intermediate relay stations [2], acting as *regenerators* or *repeaters* in the modern-day language. The role of light in such systems was simply to make the coded signals visible so that they could be intercepted by the relay stations. The opto-mechanical communication

systems of the nineteenth century were inherently slow. In modern-day terminology, the effective bit rate of such systems was less than 1 bit per second (B < 1 b/s).
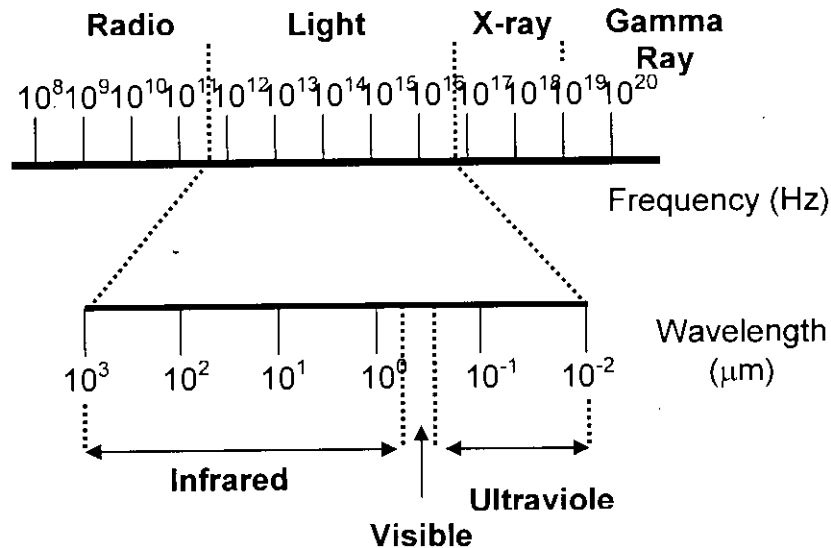
Figure 1.1: Spectrum of electromagnetic waves

1.3 Need for Fiber-Optic Communications

The advent of telegraphy in the 1830s replaced the use of light by electricity and began the era of electrical communication [3]. The bit rate B could be increased to ~10 b/s by the use of new coding techniques, such as the *Morse code*. The use of intermediate relay stations allowed communication over long distances (~1000 km). The invention of telephone in 1876 brought a major change inasmuch as electric signals were transmitted in analog form through a continuously varying electric current [4].

The development of worldwide telephone networks during the twentieth century led to many advances in the design of electrical communication systems. The use of coaxial cables in place of wire pairs increased system capacity considerably. The first coaxial-cable system, put into service in 1940, was a 3-MHz system capable of transmitting 300 voice channels or a single television channel. The bandwidth of such systems is limited by the frequency-dependent cable losses, which increase rapidly for

frequencies beyond 10 MHz. This limitation led to the development of microwave communication systems in which an electromagnetic carrier wave with frequencies in the range of 1~10 GHz is used to transmit the signal by using suitable modulation techniques. Microwave communication systems generally allow for larger repeater spacing, but their bit rate is also limited by the carrier frequency of such waves.

It was realized during the second half of the twentieth century that an increase of several orders of magnitude in the *bit rate-distance* product would be possible if optical waves were used as the carrier. However, neither a coherent optical source nor a suitable transmission medium was available during the 1950s. The invention of the laser and its demonstration in 1960 solved the first problem [5]. Attention was then focused on finding ways for using laser light for optical communications. Many ideas were advanced during the 1960s [6], the most noteworthy being the idea of light confinement using a sequence of gas lenses [7].

It was suggested in 1966 that optical fibers might be the best choice [8], as they are capable of guiding the light in a manner similar to the guiding of electrons in copper wires. The main problem was the high losses of optical fibers – fibers available during the 1960s had losses in excess of 1000 dB/km. A breakthrough occurred in 1970 when fiber losses could be reduced to below 20 dB/km in the wavelength region near 1 μm [9]. The simultaneous availability of *compact* optical sources and *low-loss* optical fibers led to a worldwide effort for developing fiber-optic communication systems [10].

1.4 Evolution of Lightwave Systems

The enormous progress in fiber-optic communication system realized over the 25-year period extending from 1975 to 2000 can be grouped into several distinct generations.

The *first generation* of lightwave systems operated near 0.8 μm wavelength at a bit rate of 45 Mb/s and allowed repeater spacing of up to 10 km. It was clear during the 1970s that the repeater spacing could be increased considerably by operating the lightwave system in the wavelength region near 1.3 μm, where fiber loss is below 1

dB/km as shown in figure 1.2. Furthermore, optical fibers exhibit minimum dispersion in this wavelength region. This realization led to a worldwide effort for the development of InGaAsP semiconductor lasers and detectors operating near 1.3 μm.

The *second generation* of fiber-optic communication systems operating at 1.3 μm became available in the early 1980s, but the bit rate of early systems was limited to below 100 Mb/s because of dispersion in multimode fibers [11]. This limitation was overcome by the use of single-mode fibers. By 1987, second-generation lightwave systems, operating at bit rates of up to 1.7 Gb/s with a repeater spacing of about 50 km, were commercially available. The repeater spacing of the second-generation lightwave systems was limited by the fiber losses at the operating wavelength of 1.3 μm (typically 0.5 dB/km). Losses of silica fibers become minimum near 1.55 μm. Indeed, a 0.2 dB/km loss was realized in 1979 in this spectral region [12].

However, the introduction of *third-generation* lightwave systems operating at 1.55 μm was considerably delayed by a large fiber dispersion near 1.55 μm. The dispersion problem can be overcome either by using dispersion-shifted fibers designed to have minimum dispersion near 1.55 μm or by limiting the laser spectrum to a single longitudinal mode. Both approaches were followed during the 1980s. Third-generation lightwave systems operating at 2.5 Gb/s became available commercially in 1990. Such systems are capable of operating at a bit rate of up to 10 Gb/s [13].

The *fourth generation* of lightwave systems makes use of *optical amplification* for increasing the repeater spacing and of *wavelength-division multiplexing* (WDM) for increasing the bit rate. The advent of WDM technique started a revolution that resulted in doubling of the system capacity every 6 months or so and led to lightwave systems operating at a bit rate of 10 Tb/s by 2001 [14]. In most WDM systems, fiber losses are compensated periodically using erbium-doped fiber amplifiers spaced 60-80 km apart.

The current emphasis of WDM lightwave systems is on increasing the system capacity by transmitting more and more channels through the WDM technique. With increasing WDM signal bandwidth, it is often not possible to amplify all channels

using a single amplifier. As a results, new kinds of amplification schemes are being explored for covering the spectral region extending from 1.45 to 1.62 μm.

The *fifth generation* of fiber-optic communication systems is concerned with extending the wavelength range over which a WDM system can operate simultaneously. The conventional wavelength window, known as the C band, covers the wavelength range 1.53-1.57 μm. It is being extended on both the long- and short-wavelength sides, resulting in the L and S bands, respectively. A new kind of fiber, known as the *dry fiber* has been developed with the property that fiber losses are small over the entire wavelength region extending from 1.30 to 1.65 μm [15]. Availability of such fibers and new amplification schemes may lead to lightwave systems with thousands of WDM channels.

The fifth-generation systems also attempt to increase the bit rate of each channel within the WDM signal. An interesting approach is based on the concept of *optical solitons* - pulses that preserve their shape during propagation in a lossless fiber by counteracting the effect of dispersion through the fiber nonlinearity.
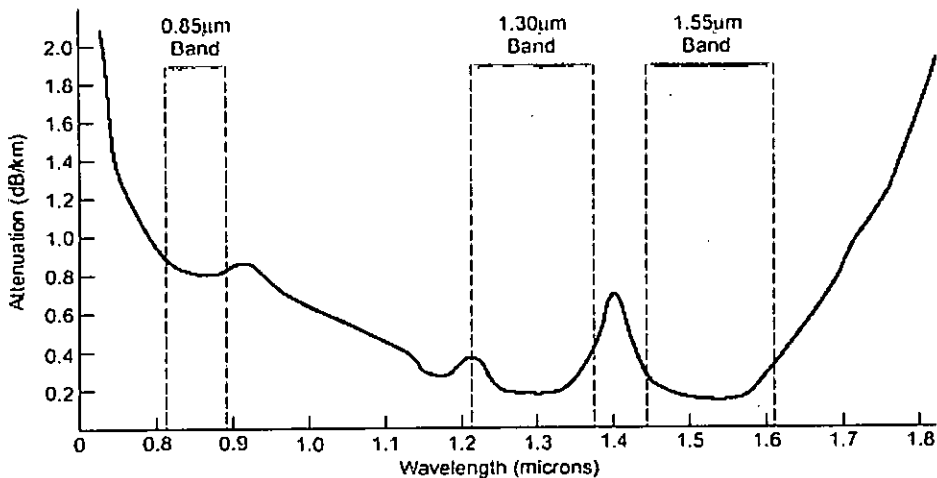
Figure 1.2: Variation of attenuation with wavelength

1.5 Components of Optical Communication

The basic optical communication system consists of three major elements: optical transmitter, optical fiber cable and optical receiver, as shown in figure 1.3.
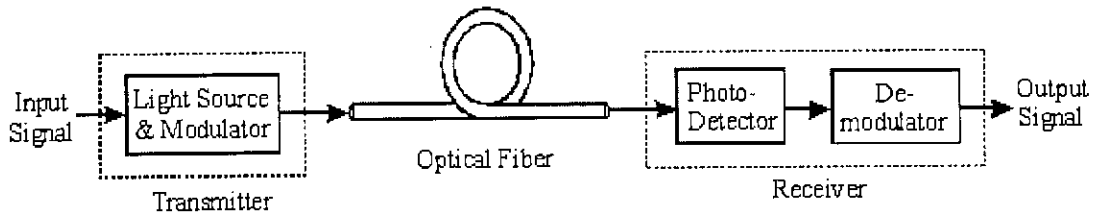
Figure 1.3: Optical fiber communication system

1.5.1 Optical Transmitters

The role of an optical transmitter is to convert the electrical signal into optical form and to launch the resulting optical signal into the optical fiber. Figure 1.4 shows the block diagram of an optical transmitter. It consists of an optical source, a modulator, and a channel coupler. Semiconductor lasers or light-emitting diodes are used as optical sources because of their compatibility with the optical-fiber communication channel. The optical signal is generated by modulating the optical carrier wave. The coupler is generally a microlens that focuses the optical signal onto the entrance plane of an optical fiber with the maximum possible efficiency. The launched power is an important design parameter. One can increase the amplifier (or repeater) spacing by increasing it, but the onset of various nonlinear effects limits how much power can be increased.
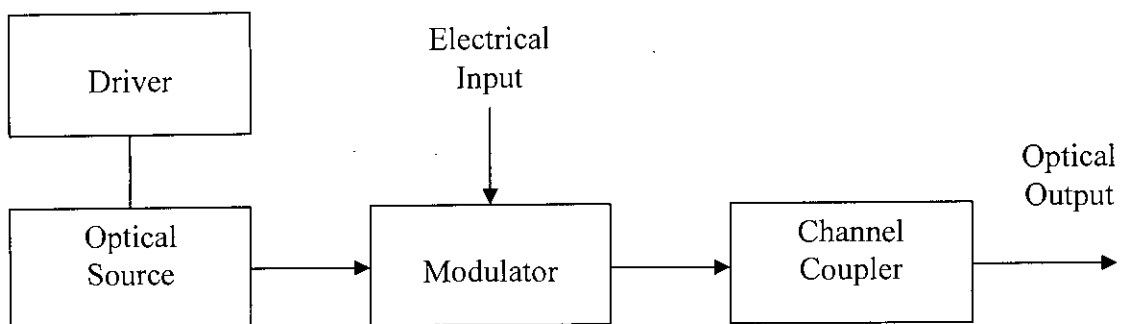
Figure 1.4: Components of an optical transmitter.

1.5.2 Optical Fibers

The role of a communication channel is to transport the optical signal from transmitter to receiver without distorting it. Most lightwave systems use optical fibers as the communication channel because silica fibers can transmit light with losses as small as 0.2 dB/km. Even then, optical power reduces to only 1% after 100km. For this reason, fiber losses remain an important design issue and determine the repeater or amplifier spacing of a long-haul lightwave system. Another important design issue is fiber dispersion, which leads to broadening of individual optical pulses with propagation.

1.5.3 Optical Receivers

An optical receiver converts the optical signal received at the output end of the optical fiber back into the original electrical signal. Figure 1.5 shows the block diagram of an optical receiver. It consists of a coupler, a photodetector and a demodulator. The coupler focuses the received optical signal onto the photodetector. Semiconductor photodiodes are used as photodetectors because of their compatibility with the whole system. The design of the demodulator depends on the modulation format used by the lightwave system. An important parameter for any receiver is the receiver sensitivity. It is usually defined as the minimum average optical power required realizing a bit error rate of 10^{-9}.
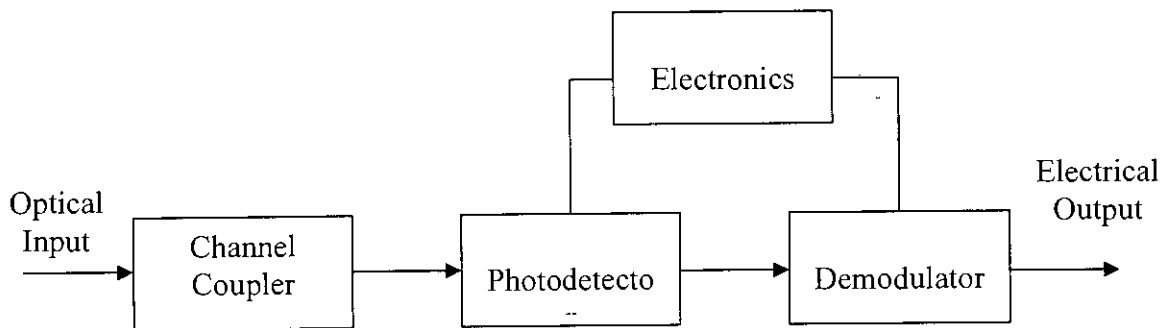
Figure 1.5: Components of an optical receiver.

1.6 Background of this study

Now a days Erbium-doped fiber amplifiers (EDFA) can periodically compensate the fiber loss at 1.55-μm. So, fiber loss is no longer a limiting factor for a long-haul fiber-optic communication system. Then, group velocity dispersion (GVD) that distorts signals remains the limiting factor in a long-haul optical communication system. Also, by using pre-, post-, or bi-end periodic dispersion compensation, one can achieve high-speed and long haul transmission system [17]-[21]. Thus the bandwidth-length product of the transmission link is no longer limited by the GVD but by higher order dispersion and fiber nonlinear effects, namely, self-phase modulation (SPM), cross-phase modulation (XPM) and four-wave mixing (FWM).

In [22] and [23], the performance of a long distance wavelength division multiplexed (WDM) system using dispersion-shifted fiber in presence of FWM and the performance of WSK technique in reducing the FWM effect have been studied. But in a WDM system using already installed standard single-mode fiber (SSMF), the dominant nonlinear effect is the SPM, which is caused by the nonlinear dependence of the refractive index on the pulse intensity [24]. Since high-speed data transmission systems require greater received power for error-free detection, the performance of dispersion compensated link is eventually degraded by the interaction of the SPM and the fiber dispersion. For a wavelength division multiplexing (WDM) it is difficult to compensate all the channels completely for dispersion [25], [26]. On the other hand, to suppress the FWM effect, GVD must not be completely compensated [27], [28].

It was shown that in strongly nonlinear transmission, the single mode fiber (SMF) must always be followed by a compensating fiber with positive residual dispersion [29], neglecting accumulated amplified spontaneous emission (ASE) noise of EDFAs. Another study on lumped compensation showed that precompensation should be employed for complete compensation [30]. In [31], bi-end compensation configuration (BECC) was considered, where two dispersive elements are placed at the input and output ends of the transmission fiber, respectively, for every compensation period. The total dispersion of the two dispersive elements was chosen two completely compensate for the accumulated second-order fiber dispersion within a compensation period. However, the transmission performance of a WDM system for

different location of dispersive element and the degree of dispersion compensation under SPM effect is yet to be reported.

1.7 Objective of this Study

The objective of this work is to study the SPM effect on the performance in-line optical amplifier fiber transmission system with dispersion compensation. Various dispersion compensation configurations, namely, post-, pre- and bi-end compensation configuration for both complete and partial dispersion compensation will be investigated. SPM-limited maximum threshold power for minimum tolerable system performance and its degradation in a cascaded optical amplifier system will be evaluated. Thus, the applicability of the compensation configurations in presence of both single channel and multi-channel WDM system will be investigated. Since the degree of the SPM effect depends on the shape of the input pulse, transmission performance for different input pulse shapes will be studied and compared.

The results of this work are expected to contribute to the design of high bit rate long-haul WDM fiber-optic communication network.

1.8 Thesis Outline

The thesis dissertation is composed of seven chapters.

Chapter 1 gives the introduction of fiber optic communication along with historical background. Recent developments in this field and the characteristics of optical fiber are also discussed. The background of this study and objective of this research work are addressed.

In chapter 2, theoretical model of optical pulse propagation within the fiber will be explained. The limiting factors governing the pulse propagation in fiber-optic communication system will be discussed and the compensation of some of the

limiting factors will also be presented. At last, the non-linear effects in a compensated transmission link will be discussed.

In chapter 3, Numerical Analysis Technique, we will describe the method Split-Step Fourier Transform (SSFT) method used in our analysis. The performance evaluation procedure, like, Signal-to-noise ration and Q parameter calculation procedure will also be given.

Chapter 4 contains the simulation results obtained for post-compensation configuration. The performance of POCC will be shown in presence of SPM with both complete and partial compensation. Then applicability of POCC in a long-haul WDM system will be described. This chapter also includes some results of the dependence of transmission performance on transmitted pulse shape.

In chapter 5, Performance Analysis of Pre-Compensation Configuration, SPM effects in PRCC will be presented. Then as in chapter 4, it will be judged whether PRCC is suitable for a long-haul WDM system.

Chapter 6 is for bi-end compensation configuration analysis. This chapter contains our proposed system for a long-haul WDM system. The chapter also includes comparison among the three compensation configurations considered in our study.

At last, in chapter 7, we draw the conclusion of our study.

Chapter 2

Theoretical Model

2.1 Introduction

In this chapter, the theoretical pulse propagation model in a fiber-optic communication and the limitations imposed by different linear and nonlinear effects will be illustrated. Here will also be explained how some effects are compensated. Then the behavior of a some-effects compensated system with non-compensated effects will also be explained.

2.2 Nonlinear Schrodinger Equation

The nonlinear Schrodinger equation (NLSE) modified to include higher-order dispersion, has been successful in accurately modeling pulse propagation in single-mode fibers in many diverse applications [32], [33], and can therefore be employed with confidence for system design considerations. It is used to model the combined effects of self-phase modulation, group-velocity dispersion and loss on pulse propagation in a single-mode fiber. The modified NLSE is given by [24]

$$i\frac{\partial A}{\partial z} = \underbrace{-\frac{i}{2}\alpha A}_{\substack{Fiber \\ Loss}} + \underbrace{\frac{1}{2}\beta_2\frac{\partial^2 A}{\partial T^2} + \frac{i}{6}\beta_3\frac{\partial^3 A}{\partial T^3}}_{Dispersion} \underbrace{- \gamma|A|^2 A}_{\substack{Self\text{-}phase \\ modulation}} \qquad (2.1)$$

where A is the slowly varying amplitude of the pulse envelope and T is measured in a frame of reference moving with the pulse at the group velocity v_g $(T = t - z/v_g)$. β_2 is second-order group velocity dispersion and β_3 is third order group velocity dispersion coefficient. α is the loss coefficient.

The three terms on the right-hand side of equation (2.1) govern, respectively, the effects of absorption, dispersion, and nonlinearity on pulses propagating inside optical

fibers. Depending on the initial width T_0 and the peak power P_0 of the incident pulse, either dispersive or nonlinear effects may dominate in the pulse evolution along the fiber.

The terms on the right-hand side of equation (2.1) govern pulse propagation inside optical fiber and specifies limit on the transmission performance. The effects of the terms on pulse propagation are discussed here.

2.3 Fiber losses

Fiber losses represent a limiting factor because they reduce the signal power in the fiber. As optical receivers need a certain minimum amount of power for recovering the signal accurately, the transmission distance is inherently limited by the fiber losses.

If P_{in} is the power launched at the input end of a fiber of length L, the output power P_{out} is given by

$$P_{out} = P_{in} \exp(-\alpha L) \tag{2.2}$$

where α includes material absorption and all other sources of power attenuation.

It is customary to express α in units of dB/km by using the relation

$$\alpha(dB/km) = -\frac{10}{L}\log_{10}(\frac{P_{out}}{P_{in}}) \approx 4.343\alpha \tag{2.4}$$

So, the transmission distance of any fiber-optic communication system is eventually limited by fiber losses. For long-haul systems, the loss limitation has traditionally been overcome using optoelectronic repeaters in which the optical signal is first converted into an electric current and then regenerated using a transmitter. Such regenerators become quite complex and expensive for WDM systems. An alternative approach to loss management makes use of optical amplifiers, which amplify the optical signal directly without requiring its conversion to the electric domain. With the advent of erbium-doped fiber amplifiers (EDFAs), fiber loss is no longer a

limiting factor even for a WDM all-optical system for its large, wide and flat gain bandwidth. Now-a-days, EDFAs are being used as power amplifiers to increase the transmitted power, as in-line amplifiers to compensate the fiber losses periodically in long-haul transmission system and as preamplifier to boost the power reaching the receiver.

But all optical amplifiers compensate fiber-loss at the expense of degradation of signal-to-noise ratio of the amplified signal because of spontaneous emission that adds noise to the signal during amplification. The SNR degradation is quantified through a parameter F_n, called the *amplifier noise figure*. For most practical amplifiers, F_n exceeds 3 dB.

2.4 Group Velocity Dispersion

The group velocity associated with the fundamental mode in a single-mode fiber is frequency dependent because of chromatic dispersion. As a result, different spectral components of the pulse travel at slightly different group velocities, a phenomenon referred to as group-velocity dispersion (GVD), intramodal dispersion or simply fiber dispersion. As a result, pulse broadens outside its dedicated bit period and causes inter-symbol interference (ISI).

| Input pulses | Optical fiber | Output pulses |
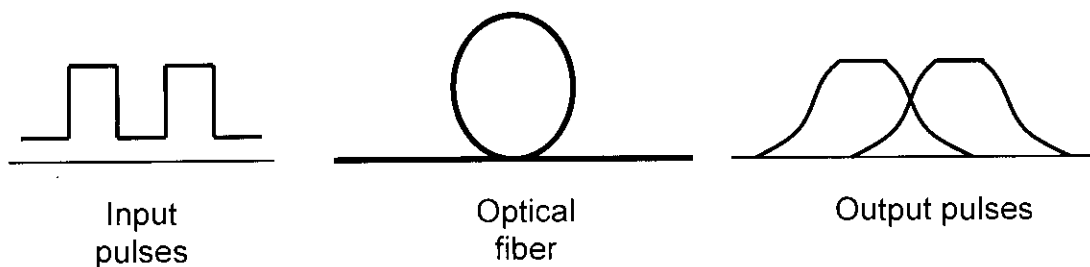
Fig. 2.1: Effect of Dispersion

2.4.1 Dispersion-induced Pulse Broadening

If amplitude of the pulse envelope is defined as $A(z,T) = \sqrt{P_0} \exp(-\alpha z/2)U(z,T)$ in equation (2.1), where P_0 is the peak power of the incident pulse and α is the attenuation coefficient, normalized amplitude $U(z,T)$ in a linear dispersive medium ($\gamma = 0$) satisfies a linear partial differential equation given by

$$i\frac{\partial U}{\partial z} = \frac{1}{2}\beta_2\frac{\partial^2 U}{\partial T^2} \tag{2.5}$$

Equation (2.5) is readily solved by using the Fourier method. If $\tilde{U}(z,\omega)$ is the Fourier transform of $U(z,T)$ such that

$$U(z,T) = \frac{1}{2\pi}\int_{-\infty}^{\infty}\tilde{U}(z,\omega)\exp(-i\omega T)d\omega \tag{2.6}$$

then it satisfies an ordinary differential equation

$$i\frac{\partial \tilde{U}}{\partial z} = -\frac{1}{2}\beta_2\omega^2\tilde{U} \tag{2.7}$$

whose solution is given by

$$\tilde{U}(z,\omega) = \tilde{U}(0,\omega)\exp\left[\frac{i}{2}\beta_2\omega^2 z\right] \tag{2.8}$$

where $\tilde{U}(0,\omega)$ is the Fourier transform of the incident field at $z = 0$ and is given by

$$\tilde{U}(0,\omega) = \int_{-\infty}^{\infty}U(0,T)\exp(i\omega T)dT \tag{2.9}$$

By substituting equation (2.8) in equation (2.6), the general solution of equation (2.5) is given by

$$U(z,T) = \frac{1}{2\pi}\int_{-\infty}^{\infty}\tilde{U}(0,\omega)\exp\left[\frac{i}{2}\beta_2\omega^2 z - i\omega T\right]d\omega \tag{2.10}$$

Equation (2.9) and (2.10) can be used for input pulses of arbitrary shapes.

Equation (2.8) shows that the effect of GVD changes the phase of each spectral component of the pulse by an amount that depends on the frequency and the propagated distance. Even though such phase changes do not affect the pulse

spectrum, they can modify the pulse shape. Actually GVD changes frequency across the pulse. This is referred to as frequency chirp. The chirp $\delta\omega$ depends on the sign of β_2. In the normal-dispersion regime ($\beta_2 > 0$), $\delta\omega$ is negative at the leading edge ($T < 0$) and increases across the pulse; the opposite occurs in the anomalous-dispersion regime ($\beta_2 < 0$).

Dispersion-induced pulse broadening is evident since different frequency components of a pulse travel at slightly different speeds along the fiber because of GVD. More specifically, red components travel faster than blue components in the normal-dispersion regime ($\beta_2 > 0$), while the opposite occurs in the anomalous-dispersion regime ($\beta_2 < 0$). The pulse can maintain its width only if all spectral components arrive together, or equivalently $\beta_2 = 0$. Any time delay in the arrival of different spectral components leads to pulse broadening. The dispersion-induced chirp broadens the pulse since different parts of the pulse develop slightly different frequencies and propagate at different speeds along the fiber.

2.4.2 Higher-order Dispersion

This section considers the effects of GVD by including both the terms involving β_2 and β_3 while still neglecting the nonlinear effects. Although the contribution of β_2 dominates in most cases of practical interest, it is sometimes necessary to include the higher-order term proportional β_3. For example, if the pulse wavelength nearly coincides with the zero-dispersion wavelength λ_D, $\beta_2 = 0$; the β_3 term then provides the dominant contribution to the GVD effects. By neglecting nonlinear terms, The NLSE for normalized amplitude $U(z,T)$ is given by the following partial differential equation

$$i\frac{\partial U}{\partial z} = \frac{1}{2}\beta_2 \frac{\partial^2 U}{\partial T^2} + \frac{i}{6}\beta_3 \frac{\partial^3 U}{\partial T^3} \qquad (2.11)$$

After solving this equation by using the Fourier technique, the transmitted field is

$$U(z,T) = \frac{1}{2\pi}\int_{-\infty}^{\infty} \tilde{U}(0,\omega)\exp\left[\frac{i}{2}\beta_2\omega^2 z + \frac{i}{6}\beta_3\omega^3 z - i\omega T\right]d\omega \qquad (2.12)$$

2.4.3 Effect of Pulse Shape on GVD

Dispersion-induced broadening is sensitive to steepness of pulse edges. In general, a pulse with steeper leading and trailing edges broadens more rapidly with propagation simply because such a pulse has a wider spectrum to start with. A super-Gaussian shape can be used to model the effects of steep leading and trailing edges on dispersion-induced pulse broadening. For a super-Gaussian pulse the normalized amplitude is generalized to take the form

$$U(0,T) = \exp[-\frac{1}{2}(\frac{T}{T_0})^{2m}] \tag{2.13}$$

where the parameter m controls the degree of edge sharpness. For, $m = 1$ this is just a Gaussian pulse. For larger values of m, the pulse becomes square shaped with sharper leading and trailing edges.

Whereas the Gaussian pulse maintains its shape during propagation, the super-Gaussian pulse not only broadens at a faster rate but also distorts in shape. The enhanced broadening of a super-Gaussian pulse can be understood by noting that its spectrum is wider than that of a Gaussian pulse because of steeper leading and trailing edges. Since the GVD-induced delay of each frequency component is directly related to its separation from the central frequency ω_0, a wider spectrum results in a faster rate of pulse broadening in a pulse with steeper leading and trailing edges.

2.5 Dispersion Management

Indeed, modern lightwave systems are often limited by the dispersive and nonlinear effects rather than fiber losses. In some sense, optical amplifiers solve the loss problem but at the same time, worsen the dispersion problem since, in contrast with electronic regenerators, an optical amplifier does not restore the amplified signal to its original state. As a result, dispersion-induced degradation of the transmitted signal accumulates over multiple amplifiers. For this reason, several dispersion-management schemes were developed during the 1990s to address the dispersion problem [34]. The group-velocity dispersion (GVD) effects can be minimized using a narrow-linewidth laser and operating close to the zero-dispersion wavelength λ_{ZD} of the fiber. However, it is not always practical to match the operating wavelength λ with λ_{ZD}.

An example is provided by the third-generation terrestrial systems operating near 1.55 μm and using optical transmitters containing a distributed feedback (DFB) laser. Such systems generally use the existing fiber-cable network installed during the 1980s and consisting of more than 50 million kilometers of the "standard" single-mode fiber with $\lambda_{ZD} \approx 1.31$ μm [14]. Since the dispersion coefficient D is approximately 17 ps/km-nm in the 1.55 μm region of such fibers, the GVD severely limits the performance when the bit rate exceeds 4 Gb/s.

A dispersion-management scheme attempts to solve this problem. The basic idea behind all such schemes is quite simple and can be understood by using the pulse-propagation equation given previously and written as

$$\frac{\partial A}{\partial z} + \frac{i\beta_2}{2}\frac{\partial^2 A}{\partial t^2} - \frac{\beta_3}{6}\frac{\partial^3 A}{\partial t^3} = 0 \qquad (2.14)$$

where A is the pulse-envelope amplitude. The effects of third-order dispersion are included by the β_3 term. In practice, this term can be neglected when $|\beta_2|$ exceeds 0.1 ps²/km. Since $|\beta_2|$ is approximately 22 ps²/km for standard single-mode fiber at 1.55 μm, we can certainly neglect β_3. Solution for $A(z,t)$ becomes as given previously,

$$A(z,t) = \frac{1}{2\pi}\int_{-\infty}^{\infty}\tilde{A}(0,\omega)\exp(\frac{i}{2}\beta_2 z\omega^2 - i\omega t)d\omega \qquad (2.15)$$

where $\tilde{A}(0,\omega)$ is the Fourier transform of $A(0,t)$.

Dispersion-induced degradation of the optical signal is caused by the phase factor $\exp(i\beta_2 z\omega^2 / 2)$, acquired by spectral components of the pulse during its propagation in the fiber. All dispersion-management schemes attempt to cancel this phase factor so that the input signal can be restored.

2.5.1 Dispersion Compensation using DCF

Among many dispersion management schemes, the use of dispersion compensating fiber (DCF) provides an all-optical technique that is capable of compensating the fiber GVD completely if the average optical power is kept low enough that the nonlinear effects inside optical fibers are negligible.

To understand the physics behind this dispersion-management technique, consider the situation in which each optical pulse propagates through two fiber segments, the second of which is the DCF. Using equation (2.15) for each fiber section consecutively, we obtain

$$A(L,t) = \frac{1}{2\pi} \int_{-\infty}^{\infty} \tilde{A}(0,\omega) \exp\left[\frac{i}{2}\omega^2(\beta_{21}L_1 + \beta_{22}L_2) - i\omega t\right]d\omega \qquad (2.16)$$

where $L = L_1 + L_2$ and β_{2j} is the GVD parameter for the fiber segment of length $L_j (j = 1, 2)$. If the DCF is chosen such that the ω^2 phase term vanishes, the pulse will recover its original shape at the end of DCF. The condition for perfect dispersion compensation is thus

$$\beta_{21}L_1 + \beta_{22}L_2 = 0,$$
$$or, \quad D_1L_1 + D_2L_2 = 0 \qquad (2.17)$$

Equation (2.17) shows that the DCF must have normal GVD at 1.55 μm ($D_2 < 0$) because $D_1 > 0$ for standard telecommunication fibers. Moreover, its length should be chosen to satisfy

$$L_2 = -(D_1 / D_2)L_1 \qquad (2.18)$$

For practical reasons, L_2 should be as small as possible. This is possible only if the DCF has a large negative value of D_2.

A practical solution for upgrading the terrestrial lightwave systems making use of the existing standard SMF fibers consists of adding a DCF module to optical amplifiers

spaced apart by ~100 km. The DCF compensates GVD while the amplifier takes care of fiber losses.

Because of a relatively small mode diameter of DCFs, the effective mode area is only ~20 μm^2. As the optical intensity is larger inside a DCF at a given input power, the nonlinear effects are considerably enhanced [35].

In DCF compensating technique, DCF can be connected at the input, output end or at both ends of the standard single-mode fiber. Depending on the position of the DCF compensation configuration is classified as – pre-, post or bi-end compensation configuration respectively.

Because of the wavelength dependence of β_2, or the dispersion parameter D as shown if figure (1.8), dispersion compensating scheme set to completely compensate at a particular wavelength, will not be able to fully compensate any other channel of different wavelengths. So, the accumulated dispersion will be different for each channel in a WDM system.

2.6 Self-Phase Modulation (SPM)

Third term on the right hand side of the nonlinear Schrodinger equation given in (2.1) represents the nonlinear effects on the pulse propagation. The lowest-order nonlinear effects in optical fibers originate from the third-order susceptibility $\chi^{(3)}$, which is responsible for phenomenon such as third harmonic generation, four-wave mixing, and nonlinear refraction. However, unless special efforts are made to achieve phase matching, the nonlinear processes which involve the generation of new frequencies (e.g. third-harmonic generation or four-wave mixing) are not efficient in optical fibers. Most of the nonlinear effects in optical fibers therefore originate from nonlinear refraction, a phenomenon that refers to the intensity dependence of refractive index resulting from the contribution of $\chi^{(3)}$, i.e., the refractive index of the fiber becomes

$$\tilde{n}(\omega, |E|^2) = n(\omega) + n_2 |E|^2 \tag{2.19}$$

where $n(\omega)$ is the linear part, $|E|^2$ is the optical intensity inside the fiber, and n_2 is the nonlinear-index coefficient related to $\chi^{(3)}$ by the relation

$$n_2 = \frac{3}{8n} \text{Re}(\chi^{(3)}_{xxxx}) \tag{2.20}$$

where Re stands for the real part and the optical field is assumed to be linearly polarized so that only one component $\chi^{(3)}_{xxxx}$ of the fourth-rank tensor contributes to the refractive index. The tensorial nature of $\chi^{(3)}$ can affect the polarization properties of optical beams through nonlinear birefringence.

The intensity dependence of the refractive index leads to a large number of nonlinear effects; the two most widely studied are self-phase modulation (SPM) and cross-phase modulation (XPM). SPM refers to the self-induced phase shift experienced by an optical field during its propagation in optical fibers. Its magnitude can be obtained by noting that the phase of an optical field changes by

$$\phi = \tilde{n} K_0 L = (n + n_2 |E|^2) K_0 L \tag{2.21}$$

where $K_0 = \frac{2\pi}{\lambda}$ and L is the fiber length. The intensity-dependent nonlinear phase shift $\phi_{NL} = n_2 K_0 L |E|^2$ is due to SPM.

In standard single-mode fiber transmission, multi-wavelength nonlinear effects have a little impact on the system performance [36]. In particular, FWM is substantially suppressed by the high chromatic dispersion and XPM introduces only a little penalty in densely spaced systems. XPM does not have a great impact on SSMF-based systems because of high walk-off.

2.6.1 SPM-induced Spectral Broadening

A general description of SPM in optical fibers requires numerical solutions of the propagation equation defined by NLSE when dispersion effect is negligible ($\beta_2 = 0$). In terms of the normalized amplitude $U(z,T)$, NSLE becomes

$$\frac{\partial U}{\partial z} = \frac{i}{L_{NL}} \exp(-\alpha z)|U|^2 U \qquad (2.22)$$

where α accounts for fiber loss. The normalized length

$$L_{NL} = (\gamma P_0)^{-1} \qquad (2.23)$$

where P_0 is the peak power and γ is related to the nonlinear-index coefficient n_2 -- $\gamma = (n_2 \omega_0)/(CA_{eff})$. Eq. (2.22) is readily solved to obtain

$$U(z,T) = U(0,T)\exp[i\phi_{NL}(z,T)] \qquad (2.24)$$

where $U(0,T)$ is the field amplitude at $z = 0$ and

$$\phi_{NL}(z,T) = |U(0,T)|^2 (z_{eff} / L_{NL}) \qquad (2.25)$$

with

$$z_{eff} = [1 - \exp(-\alpha z)]/\alpha \qquad (2.26)$$

Equation (2.24) shows that SPM gives rise to an intensity-dependent phase shift while the pulse shape governed by $|U(z,T)|^2$ remains unchanged. The nonlinear phase shift $\phi_{NL}(z,T)$ given by Eq. (2.25) increases with the propagated distance z. The quantity z_{eff} plays the role of an effective distance that is smaller than z because of fiber loss. In the absence of fiber loss, $\alpha = 0$, and $z_{eff} = z$. The maximum phase shift ϕ_{max} occurs at the pulse center located at $T = 0$. Since U is normalized such that $|U(0,0)| = 1$, it is given by

$$\phi_{max} = z_{eff} / L_{NL} = \gamma P_0 z_{eff} \qquad (2.27)$$

SPM-induced spectral broadening is a consequence of the time dependence of $\phi_{NL}(z,T)$. This can be understood by noting that a temporally varying phase implies that the instantaneous optical frequency differs across the pulse from its central value ω_0. The difference $\delta\omega$ is given by

$$\delta\omega(T) = -\frac{\partial\phi_{NL}}{\partial T} = -\frac{\partial}{\partial T}\left(|U(0,T)|^2\frac{z_{eff}}{L_{NL}}\right) \tag{2.28}$$

The time dependence of $\delta\omega$ can be viewed as a frequency chirp. The chirp is induced by SPM and increases in magnitude with the propagated distance. In other words, new frequency components are continuously generated as the pulse propagates down the fiber. These SPM generated frequency components broaden the spectrum over its initial width at z = 0. From Eq. (2.28) it is clear that, SPM-induced chirp is in the positive direction within the pulse. That is, the leading edge frequency of the pulse is down-shifted and trailing edge frequency of the pulse is up-shifted.

2.6.2 Effect of Pulse Shape on SPM-induced Spectral Broadening

The extent of spectral broadening depends on the pulse shape. Consider, for example, the case of a super-Gaussian pulse with the incident field $U(0,T)$ given by Eq. (2.13). The SPM-induced chirp $\delta\omega(T)$ for such a pulse is

$$\delta\omega(T) = \frac{2m}{T_0}\frac{z_{eff}}{L_{NL}}\left[\frac{T}{T_0}\right]^{2m-1}\exp\left[-\left[\frac{T}{T_0}\right]^{2m}\right] \tag{2.29}$$

The parameter m equals 1 for a Gaussian pulse. For larger values of m, the incident pulse becomes nearly rectangular with increasingly steeper leading and trailing edges. Fig. 2.2 shows the variation of the nonlinear phase shift ϕ_{NL} and the induced frequency chirp $\delta\omega$ across the pulse at $z_{eff} = L_{NL}$ for the case of a Gaussian pulse (m=1) and a supper-Gaussian pulse (m = 3). Since ϕ_{NL} is directly proportional to $|U(0,T)|^2$ in Eq. (2.25), its temporal variation is identical to that of the pulse intensity. The temporal variation of the induced chirp $\delta\omega$ has several interesting features. First, $\delta\omega$ is negative near the leading edge (red shift) and becomes positive near the trailing edge (blue shift). Second, the chirp is linear and positive (up-chirp) over a large central region of the Gaussian pulse. Third, the chirp is considerably larger for pulses with steeper leading and trailing edges. Fourth, super-Gaussian pulses behave differently than Gaussian pulses since chirp occurs only near pulse edges and does not have a linear variation.
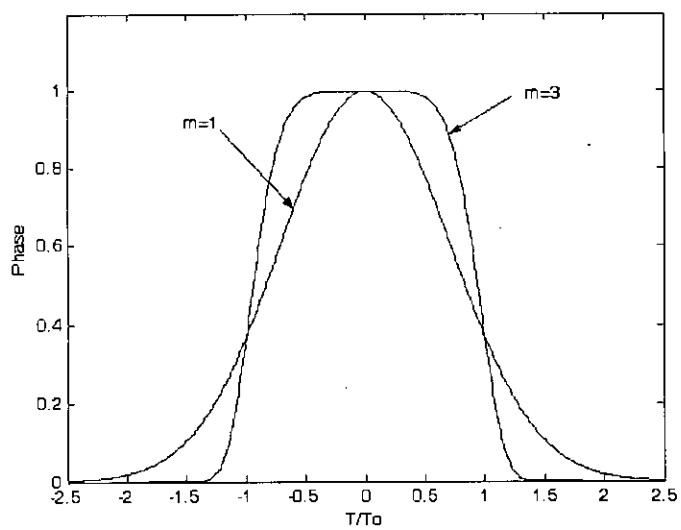
(a)
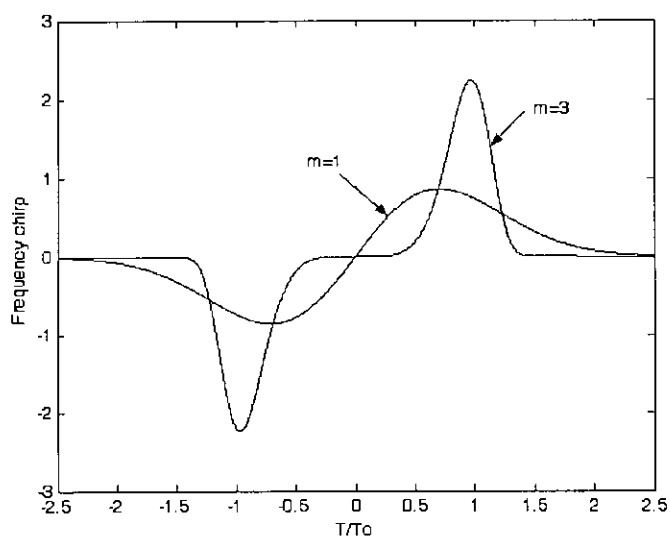
(b)

Fig. 2.2: Temporal variation of the (a) phase shift ϕ_{NL} and (b) frequency chirp $\delta\omega$ induced by SPM for the case of a Gaussian and a super-Gaussian pulse

2.7 Interaction between GVD and SPM

The SPM effects discussed above describe the propagation behavior realistically only

for relatively long pulses ($T_0 > 100 ps$) for which the dispersion length $L_D (= \dfrac{T_0^2}{|\beta_2|})$ is

much larger compared with both the fiber length L and the nonlinear length L_{NL}. As

pulses become shorter and the dispersion length becomes comparable to the fiber

length, it becomes necessary to consider the combined effects of GVD and SPM on

pulse evolution along the fiber. New qualitative features arise from interplay between

GVD and SPM. In the anomalous-dispersion regime of the fiber, the two phenomena

can cooperate in such a way that the fiber can support optical *solitons*. In normal-

dispersion regime the combined effects of GVD and SPM have found application in

optical pulse compression.

NLSE in its normalized form is given as

$$i\frac{\partial U}{\partial \xi} = \text{sgn}(\beta_2)\frac{1}{2}\frac{\partial^2 U}{\partial \tau^2} - N^2 \exp(-\alpha z)|U|^2 U \qquad (2.30)$$

where ξ and τ represent the normalized distance and time variables

$$\xi = z / L_D, \qquad \tau = T / T_0 \qquad (2.31)$$

and the parameter N is introduced by using the definition

$$N^2 = \frac{L_D}{L_{NL}} = \frac{\gamma P_0 T^2{}_0}{|\beta_2|} \qquad (2.32)$$

N governs the relative importance of the SPM and GVD effects on pulse evolution

along the fiber. Dispersion dominates for $N \ll 1$ while SPM dominates for $N \gg 1$.

For values of $N \sim 1$, both SPM and GVD play an equally important role during pulse

evolution.

The evolution of the pulse shape and the pulse spectrum for an initially unchirped

Gaussian pulse in the normal-dispersion regime ($\beta_2 > 0$) of the fiber for $N \neq 0$ is

quite different than that expected when either GVD or SPM dominates. In particular,

the pulse broadens much more rapidly compared with the case $N = 0$ (no SPM). This

can be understood by noting that SPM generates new frequency components, which

are down-shifted near the leading edge and up-shifted near the trailing edge of the pulse. Since the down-shifted components travel faster than the up-shifted components in the normal-dispersion regime, SPM leads to an enhanced rate of pulse broadening compared with that expected from GVD alone. This in turn affects spectral broadening as the SPM-induced phase shift ϕ_{NL} becomes less that that occurring if the pulse shape were to remain unchanged.

The situation is different for pulses propagating in the anomalous dispersion regime ($\beta_2 < 0$) of the fiber. The pulse broadens initially at a rate much lower than that expected in the absence of SPM and then appears to reach a steady state for transmission over several orders of dispersion length. At the same time, the spectrum narrows rather than exhibiting broadening expected by SPM in the absence of GVD. This behavior can be understood by noting that the SPM-induced chirp given by Eq. (2.28) is positive while the dispersion-induced chirp is negative for $\beta_2 < 0$. The two chirp contribution cancel each other along the pulse depending on the magnitude of N. Pulse shape adjusts itself during propagation to make such cancellation as complete as possible. Thus, GVD and SPM cooperate with each other to maintain a chirp-free pulse.

2.8 Summary

Theoretical model of pulse propagation in optical fiber in presence of both GVD and SPM has been described in this chapter. GVD effects on pulse propagation and SPM effects on pulse propagation have been described separately taking one of the effects negligible. It is found that GVD broadens the pulse and produces frequency chirping along the pulse. For a normal dispersion regime ($\beta_2 > 0$), the induced chirping is positive (frequency increases from the leading to the trailing edge). But for an anomalous dispersion regime ($\beta_2 < 0$), GVD induces a negative chirping on the pulse (frequency decreases from the leading to the trailing edge). SPM effects do not change the pulse shape in time domain but change the spectrum of the pulse. New frequency components are generated during the propagation of the pulse.

Pulse propagating in presence of both GVD and SPM behaves differently than propagating in presence of GVD or SPM alone. It is evident that SPM effects broaden a pulse at a much higher rate in normal dispersion regime ($\beta_2 > 0$) than if there were no SPM. This is because of SPM-induced frequency chirping supports GVD-induced frequency chirping. On the other hand, pulses broaden at a slower rate in presence of SPM in anomalous dispersion ($\beta_2 < 0$) regime if there were no SPM. This is because of SPM-induced frequency chirping cancels GVD-induced frequency chirping.

Chapter 3

Numerical Analysis Technique

3.1 Introduction

The nonlinear Schrodinger equation given in Eq. (2.1) governs the propagation of optical pulses inside single-mode fibers. The NLSE is a partial differential equation that does not generally lend itself to analytical solutions except for some specific cases in which the inverse scattering method can be employed. A numerical approach is therefore often necessary for an understanding of the interplay between group-velocity dispersion and self-phase modulation on optical fibers. A large number of numerical methods can be used for this purpose. These can be classified into two broad categories known as (i) the finite-difference methods and (ii) the pseudospectral methods. Generally speaking, pseudospectral methods are faster up to an order of magnitude to achieve the same accuracy. The one method that has been used extensively to solve the pulse-propagation problem in nonlinear dispersive media is the *split-step Fourier method*. The relative speed of this method compared with most finite-difference methods can be attributed in part to the use of the fast-Fourier-transform (FFT) algorithm.

3.2 Split-Step Fourier Method

To understand the philosophy behind the split-step Fourier method, it is useful to write Eq. (2.1) formally in the form

$$\frac{\partial A}{\partial z} = (\hat{D} + \hat{N})A \tag{3.1}$$

where $\hat{D}$ is a differential operator that accounts for second-order dispersion and absorption in a linear medium and $\hat{N}$ is a nonlinear operator that governs the effect of fiber nonlinearities on pulse propagation. These operators are given by

$$\hat{D} = -\frac{i}{2}\beta_2 \frac{\partial^2}{\partial T^2} - \frac{\alpha}{2} \tag{3.2}$$

$$\hat{N} = i\gamma|A|^2 \tag{3.3}$$

In general, dispersion and nonlinearity act together along the length of the fiber. The split-step Fourier method obtains an approximate solution by assuming that in propagating the optical field over a small distance h, the dispersive and nonlinear effects can be pretended to act independently. More specifically, propagation from z to $z + h$ is carried out in two steps. In the first step, the nonlinearity acts alone, and $\hat{D} = 0$ in equation (3.1). In the second step, dispersion acts alone, and $\hat{N} = 0$ in equation (3.1). Mathematically,

$$A(z + h, T) = \exp(h\hat{D})\exp(h\hat{N})A(z,T) \tag{3.4}$$

The execution of the exponential operator $\exp(h\hat{D})$ is carried out in the Fourier domain using the prescription

$$\exp(h\hat{D})B(z,T) = \{F^{-1}\exp[h\hat{D}(i\omega)]F\}B(z,T) \tag{3.5}$$

Where F denotes the Fourier-transform operation, $\hat{D}(i\omega)$ is obtained from equation (3.2) by replacing the differential operator $\partial/\partial T$ by $i\omega$, and ω is the frequency in the Fourier domain. Since $\hat{D}(i\omega)$ is just a number in the Fourier space, the evaluation of equation (3.5) is straightforward. The use of FFT algorithm makes numerical evaluation of equation (3.5) relatively fast. It is for this reason that the split-step Fourier method can be faster by up to two orders of magnitude compared with most finite-difference schemes.

The accuracy of the split-step Fourier method can be improved by adopting a different procedure to propagate the optical pulse over one segment from z to $z + h$. In this procedure equation (3.4) is replaced by

$$A(z + h, T) \approx \exp\left[\frac{h}{2}\hat{D}\right]\exp\left[\int_z^{z+h}\hat{N}(z')dz'\right]\exp\left[\frac{h}{2}\hat{D}\right]A(z,T) \tag{3.6}$$

The main difference is that the effect of nonlinearity is included in the middle of the segment rather than at the segment boundary. Because of the symmetric form of the exponential operators in equation (3.6), this method is known as the *symmetrized split-step Fourier method*. The integral in the middle exponential is useful to include the z dependence of the nonlinear operator $\hat{N}$. If the step size h is small enough, it can be approximated by $\exp(h\hat{N})$, similar to equation (3.4).

The accuracy of the split-step Fourier method can be further improved by evaluating the integral in equation (3.6) more accurately than approximating it by $h\hat{N}(z)$. A simple approach is to employ the trapezoidal rule and approximate the integral by

$$\int_z^{z+h} \hat{N}(z')dz' \approx \frac{h}{2}\left[\hat{N}(z) + \hat{N}(z+h)\right] \tag{3.7}$$

However, the implementation of equation (3.7) is not simple since $\hat{N}(z+h)$ is unknown at the mid-segment located at $z + \frac{h}{2}$. It is necessary to follow an iterative procedure that is initiated by replacing $\hat{N}(z+h)$ by $\hat{N}(z)$. Equation (3.6) is then used to estimate $A(z+h,T)$, which in turn is used to calculate the new value of $\hat{N}(z+h)$. Although the iteration procedure is time-consuming, it can still reduce the overall computing time if the step size h can be increased because of the improved accuracy of the numerical algorithm. Two iterations are generally enough in practice.

The implementation of the split-step Fourier method is relatively straightforward. As shown in figure 1, the fiber length is divided into a large number of segments that need not be spaced equally. The optical pulse is propagated from segment to segment using the prescription of equation (3.6). More specifically, the optical field $A(z,T)$ is first propagated for a distance $\frac{h}{2}$ with dispersion only using the FFT algorithm and equation (3.5). At the mid-plane $z + \frac{h}{2}$, the field is multiplied by a nonlinear term that represents the effect of nonlinearity over the whole segment length h. Finally, the

field is propagated the remaining distance $\frac{h}{2}$ with dispersion only to obtain $A(z+h,T)$. In effect, the nonlinearity is assumed to be lumped at the mid-plane of each segment (dashed line in figure 1).
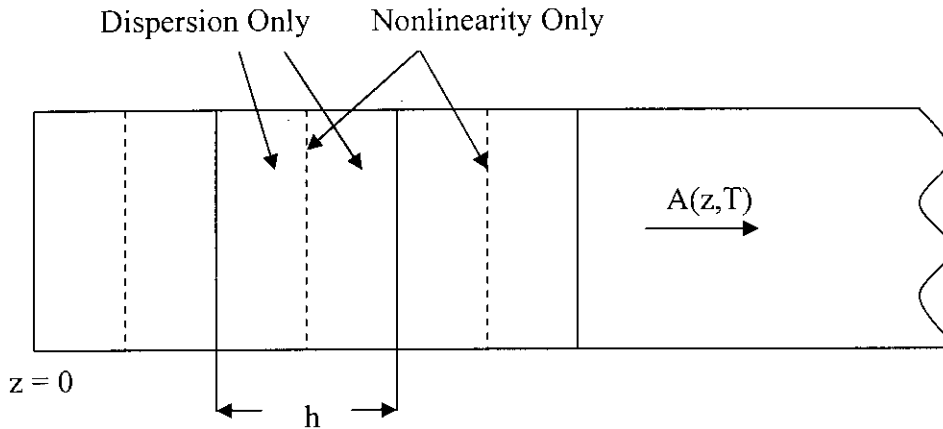
Fig. 3.1: Schematic illustration of the symmetrized split-step Fourier method used for numerical simulations. The fiber length is divided into a large number of segments of width h. Within a segment, the effect of nonlinearity is included at the mid-plane shown by a dashed line.

3.3 Transmission Performance

Optical receivers convert incident optical power P_{in} into electric current through a photodiode. The optical signal received by the receiver is already degraded by the interplay between GVD and SPM during transmission through the fiber. The pulse intensity distorts at the bit center and pulse broadens outside the dedicated bit period. As a result the magnitude of signal power received by the receiver is changed from what was transmitted and at the same time power from neighboring bits interferes into the signal power causing inter-symbol interference. So, due to degradation of pulse intensity at the bit center and inter-symbol interference, the signal content (1 or 0) may be incorrectly interpreted by the receiver.

In addition to the degraded and broadened pulse received by the receiver, a number of noise mechanisms add to the recovered electrical signal, which further mislead decision-making. The noises may come from the in-line amplifiers used to periodically compensate the fiber transmission loss or from the pre-amplifier used to increase the received power of the receiver. The noise may also originate within the receiver itself. However to evaluate performance of a system these noise mechanisms should be included.

3.3.1 Receiver Noise

Two fundamental noise mechanisms, shot noise and thermal noise [37]-[39], lead to fluctuations in the current even when the incident optical signal has a constant power. However, electrical noise induced by current fluctuations affects the receiver performance. The objective of this section is to review the noise mechanisms and then discuss the signal-to-noise ratio (SNR) in a p-i-n optical receiver.

Shot Noise:

Shot noise arises from the fact that an electric current is made up of a stream of discrete charges – namely, electrons – that are randomly generated. Thus, even when a photodetector is illuminated by constant optical power P, due to the random generation of $e - h$ pairs, the current will fluctuate routinely around an average value determined by the average optical power P.

The photodiode current generated in response to a constant optical signal can be written as

$$I(t) = I_p + i_s(t) \tag{3.8}$$

where $I_p = RP_{in}$ is the average current and $i_s(t)$ is a current fluctuation related to shot noise. Mathematically, $i_s(t)$ is a stationery random process with Poisson statistics (approximated often by Gaussian statistics). The autocorrelation function of $i_s(t)$ is related to the spectral density $S_s(f)$ by the Wiener-Khinchin theorem [39]

$$\langle i_s(t)i_s(t+\tau)\rangle = \int_{-\infty}^{\infty} S_s(f)\exp(2\pi i f\tau)df \tag{3.9}$$

where angle brackets denote an ensemble average over fluctuations. The spectral density of shot noise is constant and is given by $S_s(f) = qI_p$ (an example of white noise). Note that $S_s(f)$ is the two-sided spectral density, as negative frequencies are included in Eq. (2). If only positive frequencies are considered by changing the lower limit of integration to zero, the *one-sided* spectral density becomes $2qI_p$.

The noise variance is obtained by setting $\tau = 0$ in Eq. (3.9), i.e.,

$$\sigma_s^2 = \langle i_s^2(t) \rangle = \int_{-\infty}^{\infty} S_s(f)df = 2qI_p\Delta f \tag{3.10}$$

where Δf is the *effective noise bandwidth* of the receiver.

Since the dark current I_d also generates shot noise, its contribution is included in Eq. (3.10) by replacing I_p by $I_p + I_d$. The total shot noise is then given by

$$\sigma_s^2 = 2q(I_p + I_d)\Delta f \tag{3.11}$$

The quantity σ_s is the root-mean-square (RMS) value of the noise current induced by shot noise.

Thermal Noise:

At a finite temperature, electrons move randomly in any conductor. Random thermal motion of electrons in a resistor manifests as a fluctuating current even in the absence of an applied voltage. The load resistor in the front end of an optical receiver adds such fluctuations to the current generated by the photodiode. This additional noise component is referred to as *thermal noise*. Thermal noise can be included by modifying Eq. (3.8) as

$$I(t) = I_p + i_s(t) + i_T(t) \tag{3.12}$$

where $i_T(t)$ is a current fluctuation induced by thermal noise. Mathematically, current fluctuation induced by thermal noise $i_T(t)$ is modeled as a stationary Gaussian random process with a spectral density that is frequency independent up to $f \sim 1$ THz (nearly white noise) and is given by

$$S_T(f) = 2k_B T / R_L \qquad (3.13)$$

where k_B is the Boltzmann constant, T is the absolute temperature, and R_L is the load resistor. The autocorrelation function of $i_T(t)$ is given by

$$\langle i_T(t) i_T(t+\tau) \rangle = \int_{-\infty}^{\infty} S_s(f) \exp(2\pi i f \tau) df \qquad (3.14)$$

The noise variance is obtained by setting $\tau = 0$ and becomes

$$\sigma_T^2 = \langle i_T^2(t) \rangle = \int_{-\infty}^{\infty} S_T(f) df = (4k_B T / R_L) \Delta f \qquad (3.15)$$

where Δf is the *effective noise bandwidth*. The same bandwidth appears in the case of both shot and thermal noises. Note that σ_T^2 does not depend on input power to the receiver.

The total current noise contributed by the receiver circuit can be obtained by adding the contributions of shot noise and thermal noise. Since $i_s(t)$ and $i_T(t)$ in Eq. (3.12) are independent random processes with approximately Gaussian statistics, the total variance of current fluctuations, $\Delta I = I - I_p = i_s + i_T$, can be obtained simply by adding individual variances. The result is

$$\sigma^2 = \langle (\Delta I)^2 \rangle = \sigma_s^2 + \sigma_T^2 = 2q(I_p + I_d)\Delta f + (4k_B T / R_L)\Delta f \qquad (3.16)$$

Equation (3.16) is one of the factors that degrade the SNR of the photocurrent.

3.3.2 Optical Preamplification Noise

Optical amplifiers are routinely used for improving the sensitivity of optical receivers by preamplifying the optical signal before it falls on the photodetector. Preamplification of the optical signal makes it strong enough that thermal noise becomes negligible compared with the noise induced by the preamplifier. As a result,

the receiver sensitivity can be improved by 10-20 dB using an EDFA as a preamplifier [40]-[45].

To calculate the receiver sensitivity, we need to include all sources of current noise at the receiver. The most important performance issue in designing optical preamplifiers is the contamination of the amplified signal by the ASE [14]. Because of the incoherent nature of spontaneous emission, the amplified signal is noisier than the input signal. The photocurrent generated at the detector can be written as [14]

$$I = R\left|\sqrt{G}E_s + E_{sp}\right|^2 + i_s + i_T \tag{3.17}$$

where R is the photodetector responsivity, G is the amplifier gain, E_s is the signal field, E_{sp} is the optical field associated with the ASE, and i_s and i_T are current fluctuations induced by the shot noise and thermal noise, respectively within the receiver. The average value of the current consists of

$$\bar{I} = R(GP_s + P_{sp}) \tag{3.18}$$

where $P_s = |E_s|^2$ is the optical signal before its preamplification, and P_{sp} is the ASE noise power added to the signal with the magnitude

$$P_{sp} = |E_{sp}|^2 = S_{sp}\Delta\nu_{sp} \tag{3.19}$$

The spectral density $S_{sp}(\nu) = (G-1)n_{sp}\hbar\nu$ and $\Delta\nu_{sp}$ is the effective bandwidth of spontaneous emission set by the amplifier bandwidth or the filter bandwidth if an optical filter is placed after the amplifier. Notice that E_{sp} in Eq. (3.17) includes only the component of ASE that is copolarized with the signal as the orthogonally polarized component cannot beat with the signal [14].

The current noise $<I>$ consists of fluctuations originating from the shot noise, thermal noise, and ASE noise. The ASE-induced current noise has its origin in the beating of E_s with E_{sp} and the beating of E_{sp} with itself. To understand this beating

phenomenon more clearly, notice that the ASE field E_{sp} is broadband and can be written in the form

$$E_{sp} = \int \sqrt{S_{sp}} \exp(\phi_n - i\omega_n t) d\omega_n \qquad (3.20)$$

where ϕ_n is the phase of the noise-spectral component at the frequency ω_n, and the integral extends over the entire bandwidth of the amplifier (or optical filter). Using $E_s = \sqrt{P_s} \exp(\phi_s - i\omega_s t)$, the interference term in (3.17) consists of two parts and leads to current fluctuations of the form

$$i_{sig-sp} = 2R \int (GP_s S_{sp})^{\frac{1}{2}} \cos\theta_1 d\omega_n, \qquad i_{sp-sp} = 2R \iint S_{sp} \cos\theta_2 d\omega_n d\omega_n' \quad (3.21)$$

where $\theta_1 = (\omega_s - \omega_n)t + \phi_n - \phi_s$ and $\theta_2 = (\omega_n - \omega_n')t + \phi_n' - \phi_n$ are two rapidly varying random phases. These two contributions to current noise are due to the beating of E_s with E_{sp} and the beating of E_{sp} with itself, respectively.

$$\sigma_{sig-sp}^2 = 4R^2 GP_s S_{sp} \Delta f \qquad (3.22)$$

$$\sigma_{sp-sp}^2 = 4R^2 S_{sp}^2 \Delta\nu_{opt} \Delta f \qquad (3.23)$$

3.3.3 Inter-Symbol Interference Noise

Pulse shape broadens due to the combined effect of GVD and SPM even if dispersion is fully compensated by DCF compensating technique. Therefore, pulse intensity of one bit interferes with the pulse intensity of another. So, inter-symbol interference occurs. The interfering power from the neighboring pulse causes noise contribution to the total noise. ISI power generates noise current as the signal power generates signal current within the receiver. Besides, ISI power contributes to the shot noise and ISI power-spontaneous beat noise.

$$\sigma_{ISI}^2 = R^2 P_{ISI}^2 \qquad (3.24)$$

$$\sigma_{s(ISI)}^2 = 2qRP_{ISI} \Delta f \qquad (3.25)$$

$$\sigma_{ISI-sp}^2 = 4R^2 P_{ISI} S_{sp} \Delta f \qquad (3.26)$$

3.3.4 Total Noise

Averaging over the random phases, the total variance $\sigma^2 = <(\Delta I)>$ of current fluctuations can be written as

$$\sigma^2 = \sigma_T^2 + \sigma_{s(Total)}^2 + \sigma_{sig-sp}^2 + \sigma_{sp-sp}^2 + \sigma_{ISI}^2 + \sigma_{ISI-sp}^2 \qquad (3.27)$$

where,

$$\sigma_{s(Total)}^2 = 2q[R(GP_s + P_{sp} + P_{ISI})]\Delta f \qquad (3.28)$$

The remaining terms in Eq. (3.27) are defined in previous sections.

3.4 SNR of p-i-n Receivers

The performance of an optical receiver depends on the signal-to-noise ratio. The SNR of a receiver with a p-i-n photodiode is considered here. The SNR of any electrical signal is defined as

$$SNR = \frac{average\ signal\ power}{noise\ power} = \frac{I_p^2}{\sigma^2} \qquad (3.29)$$

where we used the fact that electrical power varies as the square of the current. $I_p = RP_{in}$ and σ^2 is given in Eq. (3.27). So, the SNR is related to the incident optical power as

$$SNR = \frac{R^2 P_{in}^2}{\sigma_T^2 + \sigma_{s(Total)}^2 + \sigma_{sig-sp}^2 + \sigma_{sp-sp}^2 + \sigma_{ISI}^2 + \sigma_{ISI-sp}^2} \qquad (3.30)$$

where $R = \eta q / h\nu$ is the responsivity of the p-i-n photodiode.

3.5 Receiver Sensitivity

Among a group of optical receivers, a receiver is said to be more sensitive if it achieves the same performance with less optical power incident on it. The performance criterion for digital receivers is governed by the $Q -$ parameter or the *bit-*

error rate (BER). BER is defined as the probability of incorrect identification of a bit by the decision circuit of the receiver. A commonly used criterion for digital optical receivers requires the BER to be below 1×10^{-9}.

The Q-Parameter

There are only two possible signal levels in binary digital communication systems and each of these signal levels may have a different average noise associated with it. This means that there are essentially two discrete signal-to-noise ratios, which are associated with the two possible signal levels. In order to calculate the overall probability of bit error, we must account for both of the signal-to-noise ratios. So, SNRs can be combined into a single quantity – providing a convenient measure of overall system quality – called the Q-parameter.

The incoming optical signal from the fiber is converted into electric current in the photodetector. Then decision circuit samples this electrical signal at the decision instant to determine whether it is 1 or 0. The sampled value I fluctuates from bit to bit around an average value I_1 or I_0, depending on whether the bit corresponds to 1 or 0 in the bit stream. The decision circuit compares the sampled value with a threshold value I_D and calls it bit 1 if $I > I_D$ or bit 0 if $I < I_D$. An error occurs if $I < I_D$ for bit 1 because of noise mechanisms discussed in this chapter. An error also occurs if $I > I_D$ for bit 0.

Both the average and variance of receiver noise are different for 1 and 0 bits since I_p equals I_1 or I_0, depending on the bit received. If σ_1^2 and σ_0^2 are the corresponding variances, Q-parameter is given by

$$Q = \frac{I_1 - I_0}{\sigma_1 + \sigma_0} \tag{3.31}$$

The Q-parameter is also useful as an intuitive figure of merit that is directly tied to the BER. For example, the BER can be improved by either (1) increasing the difference

between the high and low levels in the numerator of the Q-parameter, or (2) decreasing the noise terms in the denominator of the Q-parameter.

Finally, the Q-parameter allows simplified analysis of system performance. The most direct measure of system performance is the BER, but calculation of the BER requires evaluation of the cumulative normal distribution integral. Since this integral has no closed form solution, evaluation requires numerical integration or the use of tabulated values. A much simpler method of analyzing system performance is to optimize the Q-parameter, knowing that this will result in optimized BER. Relation between Q-parameter and BER is given by

$$BER = \frac{1}{2} erfc(\frac{Q}{\sqrt{2}}) \approx \frac{\exp(-Q^2/2)}{Q\sqrt{2\pi}} \qquad (3.32)$$

3.6 System Description

We perform computer simulations using the split-step Fourier method for dispersion compensated transmission fiber. A single channel, modulated with a 10-Gb/s nonreturn-to-zero (NRZ) bit sequence is generated through a chirp free transmitter and is launched into a link composed of spans of 100 km of standard single-mode fiber and L km of dispersion compensating fiber connected in pre-, post- or bi-end compensation configuration. The length L is varied to vary the residual dispersion accumulated at the end of the transmission fiber.

We used normalized super-Gaussian pulse shape for our numerical analysis given by

$$U(0,T) = \exp\left[-\frac{1}{2}\left[\frac{T}{T_0}\right]^{2m}\right] \qquad (3.33)$$

$$T_b = 2[2\ln 2]^{\frac{1}{2m}} T_0 \qquad (3.34)$$

where T_0 is the half-width at 1/e-intensity point. In our analysis, $m = 1.5$ is assumed.

Fiber Parameters: We used the following fiber parameters for SMF and DCF in our numerical analysis.

Parameter	SSMF	DCF
α	0.2 dB/km	0.6 dB/km
D	17 ps/km/nm	-100 ps/km/nm
$\dfrac{dD}{d\lambda}$	0.07 ps/nm²/km	0.09 ps/nm²/km
γ	1.36 W⁻¹km⁻¹	5.4 W⁻¹km⁻¹
A_{eff}	80 μm^2	20 μm^2

Table 1: Fiber parameters used in our numerical analysis

Optical Amplifier Characteristics: Optical amplifiers are assumed to be placed at regular interval in the system. Besides amplifying the signal, each amplifier adds ASE to the amplified signal. The amplifiers are assumed to have a gain characteristic that is flat with respect to wavelength.

The in-line erbium-doped fiber amplifiers (EDFAs) are supposed flat and noiseless, with gain equal to the span loss. The receiver consists of an optical preamplifier, a *0.4 nm optical filter*, and an electrical receiver. The transmission performance is evaluated considering the worst case of received geometrical eye diagram, receiver noise and the amplified spontaneous emission (ASE) noise of the optical preamplifier. The accumulated ASE noise of the in-line amplifiers has not been considered in our simulations, to highlight the effects of SPM. Because of the high fiber dispersion, the effect of nonlinear propagation on the ASE spectrum (i.e., modulation instability) is negligible [29]. Thus, the impact of the accumulated ASE noise is simply to add an

extra penalty, which decreases with the increase of input power, and which can be easily calculated as in a linear link [46].

We used the following parameter values for the pre-amplifier used in our numerical analysis.

Parameter	Values
F_n	5.5 dB
n_{sp}	1.77
ν	193.5 THz
$\hbar$	6.63×10^{-34}

Table 2: EDFA parameters used in the analysis

Photodetector Parameters: A p-i-n photodetector was used as a receiver in our analysis. We used the following parameter values for the photodetector.

Parameter	Values
R	0.8 A/w
R_L	50 ohm
q	1.6×10^{-19}
K_b	1.38×10^{-23}
I_d	10 nA
T	300^0 K

Table 3: p-i-n photodetector parameters

3.7 Summary

In this chapter, we have described the numerical analysis technique followed during our work. Since, there are no analytical solutions for NLSE, we solved it using split-step Fourier transform method using the FFT algorithm as described in this chapter. During the transmission of an optical pulse and during its detection within the receiver different noise mechanisms degrade the actual pulse shape. The noise that can be evolved and incorporated with the signal in our fiber-optic communication model using in-line EDFAs has been discussed in this chapter. Because of noise signal may be interpreted incorrectly. So, signal power should be a sufficient order of magnitude larger than the noise power. Therefore, signal-to-noise ratio is an important parameter for any transmission system. The system performance can also be judged from the value of Q-parameter or BER. We have also given the system parameters in this chapter used in our analysis.

Chapter 4

Performance Analysis of Post Compensation Configuration

4.1 Introduction

We investigated the transmission performance of post-compensated SMF transmission link. We simulated the pulse propagation in presence of both second-order GVD and SPM effects using a numerical technique, namely, the split-step Fourier transform method. SPM effects have been evaluated for a post-compensation configuration. Since SPM effects depend on the magnitude of input power, we have evaluated the maximum power levels that can be launched into a post-compensated transmission fiber in different conditions. From the output pulse of the transmission fiber, we calculated the eye opening penalty and the maximum threshold power beyond which eye penalty exceeds 3 dB at different length and at different input power levels. We also calculated the SNR and Q parameter considering optical pulse degradation due to interplay between GVD and SPM, receiver noise and preamplifier ASE noise. We also investigated the effect of pulse shape on transmission performance for a post-compensated transmission fiber. The results are presented here.

4.2 Post-Compensation Configuration

In post-compensation configuration, single-mode fiber is followed by a dispersion compensating fiber in which the sign of dispersion parameter is opposite to that of dispersion parameter of SMF. The length of DCF can be selected for complete or partial GVD compensation. The sign of dispersion parameter (D_1) of standard single-mode fiber at 1.55 µm wavelength is positive. Then, the sign of the dispersion parameter (D_2) of DCF must be negative for GVD compensation.

If DCF length satisfies equation $L_2 = -(D_1 / D_2)L_1$, where L_1 is the SMF length, then no residual dispersion exists at the end of the transmission fiber. But if DCF length L_2

is smaller than that required to satisfy this equation, there will exist positive residual dispersion as $D_1L_1 + D_2L_2$ will not vanish rather give positive number. Likewise, if L_2 is larger than that required for zero residual dispersion, there will exist negative residual dispersion at the end of the transmission fiber. It is found that, residual dispersion is a figure of merit for transmission performance. End result is different at each residual dispersion.

In our model of post-compensation configuration, we used 100 km of standard SMF followed by L km of DCF as shown in figure 4.1. Such SMF-DCF link is then followed by EDFA to exactly compensate the total fiber loss in SMF and DCF. Then such spans are repeated required number of times for a long-haul transmission link. The fiber parameters are chosen as in table 1. So when DCF length is 17 km, no residual dispersion exists. But, when DCF length is less than 17 km, positive residual dispersion exists and when DCF length is greater than 17 km, negative residual dispersion exists. In our analysis we varied DCF length to evaluate the effect of zero, positive and negative residual dispersion on self-phase modulation effect, and as a result, effect on the system performance.
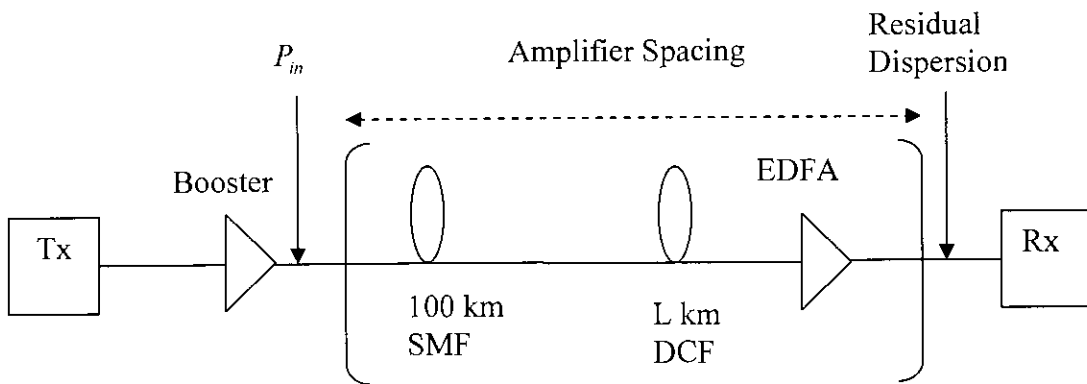
Fig. 4.1: Schematic diagram of a Post-compensation Configuration

4.3 Simulation Results

Pulse propagation in the above-described post-compensation configuration was simulated using split-step Fourier transform technique. We present here some of the simulation results to show self-phase modulation effects on transmission performance of a post-compensation configuration.

4.3.1 Complete Compensation

(a)

(c)

(b)

(d)
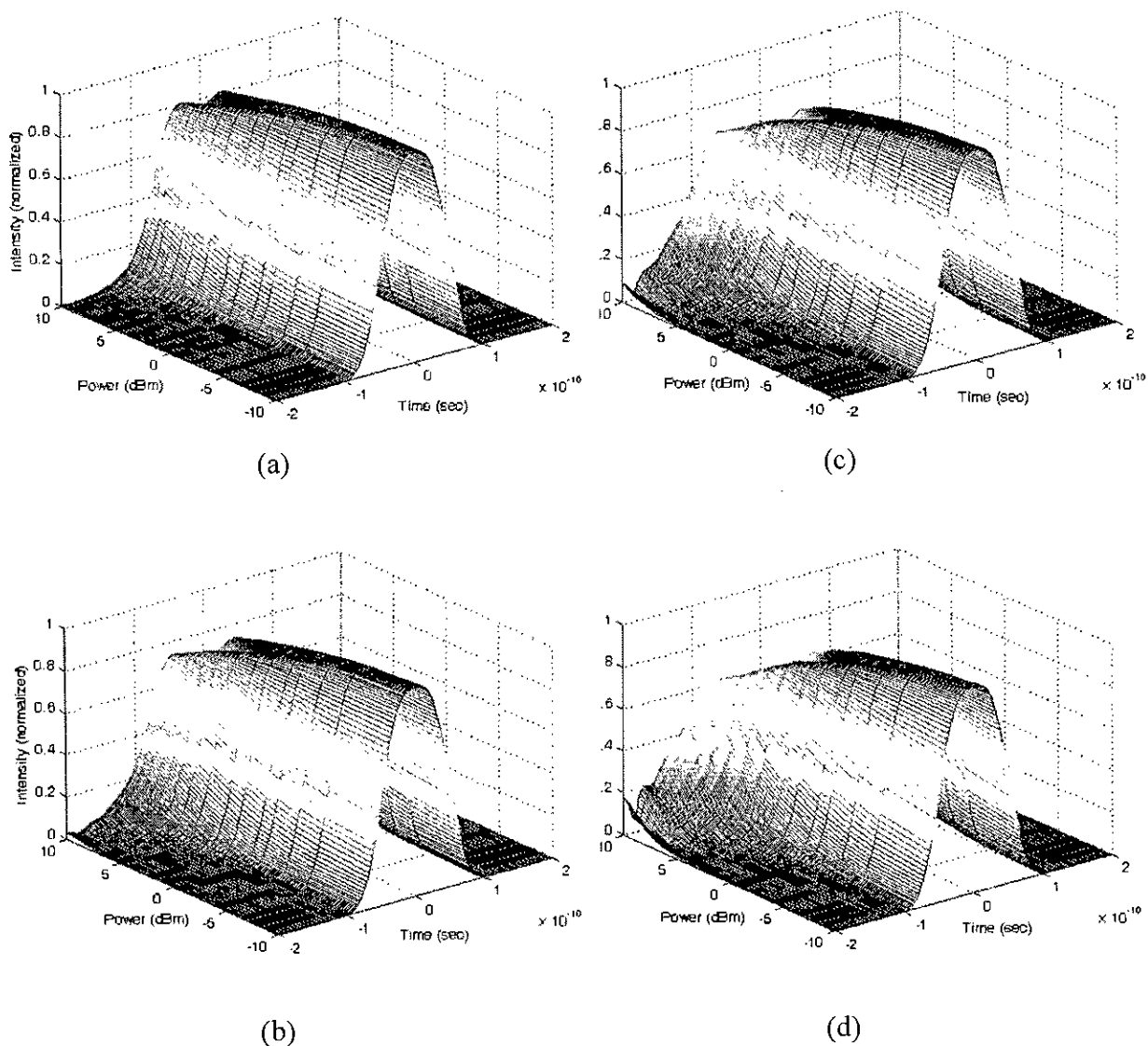
Fig.4.2: Pulse shapes at different lengths of post-compensated transmission fiber with zero residual dispersion. Input power is varied from −10dBm to 10dBm. Fiber length is (a) 1000km (b) 2000km (c) 3000km (d) 4000km
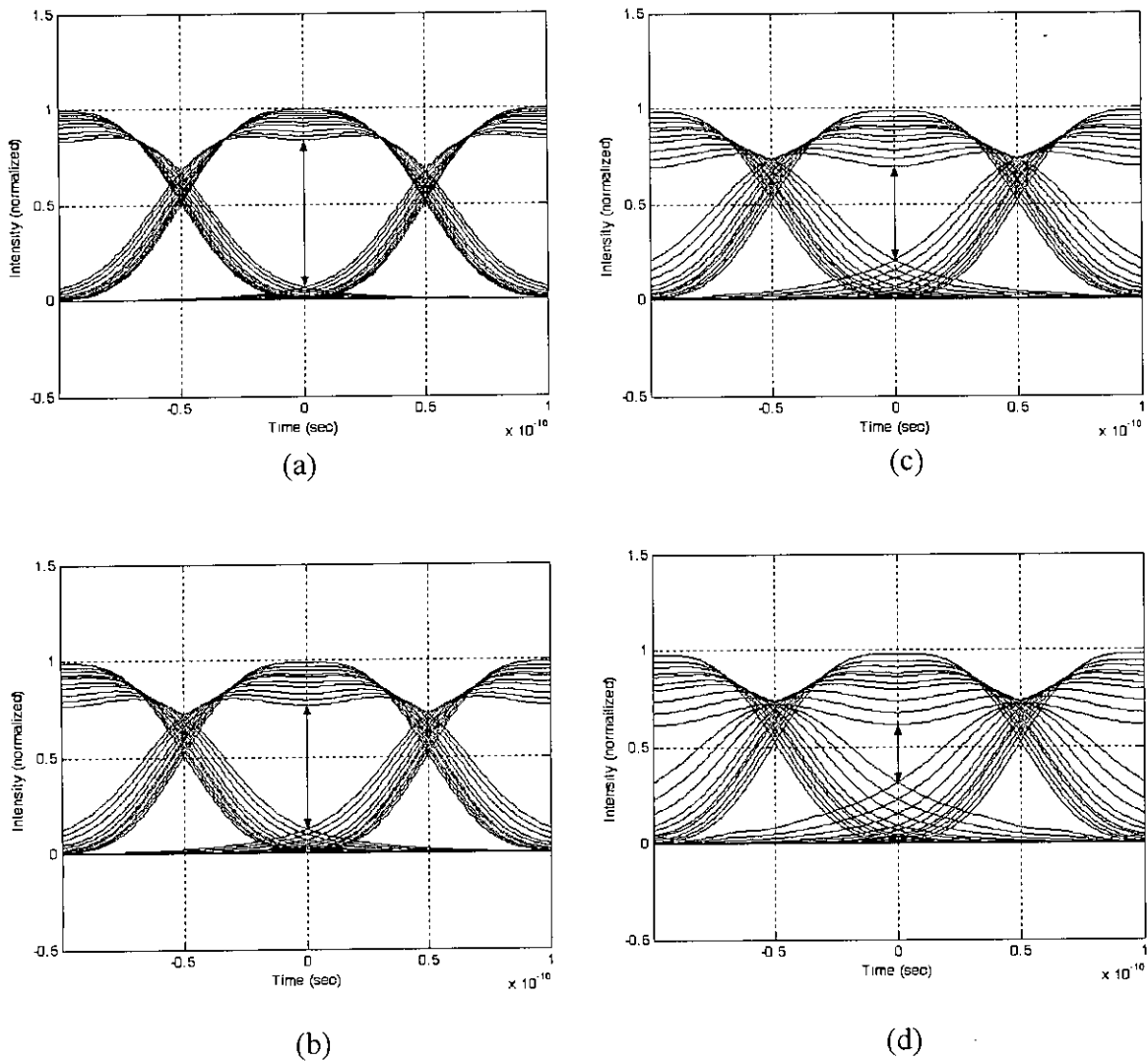
Fig.4.3: Eye diagrams at different lengths of post-compensated transmission fiber with zero residual dispersion. Input power is varied from −10dBm to 10dBm. Fiber length is (a) 1000km (b) 2000km (c) 3000km (d) 4000km

Output pulses at the end of 1000 − 4000 km transmission fiber link are given in figure 4.2. Peak powers of input pulses were varied from −10 dBm to 10 dBm. Since the degree of SPM effect is pulse peak intensity dependent, it is shown that, for a fixed length, input pulse shapes are almost restored at the output for lower input power levels (i.e., -10 dBm to −5 dBm). In these power levels, pulse broadening is almost

fully compensated by DCF. But as we increase power for input pulses, SPM effects come into play greatly and pulse shapes are no longer restored.

In case of complete dispersion compensation, there exists no residual dispersion at the end of a span. So no dispersion-accumulation happens. But as SPM produces positive frequency chirping within the pulse both in SMF and DCF, it is not compensated rather its effects accumulate from one span to another. So, we find that, for a fixed input power, output pulses at lengths 1000 km – 4000 km show distortion with length.

Eye diagrams are drawn in figure 4.3 at lengths 1000 km – 4000 km. Peak powers of input pulses were varied from –10 dBm to 7 dBm. The lowest opening at each length is for 7 dBm input power. This is also because of higher degree of SPM effect at higher input power. Still lowest opening decreases with length due to SPM effects accumulation with length. It is shown in figure 4.3 that, normalized peak intensity decreases and intensity from neighboring pulses are not zero at the bit-center of the investigating bit. And this phenomenon increases both with the increase of input pulse intensity and with the increase of transmission length. As a result, eye opening decreases for both higher power and longer transmission length.

Eye opening penalty for a post-compensated fiber link is plotted in figure 4.4 for different input power levels at transmission length 1000 km – 5000 km. Penalty is calculated from eye diagram using the formula $20\log_{10}(a/b)$, where a is the maximum eye opening at the input of the transmission fiber and b is the maximum eye opening at the output of the transmission fiber. Like the previous observations, eye-opening decreases with the increase of fiber length and input power and as a consequence eye opening penalty increases with length and with power. Increase of eye opening penalty reveals performance degradation of the system. So, we calculated the power levels beyond which eye opening penalty is beyond 3 dB. These maximum threshold power decreases in longer transmission link. Relation between maximum power threshold and transmission length is plotted in figure 4.5. It is found that maximum 8.95 dBm input power can be launched into 1000 km transmission fiber and still obtain eye penalty below 3 dB. At 2000 km this maximum power level

decreases to 6.175 dBm. For longer transmission fiber this maximum threshold power decreases further due to accumulation of SPM effects over the length of the fiber.
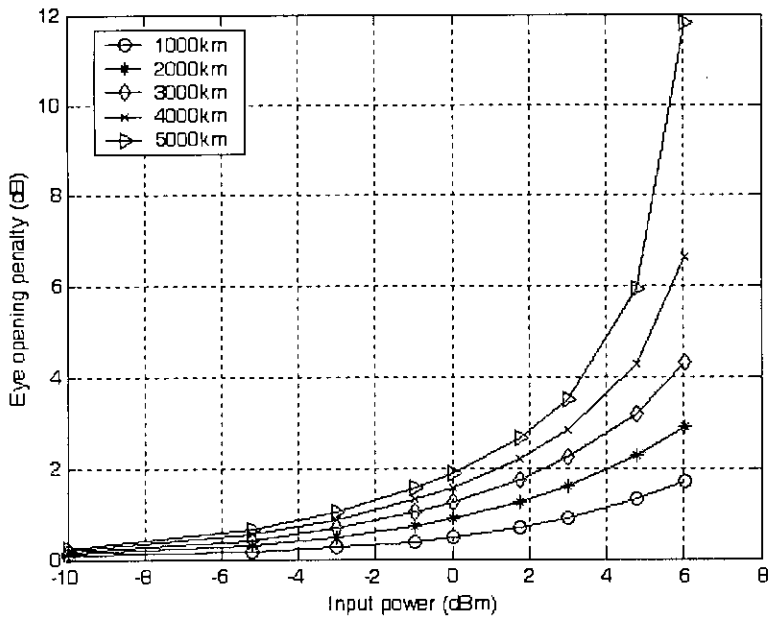
Fig.4.4: Eye opening penalty versus input power for different transmission length for post-compensation configuration with zero residual dispersion

Fig.4.5: Maximum threshold power levels (3 dB eye opening penalty) versus fiber length for post compensation configuration with zero residual dispersion

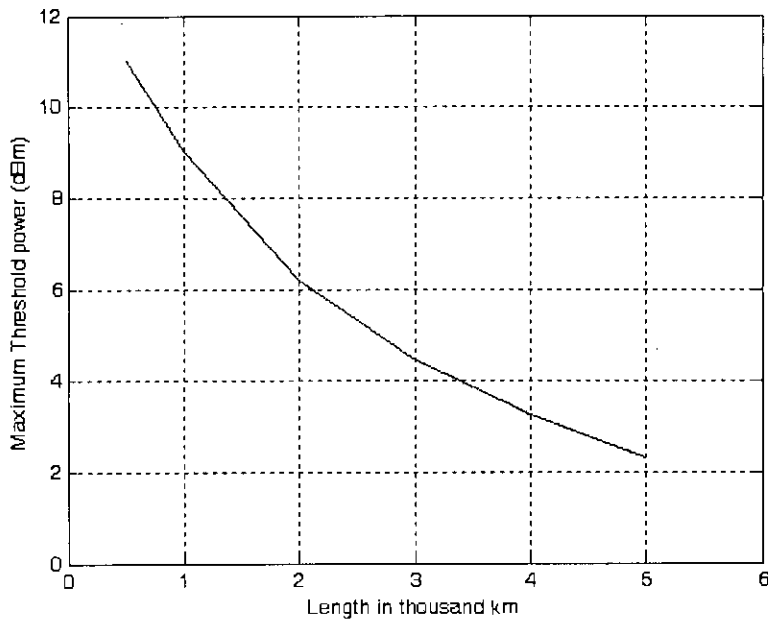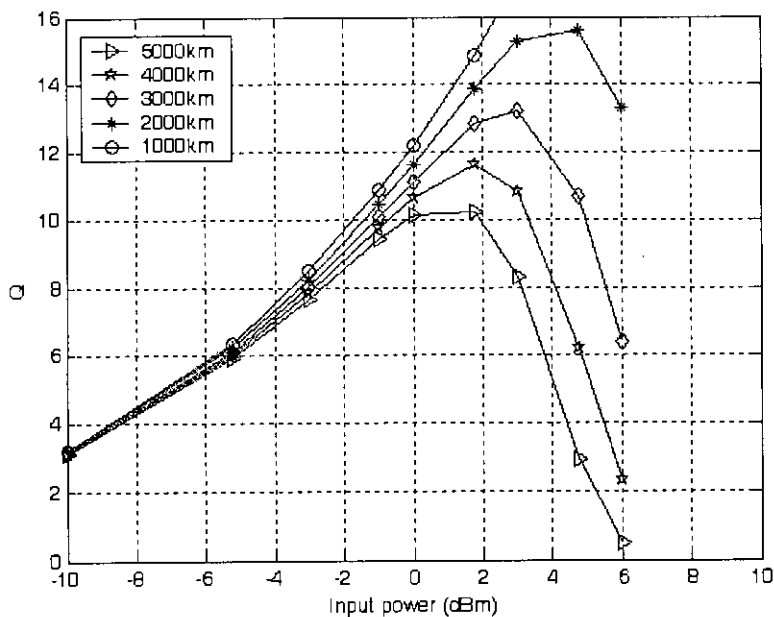**Fig.4.6:** Q parameter versus input power at different length for post-compensation configuration with zero residual dispersion
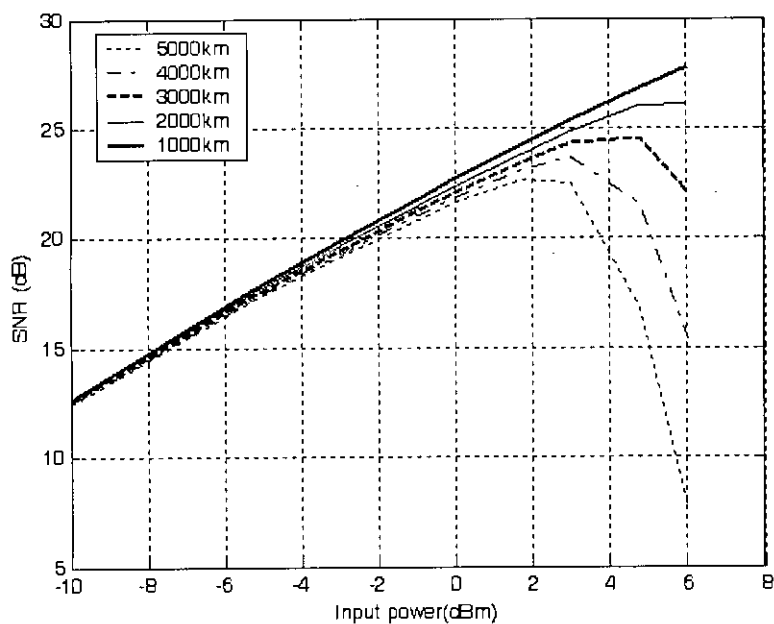
Fig.4.7: Signal-to-noise ratio versus input power at different fiber length for post-compensation configuration with zero residual dispersion
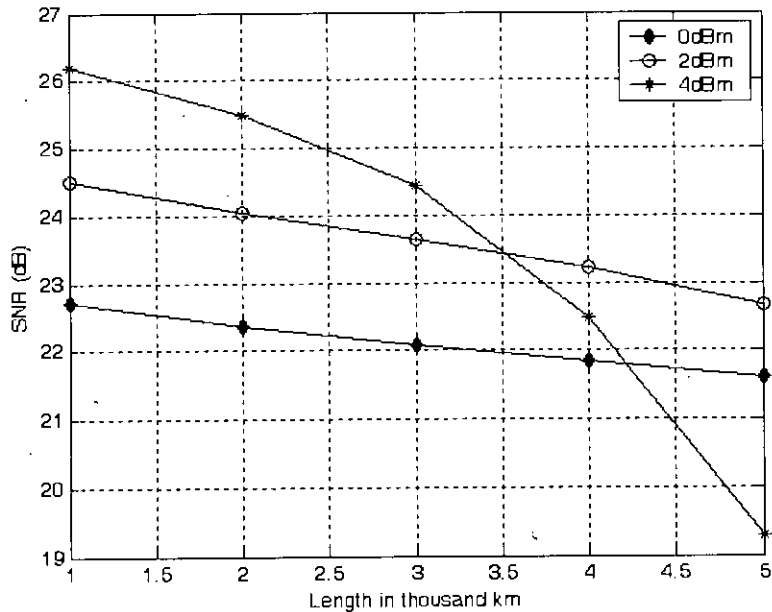
Fig.4.8: Signal-to-noise ratio versus transmission fiber length at different input power for post-compensation configuration with zero residual dispersion

Q parameter and SNR are calculated for our model of post-compensation configuration. In the calculations, with the degraded pulse shapes due to interplay between GVD and SPM, receiver noise and preamplifier ASE noise were considered. The relation of Q parameter with the input power is depicted in figure 4.6 and the relation of SNR with input power is depicted in the figure 4.7 respectively. Curves in both of the figures show an initial upward slope and then downward slope after some levels of input power. The initial increase of both Q parameter and SNR curves are clear because optically generated current at the receiver depends directly on the optical power reaching the receiver. So for higher input powers, more current induced in the receiver. But as power increases SPM effects dominate the pulse propagation and pulse broadening within SMF are not properly compensated within DCF. So, noise levels increase. As a result, both curves show a downward slope with power at higher levels.

A value of '6' for Q is the 10^{-9} BER for the transmission system. It is seen that Q versus input power curves touch this value twice. The lower value of input power indicates the minimum power that must be applied to the system to obtain 10^{-9} BER. This input power is the minimum threshold power that is less determined by SPM

effects. Shot noise, thermal noise and mainly the ASE noise of the preamplifier dominates the determination of lower threshold power level. That is why, minimum threshold powers even for 1000 and 5000 km are not far apart. Since SPM effects is not much pronounced at these power levels. Though Q parameter increases with the increase of power as received power is increased, noise level also increases. At some input power Q parameter reaches peak and then starts to decrease. We also see that, this peak value decreases for higher lengths and the input power levels at which peak value of Q parameter occurs also decreases for longer transmission fiber. Decrease of Q parameter with the increase of input power touches value of '6' again and gets below that. The maximum power levels at which Q parameter is no longer greater than '6', the system cannot provide 10^{-9} BER. Therefore, this is the maximum threshold power level that can be launched into the transmission fiber. These maximum threshold power levels are mainly determined by the nonlinear effects, namely, SPM in a dispersion compensated SMF transmission link. As a result, it is seen that, maximum threshold power at different fiber lengths are far apart since SPM effects accumulate over the length of the fiber.

Signal-to-noise ratio curves at different transmission lengths given in figure 4.7 show similar relation with input power. SPM effects on SNR of a transmission system can better be illustrated from figure 4.8 where SNR is plotted versus transmission length for different input power levels. It is shown that, for smaller transmission fiber higher input power results higher SNR. But as fiber length is increased, SNR gradually decreases due to SPM accumulation. SNR decreases at a higher rate at higher input power with the increase of fiber length as SPM effects depends on pulse intensity.

4.3.2 Partial Compensation

We have investigated transmission performance of a post-compensation configuration with partial dispersion compensation. We varied the DCF length of each span to vary the accumulated residual dispersion at the end of the transmission fiber. It is found that magnitude and sign of residual dispersion have different effects on the transmission performance due to different interplay with SPM. Simulation results at various residual dispersions are presented here.

(a)
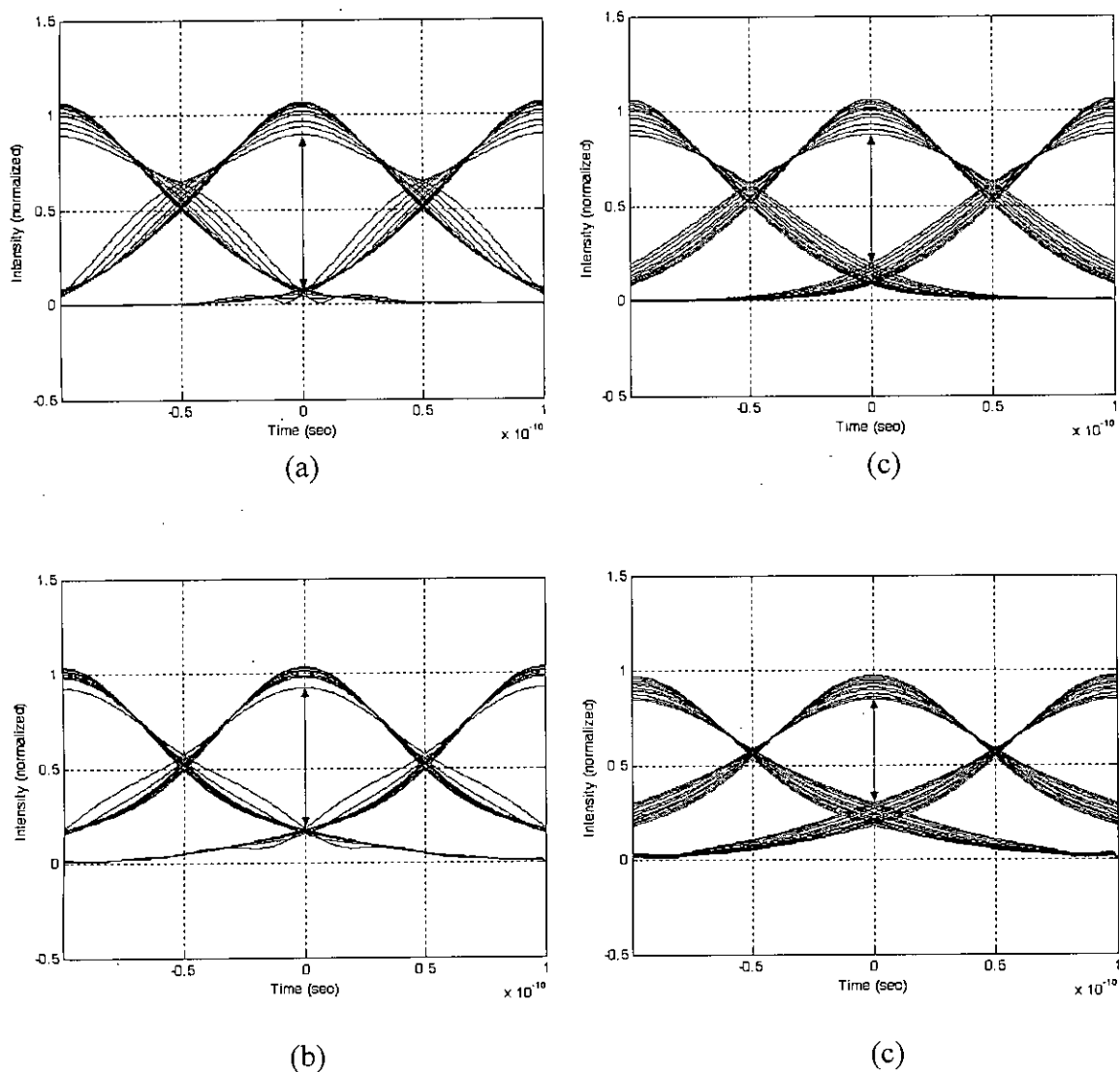
(c)

(b)

(c)

Fig.4.9: Eye diagrams at 1000 km transmission fiber with residual dispersion (a) 500ps/nm (b)1000 ps/nm (c) −500ps/nm (d) −1000ps/nm for a post-compensation configuration . Input power levels were varied from -10 dBm to 7 dBm

Eye diagrams are given in figure 4.9 for a 1000 km post-compensated transmission system. Residual dispersion varied from −1000 ps/nm to 1000 ps/nm. Input power levels were varied from −10 dBm to 7 dBm. In diagram 4.9(a) 500 ps/nm residual dispersion was considered. It is shown that, eye opening increases at lower levels of input power as input pulse compresses at the output. But with the increase of input power, SPM effects are so high that pulse broadens and eye opening decreases. The lowest eye opening in the diagram is for highest input power applied in our investigation. In 4.9(b), since residual dispersion is 1000 ps/nm, pulse distorts much. At lower input power levels, residual dispersion is almost counterbalanced be SPM induced chirping, but at higher input powers pulse broadens and eye opening decreases than 500 ps/nm. In both 4.9(c) and 4.9(d) negative residual dispersion were considered. It is found from a comparison of diagrams 4.9(a) and 4.9(b), eye opening is less with negative residual dispersion. Here at −1000 ps/nm residual dispersion it is shown that eye opening decreases so much that acceptable performance from the system may not be obtained. From a comparison of figure 4.9 with figure 4.3 it is found that eye opening is still better in 500 ps residual dispersion than in zero residual dispersion. So, 500 ps/nm residual dispersion may be the better choice for a single channel system than complete compensation.

From the discussion of section 2.4, we know that, GVD induces a negative frequency chirp (instantaneous frequency decreases from the leading to the trailing edge) on the pulse within SMF. But SPM induces a positive frequency chirp (instantaneous frequency increases from the leading to the trailing edge) on the pulse as discussed in section 2.6. Therefore, mutual interplay reduces the negative frequency chirp of the pulse. So, the propagated pulse within SMF is actually less broadened than there were no SPM. So, DCF length used for zero residual dispersion actually over-compensates the incoming pulse from SMF. This is evident from this discussion that, to obtain less distorted pulse, SMF dispersion should be designed to be under-compensated by the DCF. So, positive residual dispersion should give better eye opening than zero residual dispersion. But, if positive residual dispersion is so much to under-compensate the dispersion, then eye opening may be worse. So, there must be some optimum residual dispersion at which optimum performance would be obtained. As in figure 4.9, 500 ps/nm turns out to be optimum residual dispersion among the considered residual dispersions.

On the other hand, if DCF length is set for negative residual dispersion, pulse dispersion will be more over-compensated than zero residual dispersion. As the negative residual dispersion increases, the amount of over-compensation increases and the pulse shape distorts and the pulse broadens outside its dedicated bit period. As a result, eye opening for negative residual dispersion greatly decreases even for −1000 ps/nm residual dispersion.
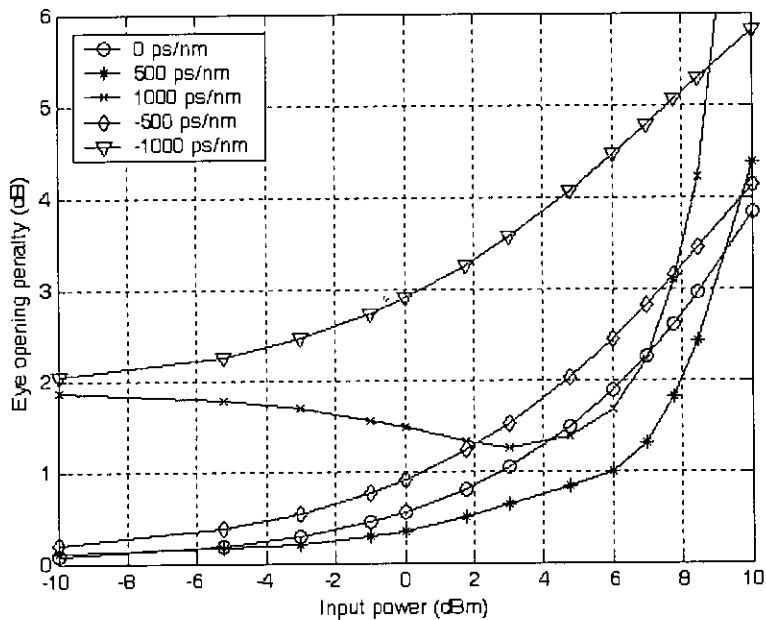

Fig.4.10: Eye opening penalty versus input power with different residual dispersion at 1000 km of a post-compensated transmission fiber
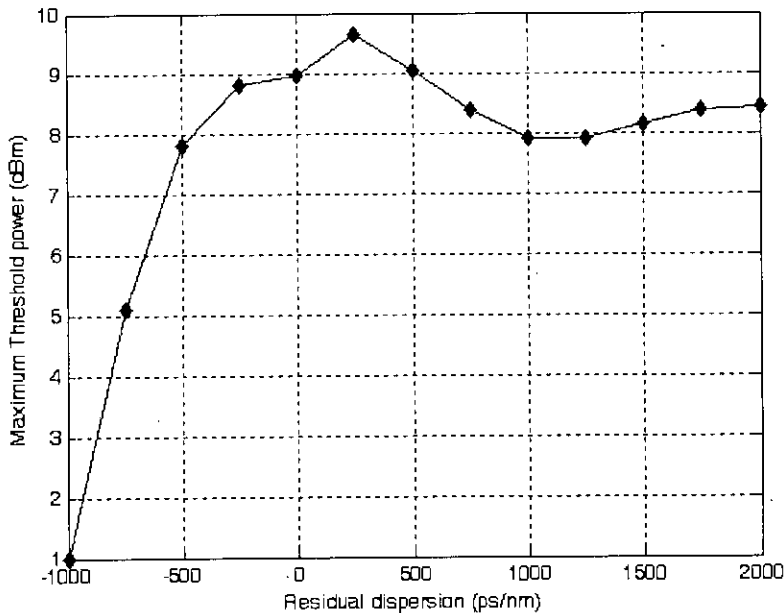
Fig 4.11: Maximum threshold power at 3 dB eye opening at 1000 km transmission fiber versus residual dispersion for a post-compensation configuration

Eye opening penalty at zero, positive and negative residual dispersion is plotted in figure 4.10 to get an idea of the performance of different residual dispersions. Input power levels were varied from −10 dBm to 7 dBm. Penalty is calculated from eye diagram using the formula $20 \log_{10}(a/b)$, where a is the maximum eye opening at the input of the transmission fiber and b is the maximum eye opening at the output of the transmission fiber. It is shown that zero residual dispersion is not the best choice for minimum eye penalty rather 500 ps/nm residual dispersion gives lower eye opening penalty. Eye opening penalty is much larger for negative residual dispersion than for positive residual dispersion especially for higher input power. From figure 4.10, it is evident that both 500 ps/nm and 1000 ps/nm residual dispersion can give better performance at higher input power levels than −500 ps/nm and −1000 ps/nm residual dispersion. Though −500 ps/nm residual dispersion can be used in the system, -1000 ps/nm residual dispersion degrades eye opening so much that it is not applicable to the transmission system.

In figure 4.11 maximum threshold power levels beyond which eye opening penalty increases beyond 3 dB are plotted versus residual dispersion. This figure gives us an

idea of maximum limit of power that can be launched into the transmission fiber and still keeping the eye opening penalty below 3 dB. It is found from the simulation results, 250 ps/nm residual dispersion allows highest input power (9.65 dBm) to be launched into a post-compensation configuration. This maximum threshold decreases very sharply with increasing negative residual dispersion. But with positive residual dispersion maximum threshold power levels remain above 8 dBm input power even at 2000 ps/nm. Nevertheless, at 1500 ps/nm and above residual dispersion, transmission system should not be designed as at these residual dispersions minimum threshold power levels increase as well. So, acceptable input power window decreases at higher positive residual dispersion.
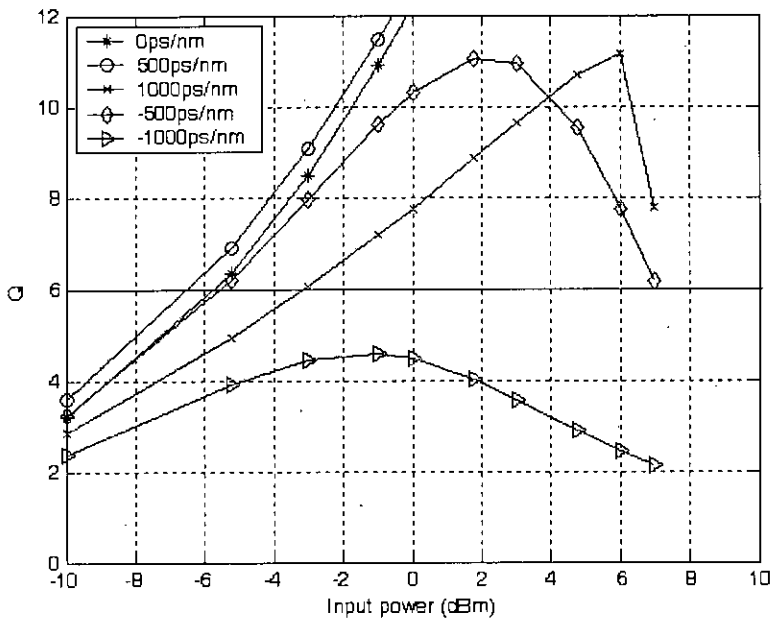
Fig.4.12: Q parameter versus input power at different residual dispersion in a 1000km post-compensated transmission fiber
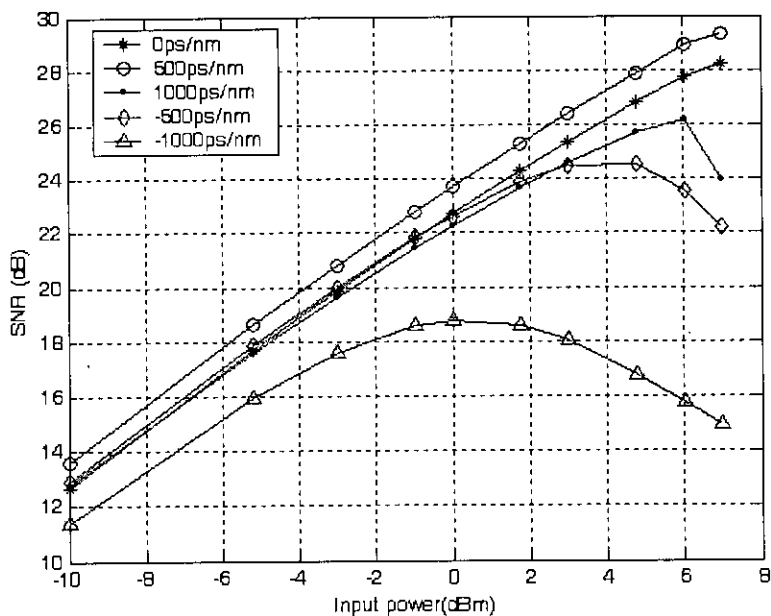
**Fig.4.13**: Signal-to-noise ratio versus input power at different residual dispersions in a 1000 km post-compensated transmission fiber

SNR and Q parameter have been plotted against input power for a 1000 km transmission link at different residual dispersions in figures 4.12 and 4.13 respectively. From the curves in both of the figures we can evaluate effect of residual dispersion on the transmission performance. It is shown from both of the figures that 500 ps/nm gives better transmission performance than any other residual dispersions. Better performance with positive residual dispersions is evident from figures 4.12 and 4.13 as both of the figures show that 500 ps/nm and 1000 ps/nm gives higher SNR and Q parameter value than that of –500 ps/nm and –1000 ps/nm residual dispersions. It is shown that, -1000 ps/nm residual dispersion results very poor SNR and Q parameter value that in a practical system this level of residual dispersion is not applicable.
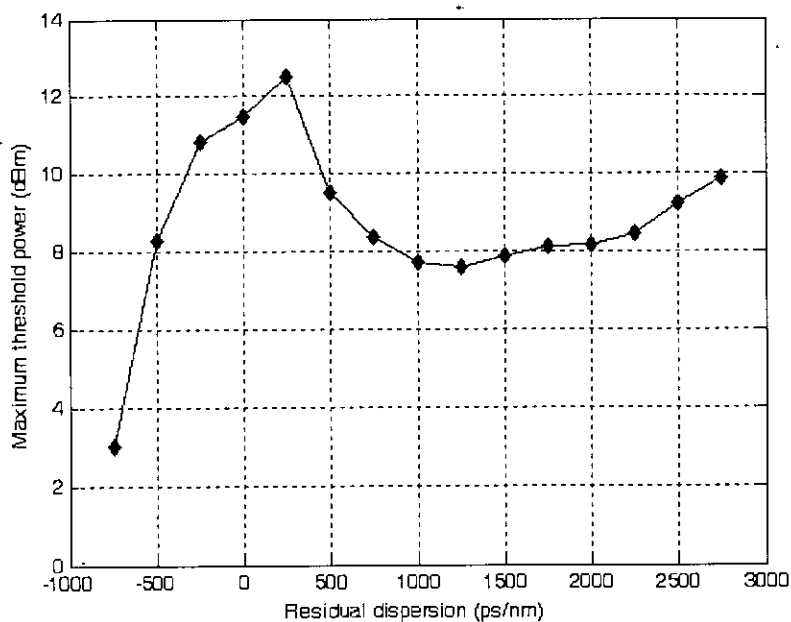
Fig. 4.14: Maximum threshold power levels at 10^{-9} BER versus residual dispersion at 1000 km of a post-compensated transmission fiber

In figure 4.14 the input power levels that can be applied to the system for a high bit rate data transmission is investigated for different residual dispersions at the end of a 1000 km post-compensated transmission fiber. It is shown in the figure that at negative residual dispersion maximum threshold that can be applied to the system decrease very sharply. Maximum threshold decreases so much at higher negative residual dispersion that, beyond -750 ps/nm residual dispersion can't give any power level for which the system performance is acceptable. On the other hand, it is shown that maximum threshold power levels are within acceptable range even for high positive residual dispersion. In our model, 250 ps/nm allows highest input power. The curve shows decrease of threshold power beyond 500 ps/nm residual dispersion. Then the threshold power again increases beyond 1500 ps/nm residual dispersion. It should be noted that, though after 1500 ps/nm residual dispersion the maximum threshold power levels increase, minimum threshold power levels also increase, to be noted, very close to the maximum threshold. So, the applicable input power window gets narrower at higher positive residual dispersion. Though maximum threshold at 2500 ps/nm residual dispersion is 9.22 dBm, minimum threshold is also very high, i.e., 6.2 dBm. So, we propose not to use the residual dispersion widow beyond 1500 ps/nm.

4.4 Use of Post-Compensation Configuration in WDM System

In an 8-channel WDM system with 0.8 nm channel spacing, total residual dispersion within the channels is approximately 550 ps/nm. So, we can select −250 ps/nm to 300 ps/nm residual dispersion region in a post compensation configuration as figure 4.14 shows that this residual dispersion window allows maximum threshold of greater than approximately 11 dBm. For a 16-channel WDM system with 0.8 nm channel spacing, total residual dispersion among the channels is 1100 ps/nm. We can choose −500 ps/nm to 600 ps/nm residual dispersion window, where maximum threshold power is approximately above 8.5 dBm. In a 32-channel WDM system, we need a total of 2200 ps/nm residual dispersion. We can choose from −500 ps/nm to 1700 ps/nm residual dispersion window where maximum threshold power is approximately above 8 dBm.

4.5 Effect of Pulse Shape on Transmission Performance

Both GVD of fiber and SPM effects due to nonlinear dependence of fiber refractive index on pulse intensity depend on pulse shape. So, in addition to the dispersion compensating technique and magnitude of residual dispersion, pulse shapes determine the transmission performance as well. A Gaussian pulse shows low level of pulse broadening due to GVD and low level of spectrum broadening due to SPM, whereas super-Gaussian pulse with very sharp leading and trailing edges shows much higher GVD-induced pulse broadening and SPM-induced spectrum broadening. As a result, propagating pulse distortion is different in different input pulse shapes.

In section 2.4.3, it is discussed that dispersion-induced broadening is sensitive to steepness of pulse edges. In general, a pulse with steeper leading and trailing edges broadens more rapidly with propagation simply because such a pulse has a wider spectrum to start with. Besides, SPM-induced frequency chirp is considerably larger for pulses with steeper leading and trailing edges. So, interplay between GVD and SPM varies according to the pulse shape and actually the SPM effects are more serious for pulses with steeper leading and trailing edges.

In figure 4.15, eye diagrams are drawn for various input pulse shapes. We simulated using a super-Gaussian pulse as given in equation (2.13), as $U(0,T) = \exp[-\frac{1}{2}(\frac{T}{T_0})^{2m}]$ where steepness of the pulse is controlled by the value of m. When $m = 1$, the pulse is simply a Gaussian pulse. Eye diagrams are drawn for different values of m to show the effects of pulse steepness on the pulse propagation. It is shown from the figure that, when $m = 1$, the pulse shape is restored at the end of the transmission fiber even at the high level of input power. But as value of m is increased, the pulse's leading and trailing edges become steep and as a result, both GVD and SPM effects are higher. So, pulse shapes are not restored at the end of the transmission fiber. For higher levels of input powers, the eye opening degrades much due to the higher SPM effects at that power levels.
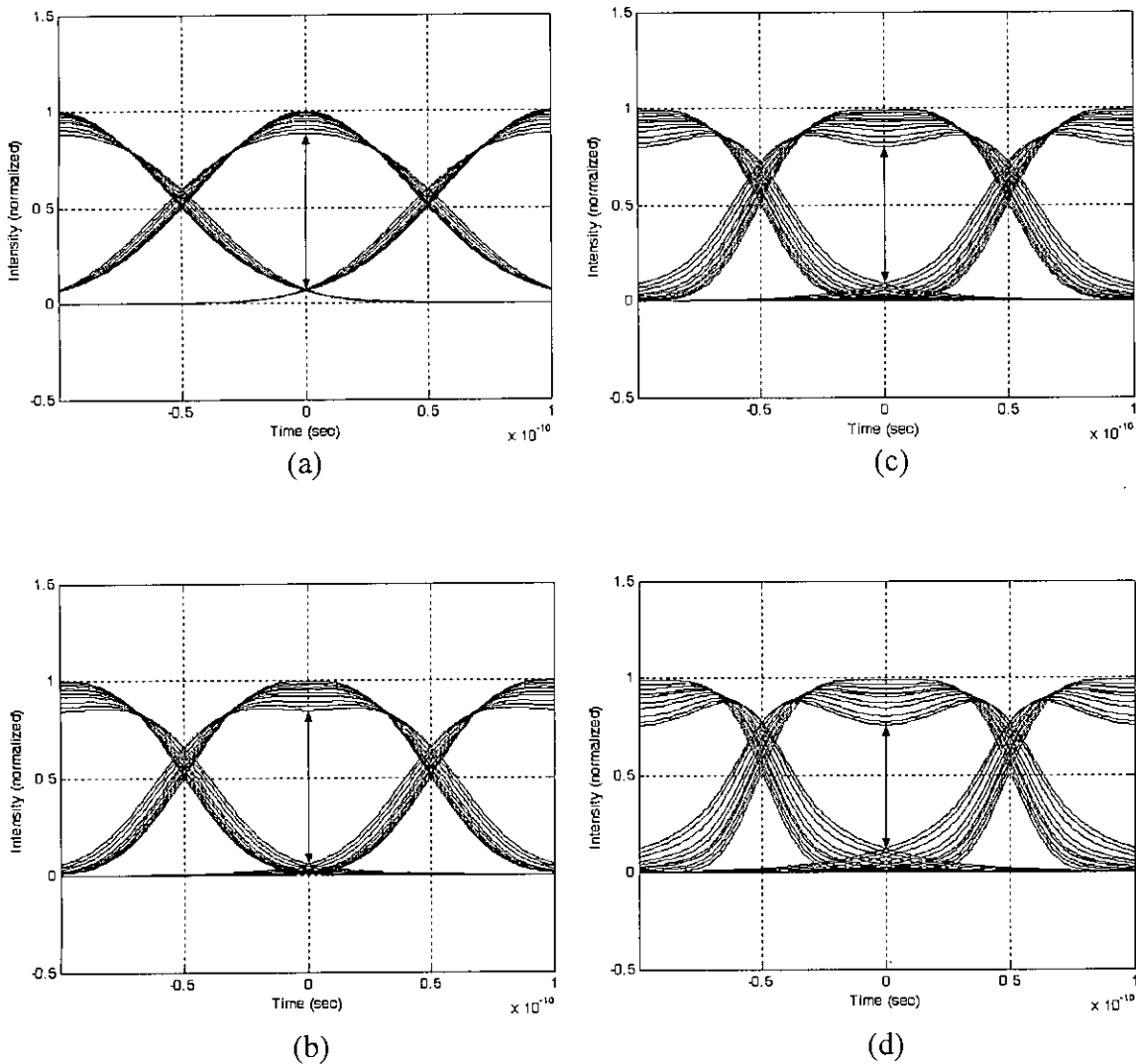
Fig. 4.15: Eye diagrams at post-compensated 1000 km transmission fiber at different input power. Input pulse is a super-Gaussian pulse with m - (a) 1 (b) 1.4 (c) 1.8 (d) 2.2. Input power varied from −10 dBm to 7 dBm.

The eye opening penalty at 1000 km transmission fiber with variable steepness of pulse edges are drawn in figure 4.16. It is shown that, eye opening penalty increases with the input power at a higher rate with pulses of steeper leading and trailing edges. This phenomenon is better illustrated in figure 4.17 where eye-opening penalty is drawn with relation to steepness of the pulse at different levels of input power. It is shown that at each input power levels, eye-opening penalty increases with the increase of m. Moreover, eye-opening penalty is higher at higher input power for same value of m. It is interesting to note from the figure that, eye opening penalty curves at each input power level show a declination initially with the increase of m. This happens because for a Gaussian pulse intensity of the neighboring pulses does

not become zero at the bit center of the investigating pulse, rather neighboring pulse has significant intensity at the pulse center. But with the increase of steepness of the pulse, this inter-symbol interference decreases and as a result, eye-opening penalty shows declination initially with the increase of pulse steepness.
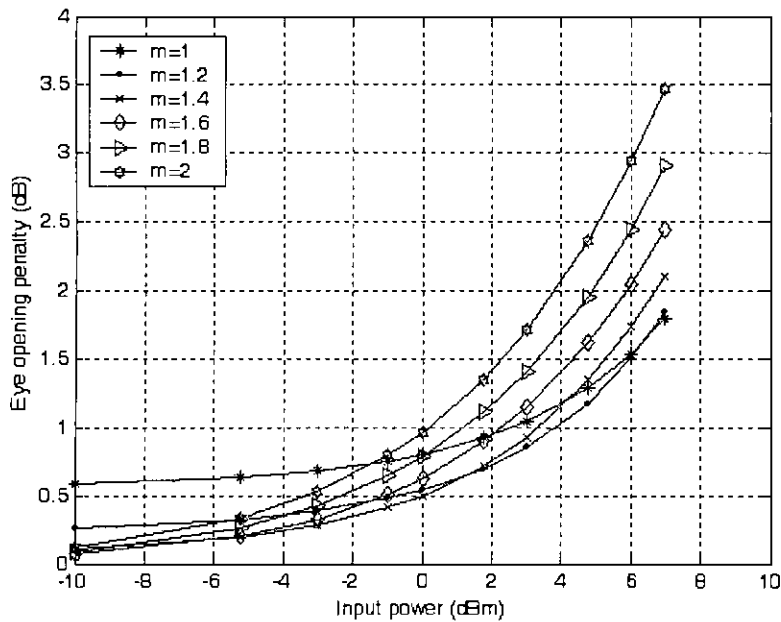
Fig. 4.16: Eye opening penalty versus m of a super-Gaussian pulse at 1000 km of a post-compensated transmission link
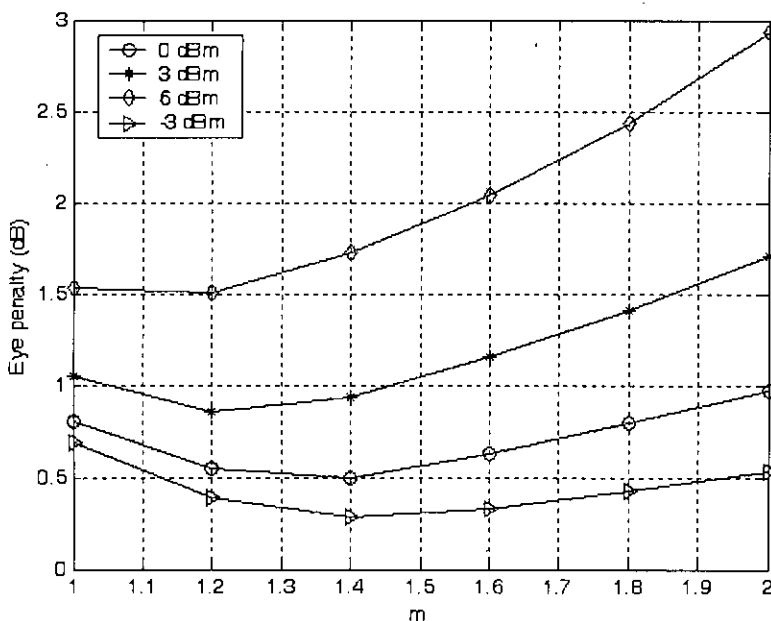
Fig. 4.17: Eye penalty versus steepness of input pulse shape (m) at different input power levels at a post-compensated 1000 km transmission link
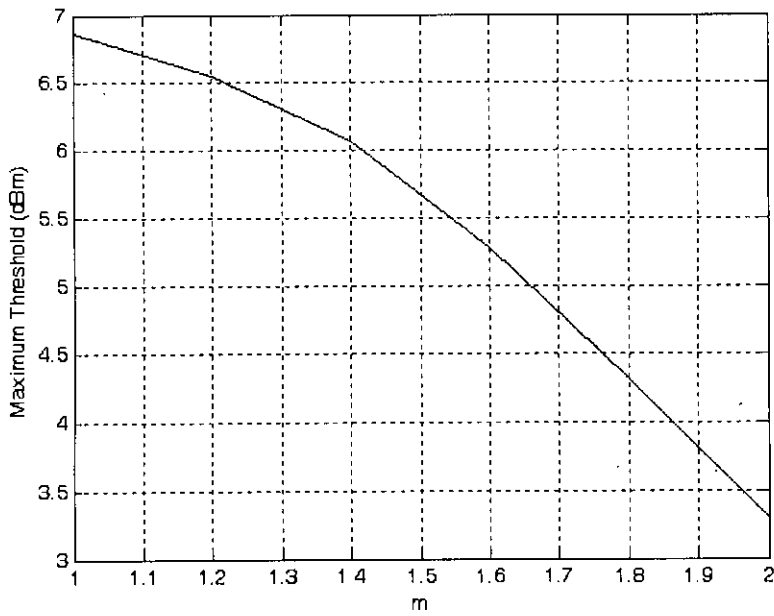
Fig. 4.18: Maximum threshold power at 3 dB eye opening penalty versus steepness of the input pulse shape (m) at 2000 km of a post-compensated transmission link
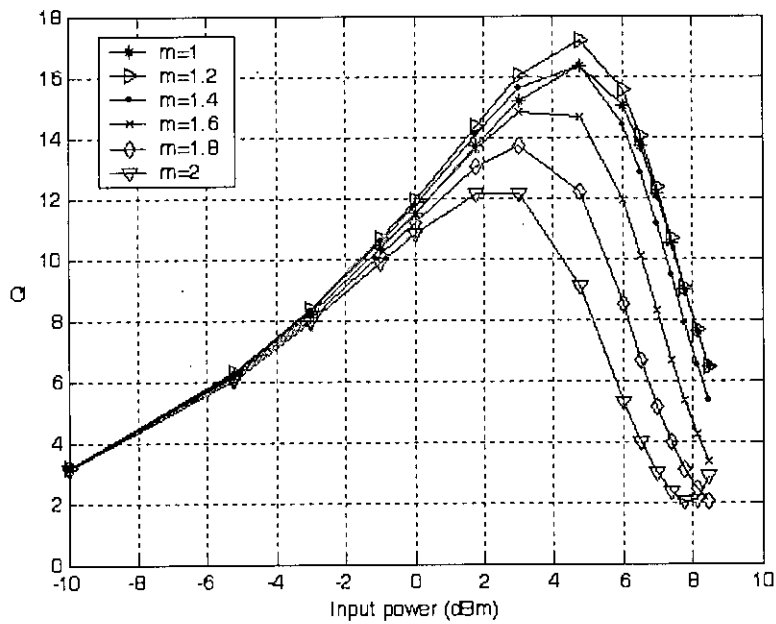
Fig. 4.19: Q parameter versus input power for different input pulse shape (m) at 2000 km of a post-compensated transmission link
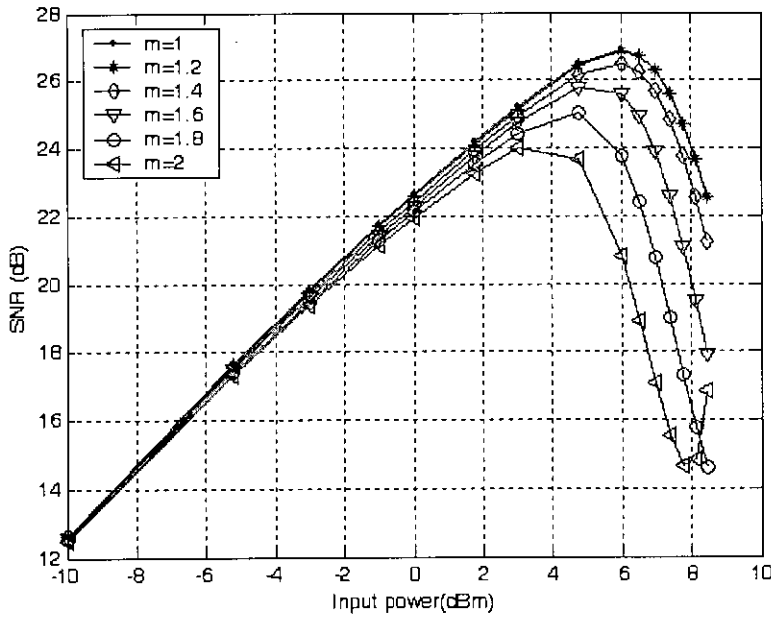
Fig. 4.20: Signal-to-noise ratio versus input power for different pulse shape (m) at 2000 km of a post-compensated transmission link

Maximum power levels beyond which eye opening penalty is greater than 3 dB for different pulse shapes at 2000 km of transmission fiber is given in figure 4.18. It is shown that maximum threshold power reduces much for steeper leading and trailing edges. For $m = 1$, maximum power that can be applied still obtaining 3 dB eye opening penalty is 6.87 dBm, whereas this value becomes only 3.3 dBm for a super-Gaussian pulse with $m = 2$. The transmission performance for different input pulse shapes have been evaluated and the results are plotted in figure 4.19 and 4.20. In figure 4.19, Q parameter is plotted against m and in figure 4.20 SNR is plotted against m. Both of the figures represent the philosophy described so far. That is - for an input pulse with steeper leading and trailing edges pulse stretching in SMF and pulse recompression in DCF are disturbed more and as a result, Q parameter and SNR both decrease at a fixed power for higher value of m.

4.6 Summary

In this chapter, we have discussed the effects of SPM in optical fiber transmission system with dispersion compensated by a DCF connected at the end of the transmission link. We have shown the effects of zero, positive and negative residual dispersions on the transmission performance. We put our emphasis especially on the self-phase modulation-limited maximum threshold power that can be applied to the system and still achieving required performance (i.e., 10^{-9} BER). The most remarkable observation that can be made from the above analysis that in post-compensation scheme, residual dispersion exhibits higher maximum threshold than zero dispersion. Our observation turns out to be same what was asserted in [29]. Moreover, we emphasize that our analysis permits to verify some other results present in the literature, for example that the region corresponding to positive residual dispersion assures, in general, better performances than the negative ones for a post-compensation configuration. This is due to the pulse compression effect induced by SPM during its propagation within SMF.

Moreover, we have discussed the feasibility of application of post-compensation configuration in a WDM system. It is found that, for an 8-channel WDM system, the region can be selected to contain both negative and positive residual dispersion. But for 16-channel and 32-channel WDM system we will have to extend the residual dispersion window toward the positive residual dispersion region.

Chapter 5

Performance Analysis of Pre-Compensation Configuration

5.1 Introduction

In this chapter, we investigate the transmission performance of a pre-compensated transmission link. We simulated the pulse propagation in an in-line optical amplifier dispersion compensated system in presence of both second-order GVD and SPM effects using split-step Fourier transform method. From the obtained output pulse we determine eye diagram at different lengths and at different residual dispersions. Then we determine the maximum threshold power levels at different lengths and at different residual dispersions of transmission fiber. Thus we find out best suitable residual dispersion region in a pre-compensation configuration for a WDM system.

5.2 Pre-Compensation Configuration

In pre-compensation configuration, DCF is followed by standard single-mode fiber. Residual dispersion can be varied in the same way as in the post-compensation configuration. Since SPM effect is different on the propagating pulse in a fiber with positive dispersion parameter than in a fiber with negative dispersion parameter, interplay between GVD and SPM changes much in PRCC than POCC.
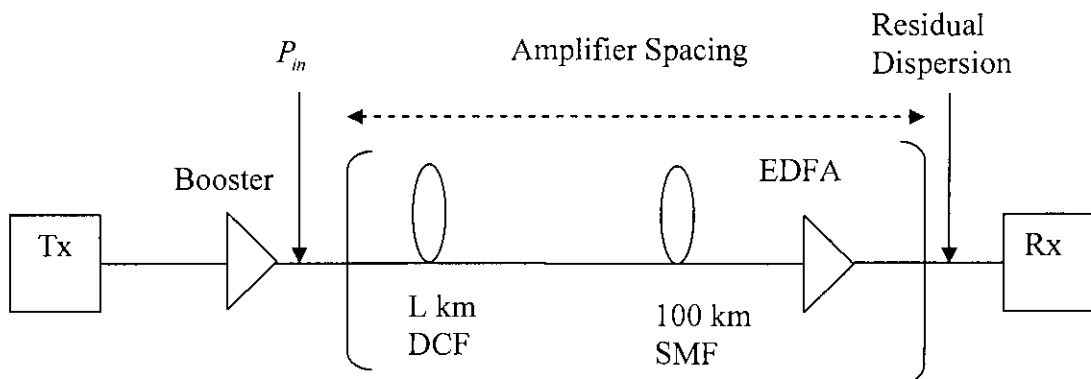

Fig. 5.1: Schematic diagram of pre-compensation Configuration

In our model of pre-compensation configuration, L km of dispersion compensating fiber (DCF) precedes 100 km of standard single-mode fiber (SMF) and the fiber losses are compensated periodically for such DCF-SMF links as shown in figure 5.1. A single channel, modulated with a 10-Gb/s nonreturn-to-zero (NRZ) bit sequence, generated through a chirp free transmitter, is launched into DCF and gets chirped and broadened due to interaction between GVD and SPM. This chirped and broadened pulse is recompressed during its propagation through the SMF. As in post-compensation, 17 km of DCF results zero residual dispersion for 100 km of SMF. DCF length of higher than 17 km and lower than 17 km result negative and positive residual dispersion respectively.

5.3 Simulation Results

Pulse propagation in the above-described pre-compensation configuration was simulated using split-step Fourier transform technique. We present here some of the simulation results to show self-phase modulation effect on transmission performance of a pre-compensated fiber link.

5.3.1 Complete Compensation

Transmission fiber imposes a dispersion-induced chirp on the pulse during its propagation. If the initial chirp is in the opposite direction of that imposed by GVD, the two tend to cancel each other, resulting in an output pulse narrower than the input pulse. The exact chirp cancellation occurs only at a specific distance. In the time domain, the compression process can be visualized as follows. Different frequency components of the pulse travel at different speeds in the presence of GVD. If the leading edge of the pulse is delayed by just the right amount to arrive nearly with the trailing edge, the output pulse is compressed. Positively chirped pulses (frequency increasing toward the trailing side) require anomalous or negative GVD (β_2) in order to slow down the red-shifted leading edge. By contrast, negatively chirped pulses require normal or positive GVD (β_2) to slow down the blue-shifted leading edge.

(a)　　　　　　　　　　　(b)
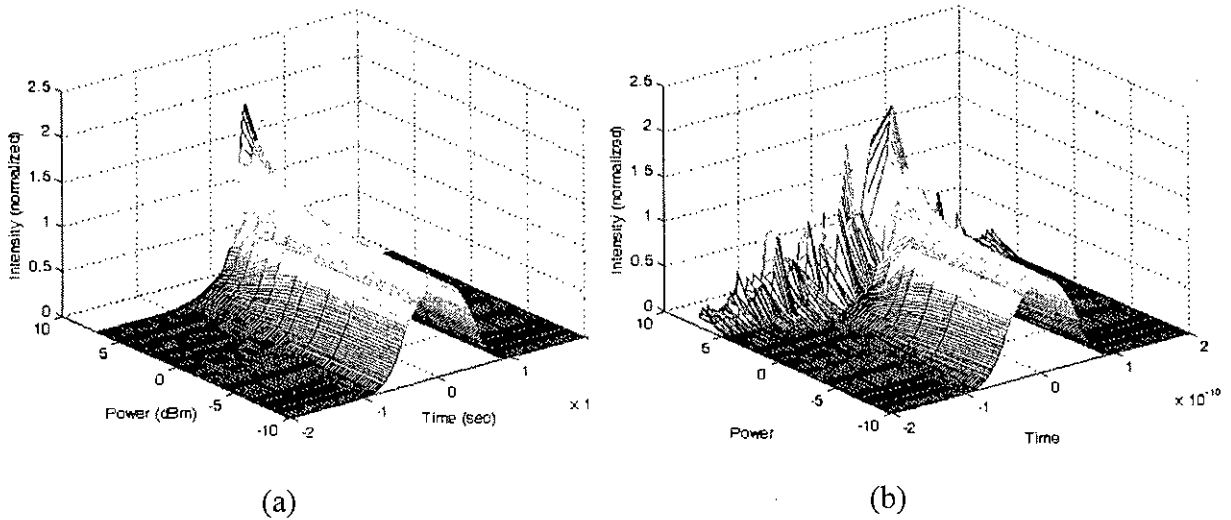
Fig.5.2: Pulse shapes versus input power at fiber length (a) 1000 km (b) 2000 km in pre-compensation configuration with zero residual dispersion. Input power is varied from −10 dBm to 7 dBm

(a)　　　　　　　　　　　(b)
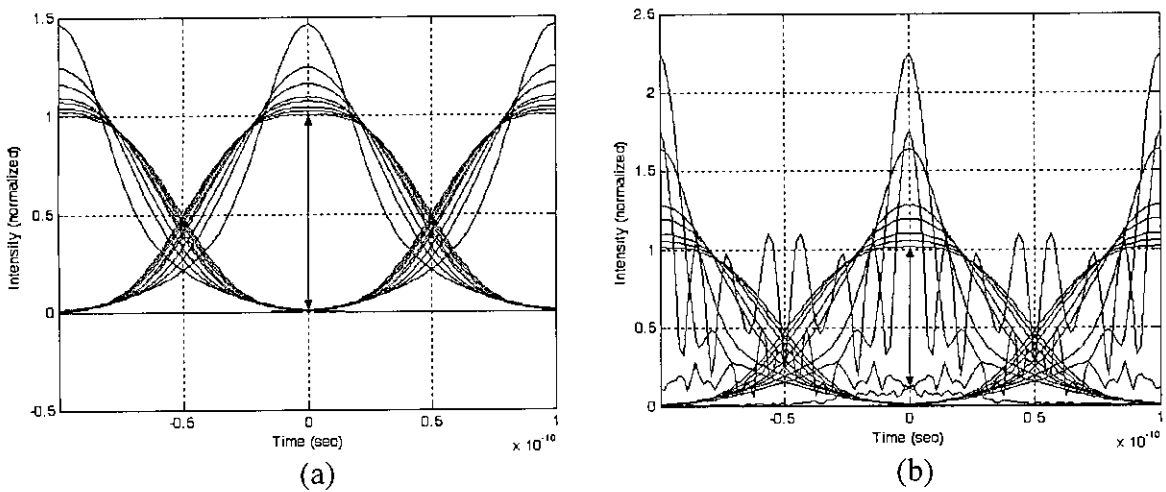
Fig.5.3: Eye diagrams at zero residual dispersion for different input powers at fiber length (a) 1000 km (b) 2000 km in pre-compensation configuration

In DCF the transmitted pulse is positively chirped (frequency increases from the leading toward the trailing edge). The leading edge frequency is down shifted and the trailing edge frequency is up shifted. SPM produces new frequency components within the transmitted pulse and imposes chirping on the pulse also in the positive direction. It is to be noted that since SPM depends on intensity of the pulse, its effects

are imposed on the pulse up to some km of fiber. Due to loss, pulse intensity decreases and SPM effects get less and less serious down the fiber link. In our model, the pulse intensity is attenuated almost 30 dB. So, down the fiber, intensity dependent non-linear effect is not serious.

The extra-chirped pulse due to SPM enters SMF. The chirping induced in SMF is opposite to that induced in DCF. For zero residual dispersion chirping induced by DCF is cancelled by chirping induced by SMF. But as the pulse contains extra chirping and frequency components, it gets compressed. Since nonlinearity in the induced frequency chirping is increased at higher input power due to SPM and this effect accumulates over fiber length, pulse distortion increases both at higher input power and at longer fiber link.

Propagated pulses at the end of 1000 km – 2000 km transmission link are given in figure 5.2. Peak powers of input pulses were varied from –10 dBm to 7 dBm. The curves show that, pulses gradually compress with the increase of input power. But at some level of input power, compression is maximum and pulses can no longer be compressed. Since the degree of SPM effect is pulse peak intensity dependent, it is shown that, for a fixed length input pulse shapes are almost restored at the output for lower input power levels (i.e., -10 dBm to 0 dBm). In these power levels, pulse broadening in DCF is successfully compressed within SMF. But as we increased power for input pulses, compression is maximum at some input power level and the pulse gets distorted and the pulse intensity oscillates.

Dispersion is completely compensated in each span. So no dispersion-accumulation happens. But as SPM produces chirping always in the positive direction, it is not compensated rather its effects accumulate from one span to another. So, we find that, for a fixed input power, output pulses at lengths 1000 km and 2000 km show higher degree of distortion at higher length.

Eye diagrams at (a) 1000 km and (b) 2000 km are drawn in figure 5.3. Maximum input power that used in our simulation is 4.77 dBm (3 mW). It is shown that pulses are compressed up to this power level at both 1000 km and 2000 km. But at 2000 km transmission fiber pulse compression is so high that at 4.77 dBm input power pulse

shape is no longer restored rather its magnitude fluctuate seriously. Further increase of input power, distorts the pulse shape so much that the compensation technique is no longer suitable to be used at a power level beyond this value.
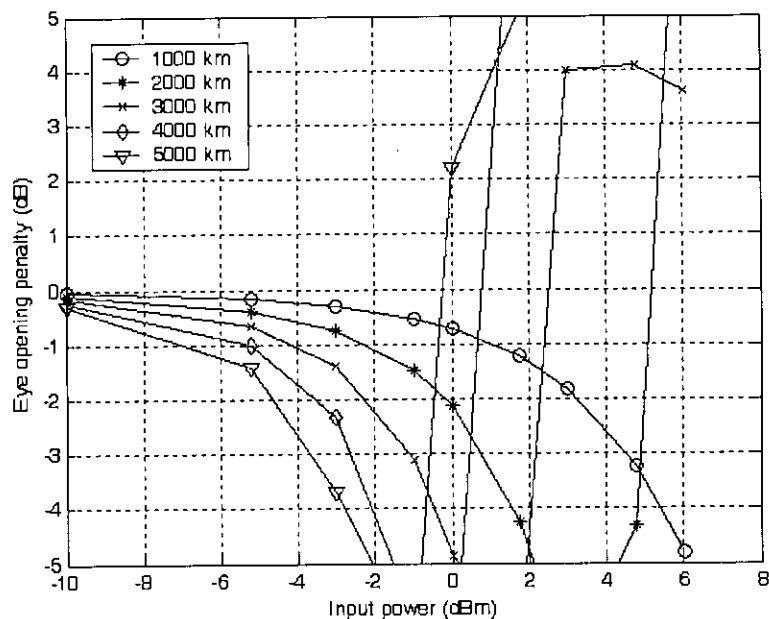
Fig. 5.4: Eye opening penalty versus input power at different fiber lengths for a pre-compensation configuration with zero residual dispersion

Eye opening penalty versus input power for a pre-compensated transmission fiber is plotted in figure 5.4 at 1000 km – 5000 km. All curves show decrease of eye opening penalty as input pulses are compressed for lower levels of input power and then a sharp increase of eye opening penalty due to pulse distortion. This is because of higher degree of SPM effect at higher input power. As SPM effects are not compensated by any opposing effect, it accumulates over the length. This accumulation effect is evident from the curves as we see that pulse compression is higher for a fixed input power for longer transmission length and pulse distortion also happens earlier at longer transmission fiber.
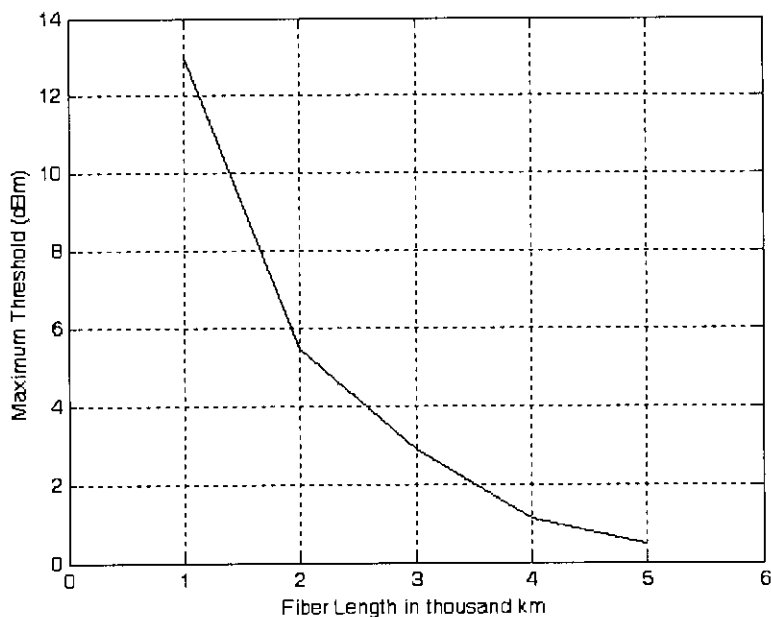
Fig. 5.5: Maximum threshold power versus transmission fiber length for pre-compensation configuration with zero residual dispersion
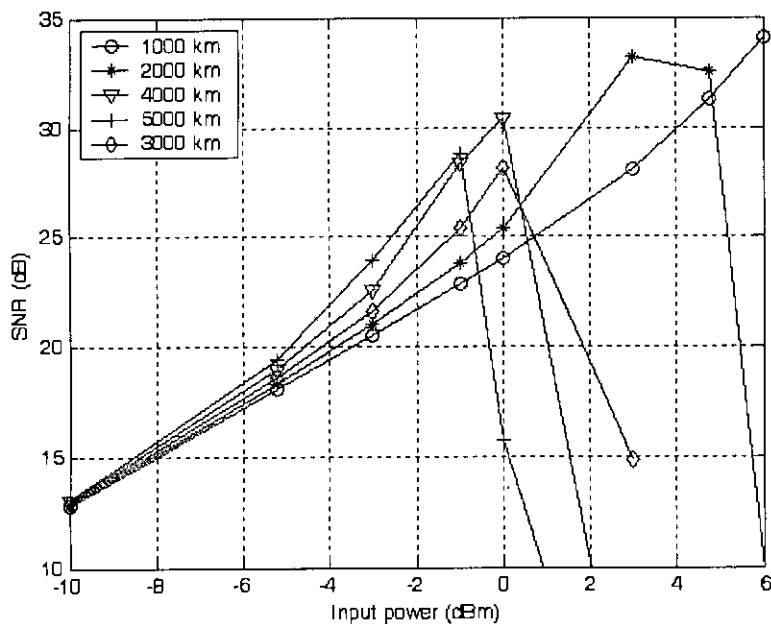
Fig. 5.6: Signal-to-noise ratio versus input power at different length of transmission fiber for pre-compensation configuration with zero residual dispersion

In figure 5.5, we plot 3 dB eye opening penalty points versus fiber length. It is shown that, maximum threshold power decreases very sharply with the increase of length. At

1000 km we can apply up to 13 dBm input power and still achieve 3 dB eye opening penalty. But at 2000 km, we can apply only 5.5 dBm and still achieve 3 dB eye opening penalty. The maximum threshold power that can be applied decreases further at 3000 km and upward.

SNR versus input power relation for a pre-compensation configuration is plotted in figure 5.6 where GVD is completely compensated. Receiver noise and preamplifier ASE noise are considered with the distorted pulse due to propagation in presence of both GVD and SPM in the calculation of SNR. At lower levels of input power, SNR is mainly determined by ASE noise of preamplifier. SPM effects are stronger at high input power and then it dominates the determination of SNR. The rate of increase of SNR at lower power levels is shown to be higher than that of in post-compensation configuration as shown in figure 4.7. This is because of the pulse compression in a pre-compensated transmission link with zero residual dispersion.

5.3.2 Partial Compensation

We have investigated transmission performance of a pre-compensation configuration with partial dispersion compensation. We varied the DCF length of each span to vary the accumulated residual dispersion at the end of the transmission fiber. It is found that magnitude and sign of residual dispersion have different effects on the transmission performance due to different interplay with SPM. Simulation results at various residual dispersions are presented here.

(a)

(c)

(b)

(d)
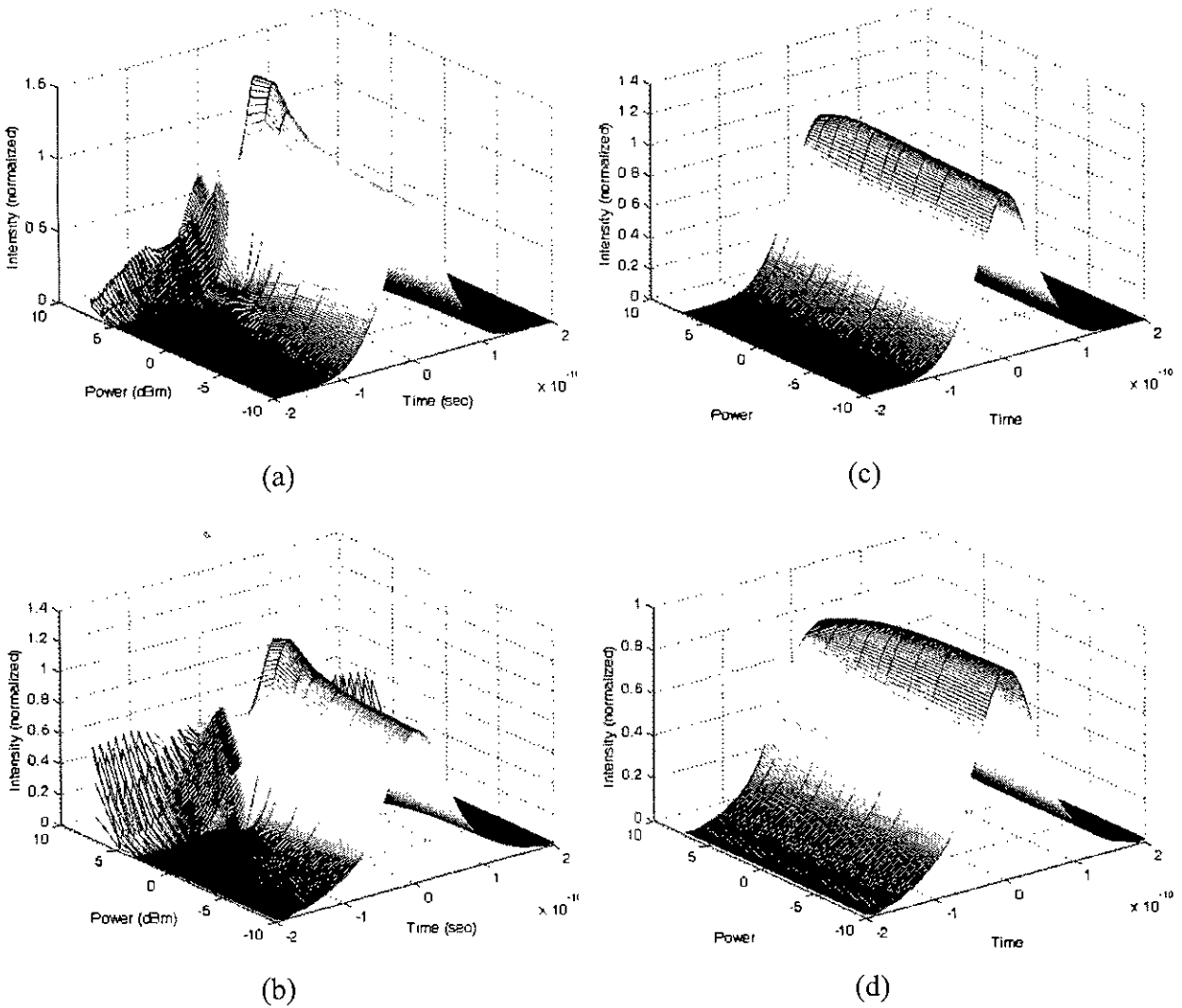
Fig. 5.7: Pulse shapes at 1000 km versus different input power at residual dispersion (a) 500ps/nm (b) 1000ps/nm (c) -500ps/nm (d) –1000ps/nm for pre-compensation configuration

(a)

(c)

(c)

(d)
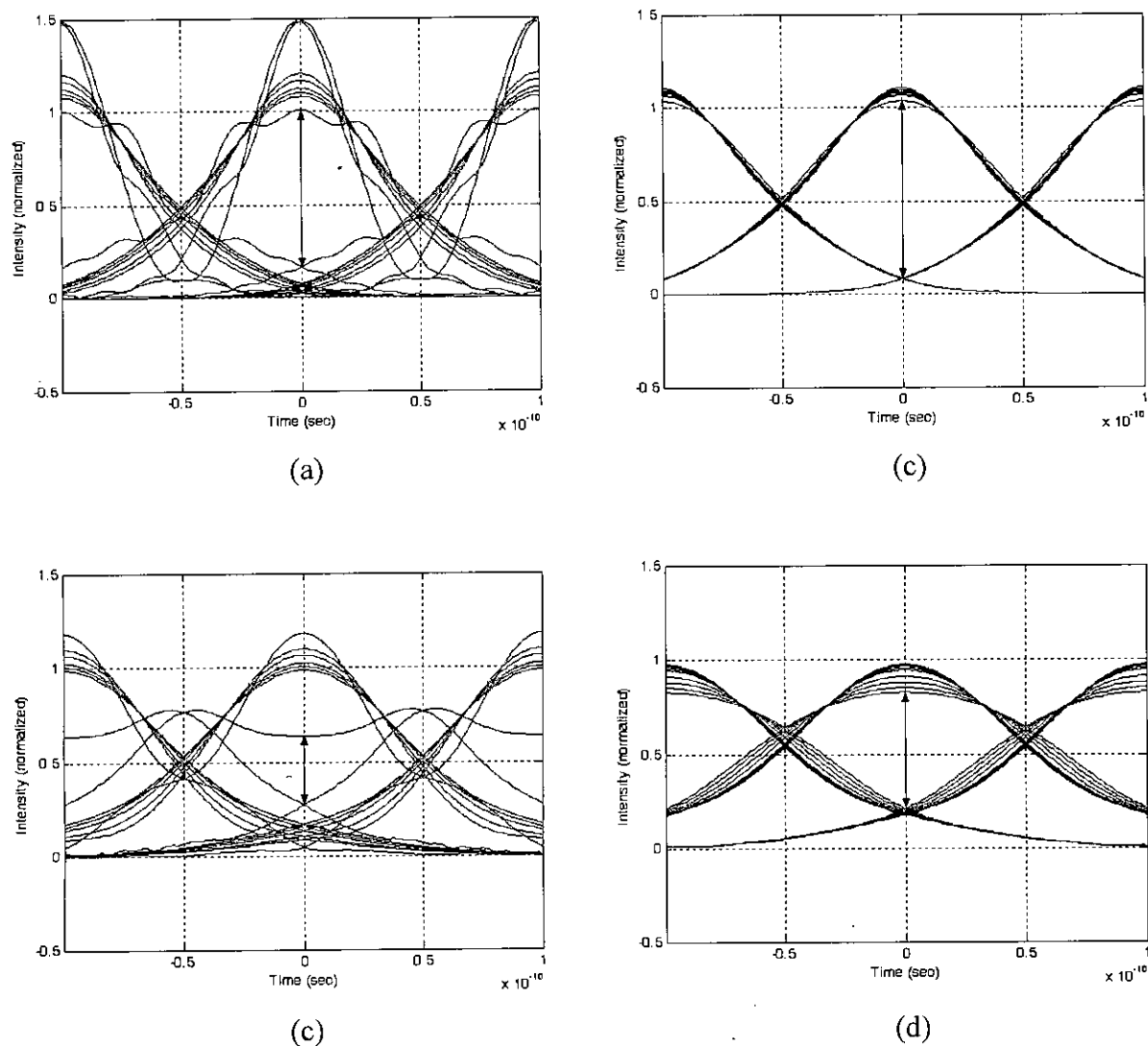
Fig. 5.8: Eye diagrams versus input power with different residual dispersion (a) 500 ps/nm (b) 1000 ps/nm (c) −500 ps/nm (d) −1000 ps/nm for pre-compensation configuration at 1000 km of transmission fiber

In figure 5.7 pulse shapes are drawn at 1000 km for various residual dispersion. Input power varied from −10 dBm to 7 dBm. Eye diagrams at various residual dispersions at 1000 km of transmission fiber for different input power levels are drawn in figure 5.8. We varied input power levels from −10 dBm to upward. In 5.8(a) 500 ps/nm residual dispersion was considered. Here, maximum input power that was applied to the system was 3.5 mW. It is seen from the diagram that pulse compresses and as a result eye opening increases up to 3 mW input power. At 3.5 mW pulse can no longer compress. So a distorted pulse is found. As a result, eye opening decreases at 3.5 mW

input power. If input power is further increased, eye opening will be closed enough to be applicable in any practical purpose. Eye diagram for 1000 ps/nm residual dispersion is drawn in 5.8(b). Here, pulse compresses up to 2 mW of input power. But at 2.5 mW input power pulse distorts and broadens that eye opening is reduced very much. So, it is evident that 1000 ps/nm residual dispersion is not a suitable value for a pre-compensation configuration. In 5.8(c) eye diagram is drawn for −500 ps/nm residual dispersion. Eye opening is very wide for this value of residual dispersion for the input power levels used in the diagram. Input power was varied up to 7 dBm. Lowest opening shown in the diagram is for 7 dBm of input power. In 5.8(d) eye diagram for −1000 ps/nm residual dispersion at 1000 km of transmission fiber is drawn. Up to 7 dBm input power is applied to see the SPM effect on the pulse transmission in a pre-compensation configuration at this value of residual dispersion. Eye opening degrades due to large value of residual dispersion. Eye opening decreases with the increase of input power. Minimum eye opening is for maximum input power.

Eye opening penalty curves are plotted versus input power at different residual dispersions in figure 5.9. It is shown that, at 0 ps/nm residual dispersion eye penalty decreases as the pulse compresses. The degree of compression increases with the increase of input power. This is because of positive chirping induced by SPM increases with the increase of input power. At 500 ps/nm residual dispersion pulse compresses more than at 0 ps/nm residual dispersion but breaks down at some threshold power (~5 dBm) and as a result, eye penalty increases sharply. At −500 ps/nm residual dispersion, though pulse is not compressed much but shows very small increase of eye penalty with the increase of input power. This happens because of cancellation of residual dispersion effect by the SPM induced chirping up to much higher levels of input power. Both at −1000 ps/nm and 1000 ps/nm residual dispersions, eye penalty curves show that, penalty increases substantially even at lower levels of input power.
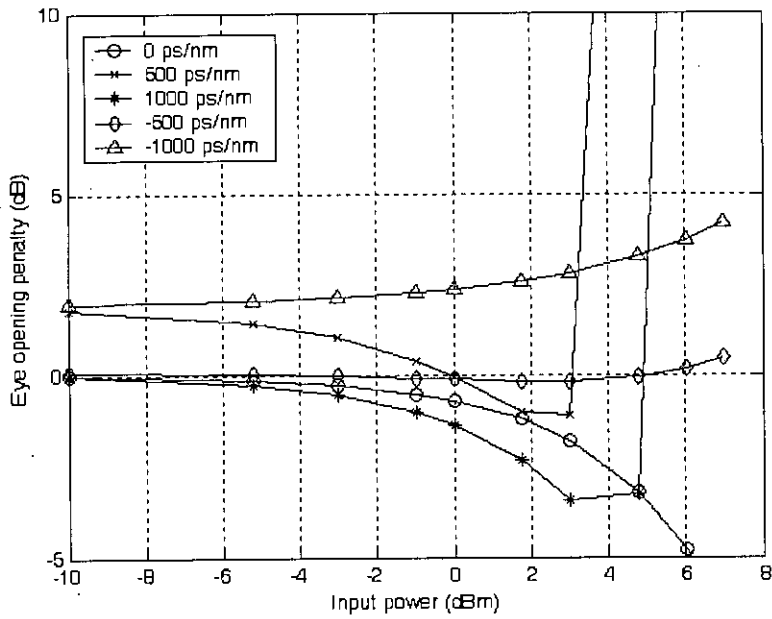
Fig. 5.9: Eye opening penalty versus input power at different residual dispersion for pre-compensation configuration at 1000 km transmission fiber
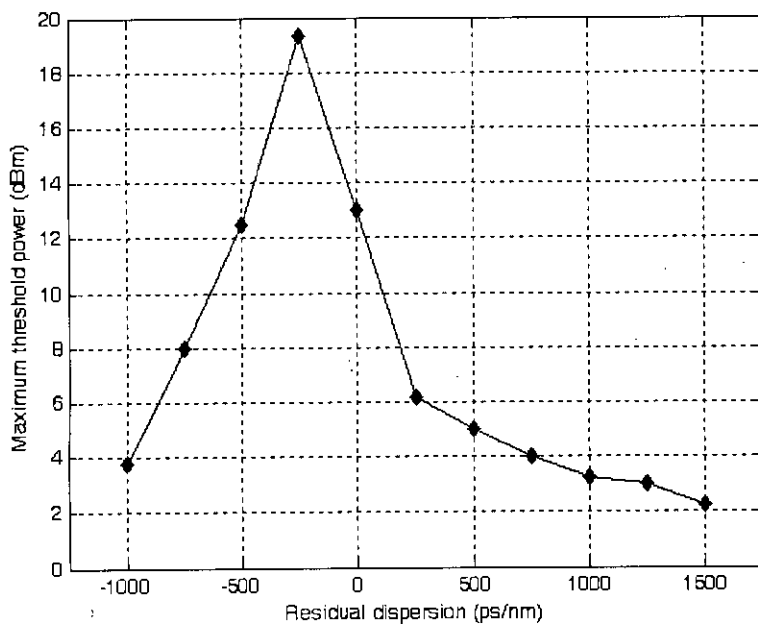

Fig. 5.10: Maximum threshold power at 3 dB eye opening penalty versus residual dispersion at 1000 km for pre-compensation configuration

(

In figure 5.10 maximum threshold power at 3 dB eye opening penalty is plotted versus residual dispersion at 1000 km of a pre-compensated transmission fiber. It is found that, zero residual dispersion is not the optimum residual dispersion for maximum threshold power rather –250 ps/nm residual dispersion allows higher input power to be applied to the pre-compensation system. So, for the fiber parameters selected in our analysis, -250 ps/nm residual dispersion is the best choice among the values analyzed. It is shown that, maximum threshold power decreases sharply at both positive and negative residual dispersion region. But at negative residual dispersion region, rate of decrease is higher and it is found that beyond –1000 ps/nm residual dispersion we can not get any residual dispersion region that provide 3 dB eye opening penalty. On the other hand, the region extends toward 1500 ps/nm and even higher residual dispersion. So, if we have to select narrow region of residual dispersion, it can be selected from negative residual dispersion region. But if wide residual dispersion region is to be selected, we have to move to positive residual dispersion region.

Signal-to-noise ratio versus input power curves are plotted in figure 5.11 at –1000 ps/nm to 1000 ps/nm residual dispersion at 1000 km transmission fiber. It is shown that stable relationship is obtained at –500 ps/nm among the residual dispersions considered in this figure. It is worth noticing that better result can be obtained at positive residual dispersion (i.e., 500 ps/nm) if the input power is kept substantially low (i.e., less than 1 dBm).

Maximum power that can be applied to the transmission link and still obtain a minimum of 10^{-9} BER is plotted against residual dispersion in figure 5.12. Maximum threshold power is shown to be highest at –250 ps/nm residual dispersion among the residual dispersion values considered in our analysis. But in pre-compensated link, the maximum threshold power decreases very sharply at both negative and positive residual dispersion region. At 1250 ps/nm negative residual dispersion and at higher negative residual dispersion the 10^{-9} BER can't be achieved. Similarly at 1500 ps/nm positive residual dispersion and higher positive residual dispersion 10^{-9} BER can't be achieved.
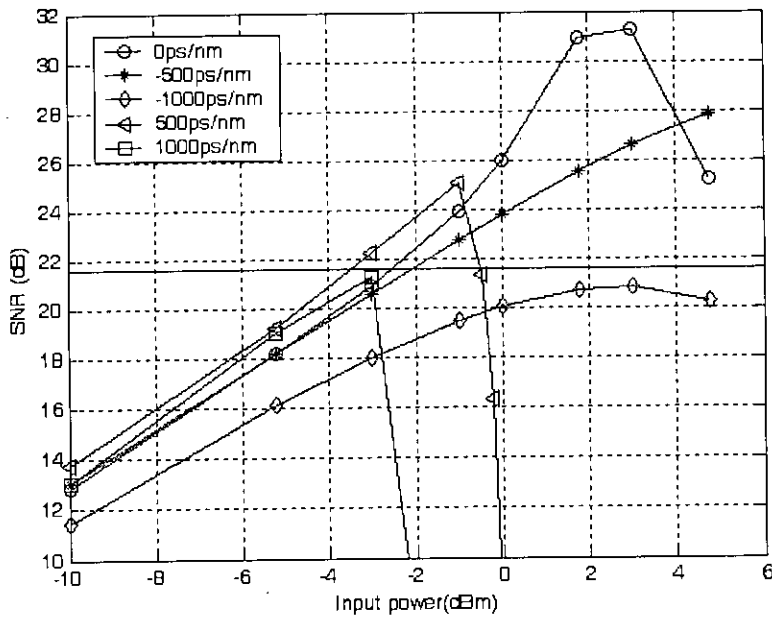
Fig. 5.11: Signal-to-noise ratio versus input power for a pre-compensated transmission fiber. Residual dispersion is varied from −1000ps/nm to 1000ps/nm.
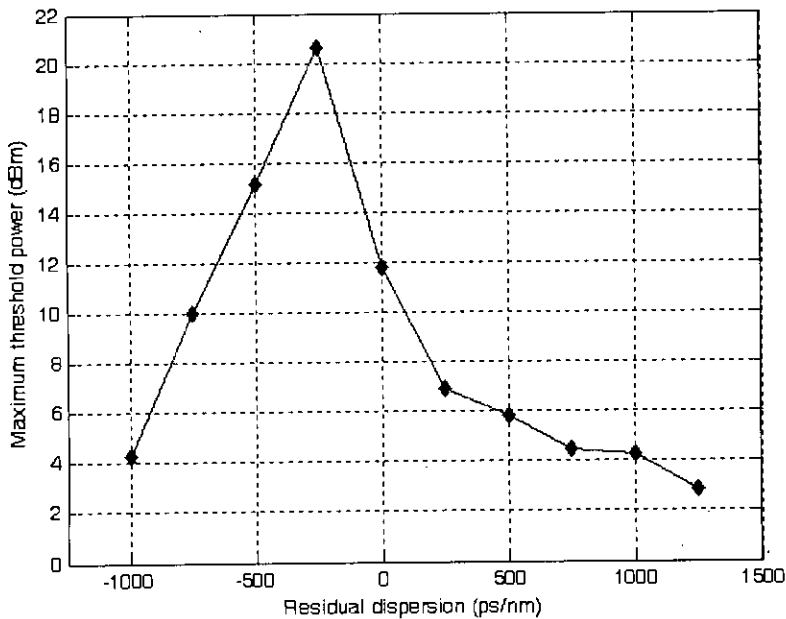

Fig. 5.12: Maximum threshold power at 10^{-9} BER at 1000 km pre-compensated transmission fiber versus residual dispersion

5.4 Use of Pre-Compensation Configuration in a WDM System

When a single channel is transmitted through the system, we can choose zero, -250 ps/nm or −500 ps/nm residual dispersion with −250 ps/nm residual dispersion resulting the best possible performance. If multiple channels are transmitted we will have to select the channel wavelengths in such a way so that for all channels input power levels can be as high as possible to maintain better SNR at high bit rate. For the fiber parameters chosen in our analysis, for an 8-channel WDM system with 0.8 nm channel spacing, total residual dispersion within the channels will be approximately 550 ps/nm at 1000 km transmission fiber. So, we can choose −550 ps/nm to 0 ps/nm residual dispersion region for this purpose. Maximum threshold power at this region is greater than 12 dBm. But for a 16-channel system, the channels will exhibit a total of 1100 residual dispersion at 1000 km transmission fiber. From figure 5.12 it is shown that, we will have to select residual dispersion region for such a WDM system where maximum input power can be as low as 8 dBm. We can select the region between −850 ps/nm and 250 ps/nm. For a 32-channel, we need 2200 ps/nm residual dispersion window to accommodate all the channels with 0.8 nm spacing at 1000 km transmission fiber. But it is difficult to select 2200 ps/nm residual dispersion region from figure 5.12 for pre-compensation configuration. We will have to move to positive residual dispersion region. But the selected window will have as low as less than 5 dBm maximum threshold power.

5.5 Summary

We have discussed the transmission performance of a pre-compensation configuration in this chapter. Power margins that can be applied to the system at different transmission length have been evaluated. It is found that power margin decreases sharply with length in a pre-compensation configuration. Though for 1000-km transmission link 13 dBm power can be launched, only 5.5 dBm power can be launched in 2000-km transmission link. Performance analysis with different magnitude of residual dispersion provides us to choose the optimum residual dispersion. It is found that zero residual dispersion is not the best choice rather −250 ps/nm residual dispersion allows maximum input power. Since a WDM system

implementation always requires to study the system at residual dispersion, we can have an idea of performance of pre-compensation technique when multiple number of channels are applied from the discussion.

Chapter 6

Performance Analysis of Bi-end Compensation Configuration

6.1 Introduction

The transmission performance of bi-end compensation configuration in presence of SPM will be presented and analyzed in this chapter. The performance will be evaluated by simulating the pulse propagation in presence of both second-order GVD and SPM effects using a numerical technique, namely, the split-step Fourier transform method. As we did in chapters 4 and 5, the maximum power levels that can be applied to the transmission system will be quantified. From the simulation of pulse propagation eye diagrams will be drawn. Then performance of the compensation configuration will be calculated considering receiver and pre-amplifier characteristics. We calculated the eye opening penalty and the maximum threshold power beyond which eye penalty exceeds 3 dB at different length and at different input power levels. We also calculated the SNR and the Q parameter considering optical pulse degradation due to interplay between GVD and SPM, receiver noise and preamplifier ASE noise. The results are presented here.

6.2 Bi-end compensation configuration

In bi-end compensation configuration, dispersion compensating fiber is connected at the both ends of the single-mode fiber. The combined length of DCF at the both end can be selected to compensate GVD completely or partially. Since the sign of dispersion parameter (D_1) of standard single-mode fiber at 1.55 μm wavelength is positive, the sign of the dispersion parameter (D_2) of DCF must be negative for GVD compensation.

If total length of DCF at both ends satisfies equation $L_{DCF} = -(D_1 / D_2)L_{SMF}$, where L_{SMF} is the SMF length, then no residual dispersion exists at the end of the transmission fiber. But if total length of DCF L_{DCF} is smaller than that required to

satisfy the equation, there will exist positive residual dispersion as $D_1 L_{SMF} + D_2 L_{DCF}$ will not vanish rather give positive number. Likewise, if L_{DCF} is larger than that required for zero residual dispersion, there will exist negative residual dispersion at the end of the transmission fiber. We varied L_{DCF} to show the effect of residual dispersion on the transmission performance of bi-end compensation configuration.

In our model of bi-compensation configuration, we used L_1 km of DCF connected at the input end of the SMF and L_2 km of DCF connected at the output end of the DCF as shown in figure 6.1. Total length of the DCF is set to compensate the GVD of the SMF. To compensate completely the GVD of SMF, L_1+L_2 must be 17 km of length. To vary the residual dispersion we vary only L_2. For zero residual dispersion we select $L_1=L_2$.
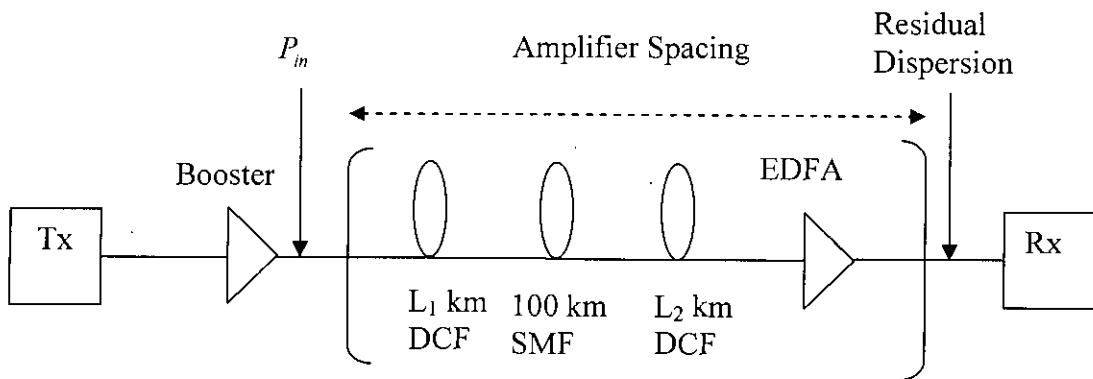
Fig. 6.1: Schematic diagram of bi-end compensation configuration

6.3 Simulation Results

Pulse propagation in the above-described bi-end compensation configuration was simulated using split-step Fourier transform technique. We present here some of the simulation results to show self-phase modulation effect on transmission performance.

6.3.1 Complete Compensation
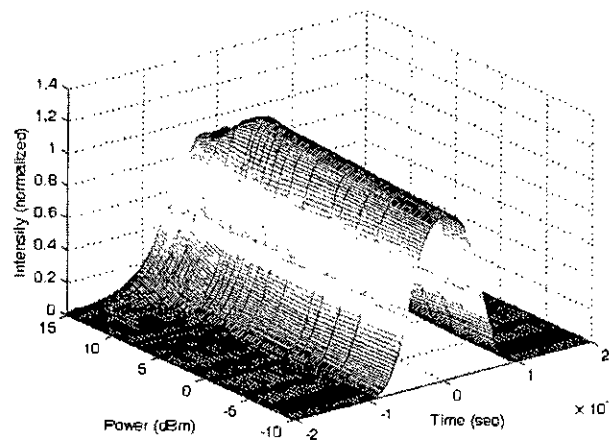
(a)
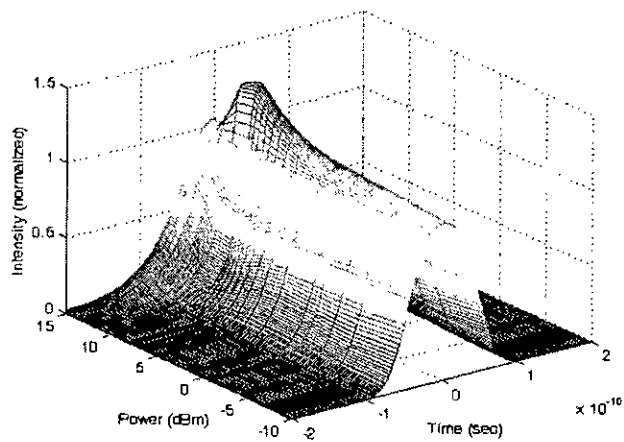
(c)
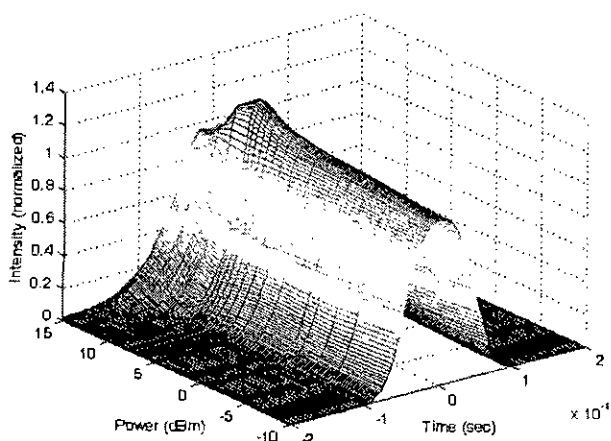
(b)
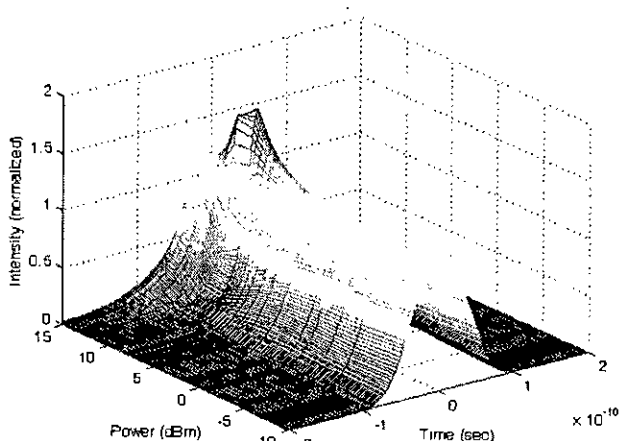
(d)

Fig. 6.2: Pulse shapes at different input power levels at (a) 1000 km (b) 2000 km (c) 3000 km (d) 4000 km for BECC with zero residual dispersion

(a)

(c)

(b)

(d)
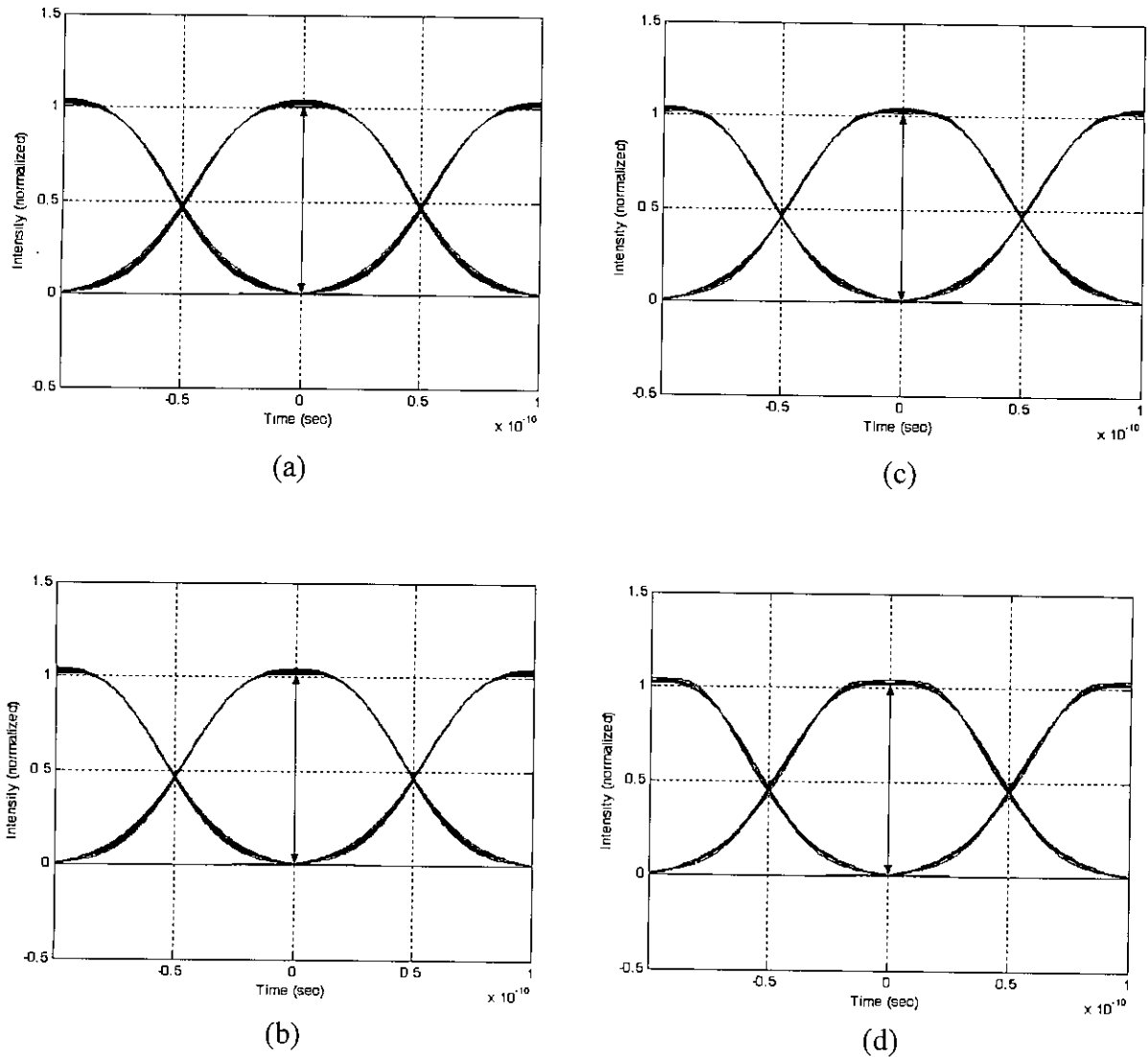
Fig.6.3: Eye diagrams at (a)1000 km (b) 2000 km (c) 3000 km (d) 4000 km at different power levels for BECC with zero residual dispersion. Input power is varied from −10 dBm to 7 dBm.

Propagated pulses at the end of 1000 km − 4000 km transmission link are given in figure 6.2. Peak power of input pulses were varied from −10 dBm to 15 dBm. It is shown that, in bi-end compensation configuration pulse shape distortion is less up to much higher levels of input power. Pulse gets compressed due to SPM effect in a bi-end compensation configuration. As input power is increased, SPM induced chirping and new frequency component generation increases, and as a result, pulse compression increases with power. But after some maximum input power level pulse

can no longer compress. As the nonlinear chirping induced by SPM increases so much, pulse gets distorted at higher input power levels. Since SPM accumulates over the length, pulse compression is higher at lower input power levels and distortion of pulses happen at lower input power at longer transmission link. In 6.2(a) pulse shapes at 1000 km for different input power levels are drawn. It is found that pulse shapes are almost restored up to 10 dBm of input power levels. After 10 dBm input power, pulses distort. But up to 15 dBm the distortion is not high in a bi-end compensation configuration at 1000 km. In 6.2(b), 6.2(c) and 6.2(d) pulse shapes are drawn at 2000 km, 3000 km and 4000 km respectively. Due to accumulation of SPM effects with length, it is found that pulse compression is higher at same power at longer transmission link.

Since we used L_{DCF} of 17 km, dispersion is completely compensated in each span. So no dispersion-accumulation happens. But as SPM produces positive frequency chirping within the pulse both in SMF and DCF, it is not compensated rather its effects accumulate from one span to another. So, we find that, for a fixed input power, output pulses at lengths 1000 km – 4000 km show distortion with length.

Eye diagrams are drawn in figure 6.3 at lengths 1000 km – 4000 km. Peak power of input pulses were varied from –10 dBm to 7 dBm. Eye diagrams show increase of eye opening at these power levels with the increase of input power levels due to compression effect. So, actually highest opening is for 7 dBm and lowest opening is for –10 dBm input power. The pulse shapes show slight compression up to this power levels. But if power is increased beyond limit, the pulse compression reaches maximum and as a result it distorts and the opening decreases. Since up to 7 dBm input power levels the pulses do not broaden, rather compress, inter-symbol interference from the neighboring pulses is minimum and this causes to increase the eye opening.
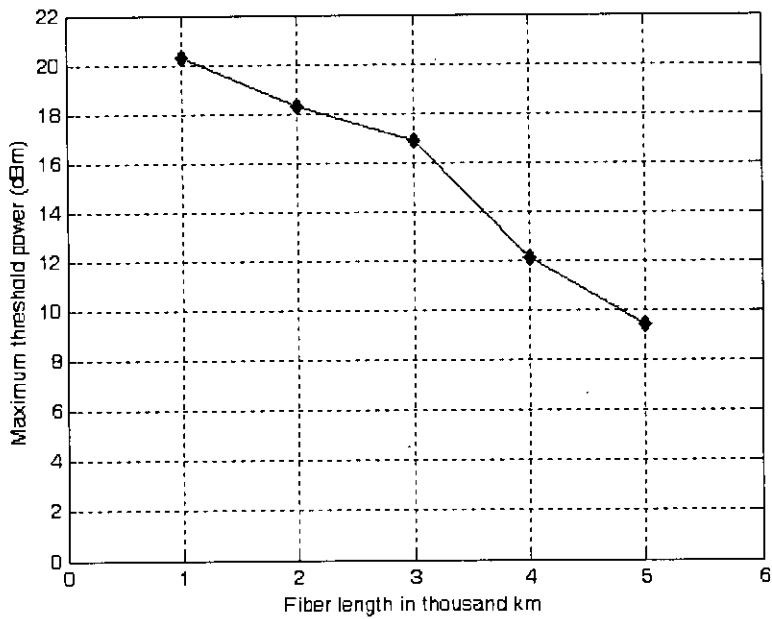
Fig. 6.4: Maximum power threshold at 3 dB eye penalty versus fiber length for BECC with zero residual dispersion
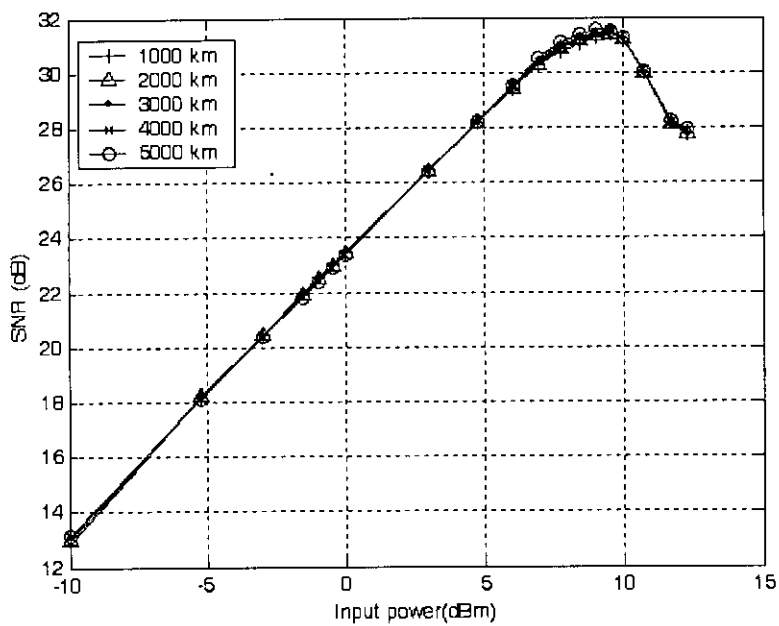

Fig. 6.5: SNR versus input power at 1000 km – 5000 km transmission fiber for BECC with zero residual dispersion

Maximum threshold power levels below which eye opening penalty is less than 3 dB are plotted against fiber length in figure 6.4. Eye penalty was calculated using the formula $20\log_{10}(a/b)$, where a is the maximum eye opening of the pulse at the input of the transmission fiber and b is the maximum eye opening at the output of the transmission fiber. Maximum threshold power level decreases with the increase of fiber length. Since no dispersion accumulation occurs with the length of the fiber, this decrease of threshold power is due to SPM effects accumulation. It is shown that, maximum threshold power is 20.3 dBm for 1000 km transmission fiber. This value is greater than that of both of post- and pre-compensation configuration. It is found that, even at 5000 km transmission fiber 9.4 dBm power can be applied and still the power penalty remains within 3 dB penalty.

Transmission performance of the bi-end compensation configuration is depicted as SNR with respect to input power levels at 1000 km – 5000 km of transmission fiber lengths. As in eye opening penalty curves in figure 6.5, SNR curves show almost same values at different transmission lengths up to the input power levels considered in the analysis. For each curve, SNR increases with input power up to approximately 10 dBm. That means SPM effects up to approximately 10 dBm are not serious for a bi-end compensation configuration. After increasing the input power above 10 dBm, SPM effects start to degrade the pulse shapes and as well as the eye opening and as a result, SNR starts to fall. Nevertheless SNR shows minimum required value at much higher value of 10 dBm. So, it is evident that bi-end compensation configuration allows much higher input powers for high bit rate long-haul transmission system and still keeping the SPM effect negligible.

6.3.2 Partial Compensation
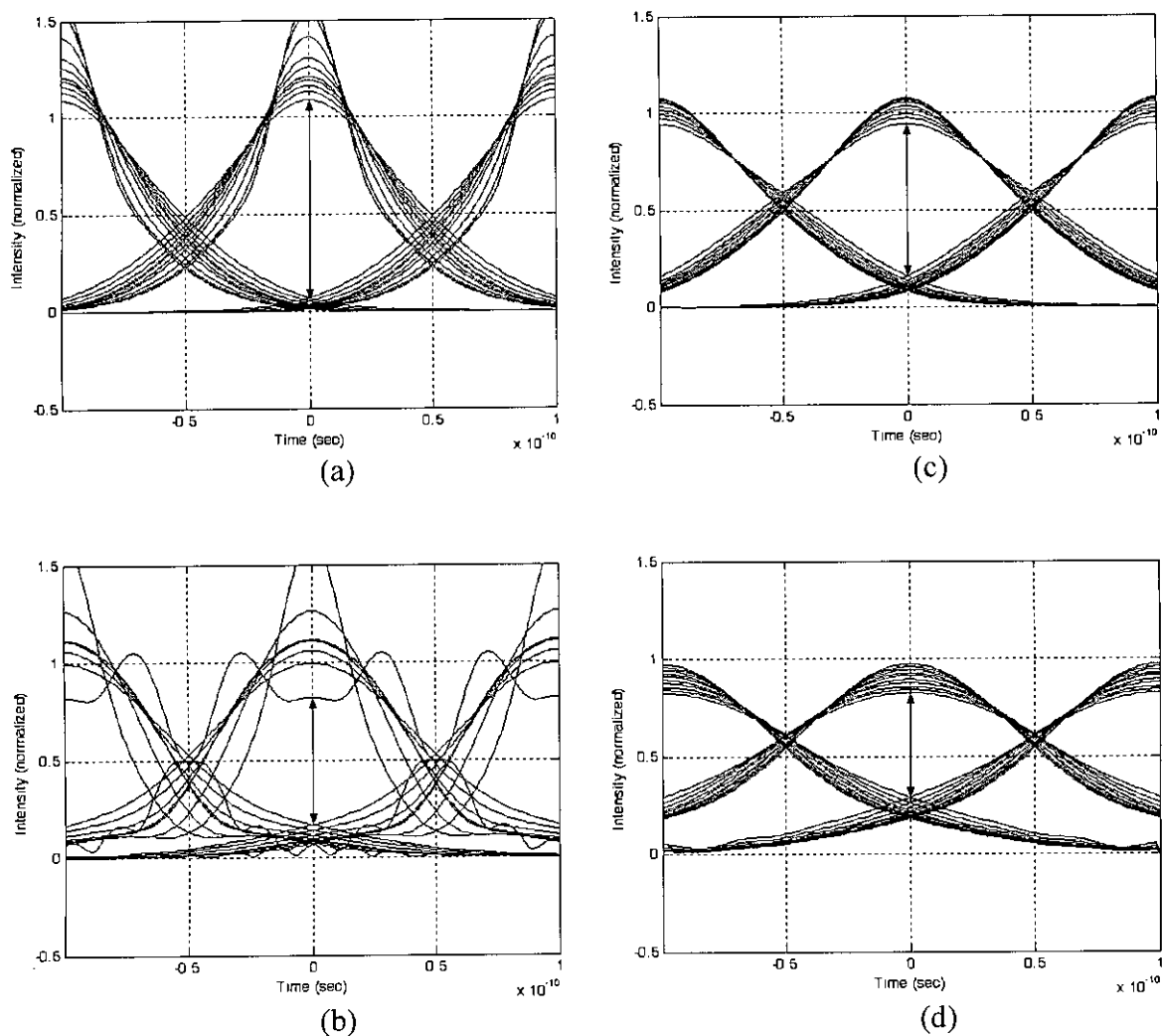
Fig. 6.6: Eye diagrams at 1000 km for bi-end compensated transmission link with (a) 500 ps/nm (b) 1000 ps/nm (c) –500 ps/nm (d) –1000 ps/nm residual dispersion

Eye diagrams at various residual dispersions at 1000 km of transmission fiber for different input power levels are given in figure 6.6. We varied input power from –10 dBm to upward. For figure 6.6(a), 6.6(c) and 6.6(d) maximum input power used was 7 dBm. For figure 6.6(b) maximum 5 dBm input power was used. Figure 6.6(a) shows that, eye opening increases with the increase of input power due to compression effect in presence of SPM. Highest eye opening is for the 7 dBm of input power. This effect is better illustrated in figure 6.7 where we plotted eye opening penalty versus input power levels for various residual dispersions. There it is shown that, eye opening

penalty gradually decreases with the increase of input power up to 7 dBm. In 6.6(b) eye diagram is drawn for 1000 ps/nm residual dispersion. Here, also pulse compression occurs at lower input powers. But after application of 5 dBm of input power it is shown that pulse can no longer be compressed and as a result, pulse distorts due to the interplay between GVD and SPM. This effect is further illustrated in figure 6.7 where it is shown that eye opening increases very sharply after 3 dBm of input power. In 6.6(c), eye diagram for −500 residual dispersion is drawn. Here, minimum eye opening is for maximum input power (i.e., 7 dBm) and maximum eye opening is for minimum input power (i.e., -10 dBm). It is clear from the diagram that pulse compresses only for low levels of input power. At higher power level, such as at 3 dBm input power, pulse broadens. As a result peak power decreases and interferes in the neighboring pulses. Eye diagram for −1000 ps/nm residual dispersion is drawn in figure 6.6(d). Due to high residual dispersion, interplay between GVD and SPM broadens the pulse so much that eye opening decreases greatly for 7 dBm input power. Eye diagram shows degradation even in −10 dBm of input power where SPM effect is very low. This is mainly because GVD is over compensated at such a high level of residual dispersion.

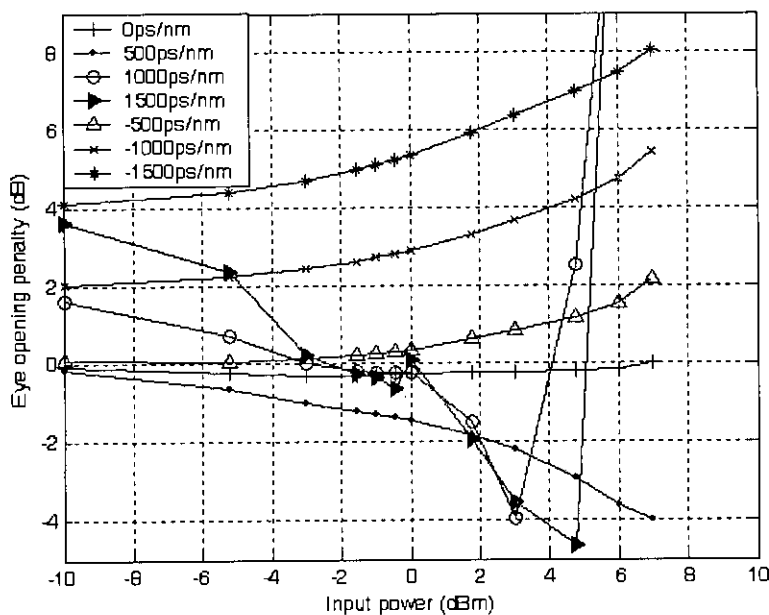**Fig.6.7:** Eye opening penalty versus input power for BECC with different residual dispersions at 1000 km transmission fiber
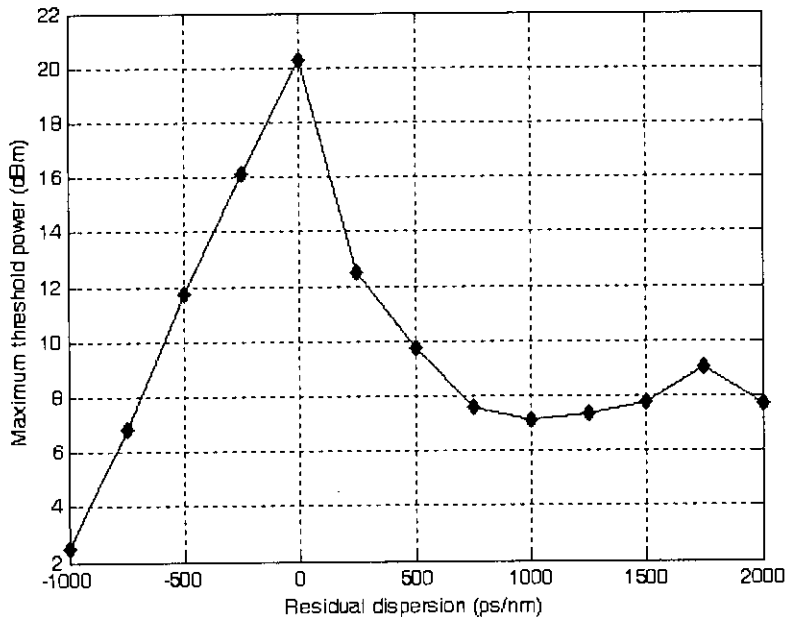

Fig. 6.8: Maximum threshold power at 3 dB eye penalty versus residual dispersion for BECC at 1000 km of transmission fiber

Eye opening penalty is plotted versus input power levels at different residual dispersions at 1000 km of bi-end compensated transmission fiber in figure 6.7.

Residual-dispersions were varied from −1500 ps/nm to 1500 ps/nm. Curve for each residual dispersion shows huge difference from one another. So, residual dispersion is an important consideration of system design. At 0 ps/nm residual dispersion, eye opening is always close to zero up to maximum power level (i.e., 7 dBm) of our investigation. At 500 ps/nm residual dispersion, eye opening penalty curve is even below the curve of 0 ps/nm residual dispersion for the power levels of our investigation. Eye penalty at 1000 ps/nm shows decrease with power initially but after some input power levels (i.e., 3 dBm), it shows steep rise with input power. 1500 ps/nm residual dispersion curve shows similar behavior as 1000 ps/nm residual dispersion except that eye penalty is also higher at low level of input power. For negative residual dispersion, curves show an increase of eye penalty with the input power and this phenomenon is higher in higher negative residual dispersion. At −1500 ps/nm residual dispersion, eye opening penalty is always higher than 3 dB penalty that this level of residual dispersion is totally unusable in a practical system.

Maximum threshold power at 3 dB eye opening penalty is plotted versus residual dispersion at 1000 km of transmission fiber in figure 6.8. It is found that, zero residual dispersion allows highest maximum threshold power to be applied to the system. Maximum threshold power levels decrease at both negative and positive end of the zero residual dispersion. The rate of decrease is much faster in the negative residual dispersion region. For negative residual dispersion beyond −1000 ps/nm 3 dB eye opening is not available at all, whereas even at 2000 ps/m positive residual dispersion 3 dB eye opening penalty is possible at 8 dBm. But, though maximum threshold power shows increasing after 1000 ps/nm residual dispersion in figure 6.8, it worth noticing that after this residual dispersion, minimum threshold also increases. After 2000 ps/nm residual dispersion, minimum threshold voltage is found to be very near to the maximum threshold. So, in using the system at such levels of residual dispersion, the input power window that will give us acceptable output performance is very limited. So, we propose that, the system must not be operated at residual dispersion beyond 1500 ps/nm.
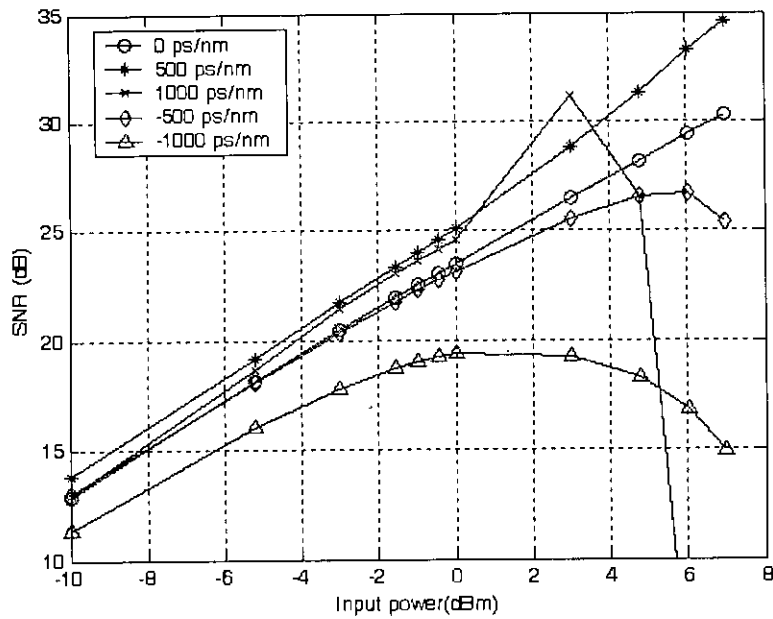
Fig. 6.9: SNR versus input power for BECC at 1000 km transmission fiber with different residual dispersion
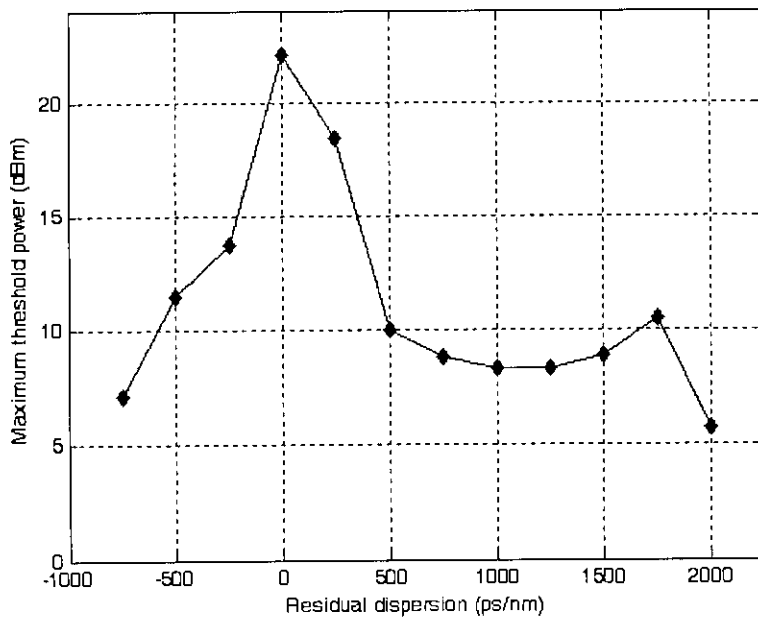

Fig. 6.10: Maximum threshold power at 10^{-9} BER at 1000 km transmission fiber versus residual dispersion in BECC

SNR characteristics of the bi-end compensation configuration are plotted in figure 6.9 at various residual dispersion for both positive and negative values. It is shown from the figure that SNR characteristic is better at 500 ps/nm than at 0 ps/nm residual dispersion at least up to power levels of our investigation. SNR curve for 1000 ps/nm shows sharp decrease of SNR after 5 dBm of input power and so does not give acceptable performance level. Though −500 ps/nm residual dispersion is shown to be acceptable even at more than 7 dBm of input power, -1000 ps/nm negative residual dispersion gives very poor performance that may not be sufficient for minimum required performance. So, bi-end compensation configuration at −1000 ps/nm and any higher value of negative residual dispersion should not be used as per our analysis.

Maximum threshold power levels that can be applied to the transmission system and still obtain 10^{-9} BER are plotted versus residual dispersions in figure 6.10. It is shown that, maximum input power of 22 dBm can be applied to a bi-end compensation configuration system with zero residual dispersion. It is also found that, apart from post- and pre-compensation configuration, zero residual dispersion gives the highest allowable input power in a BECC. Moreover, positive residual dispersion is shown to offer required transmission performance better than negative residual dispersion. In positive residual dispersion region 10^{-9} BER is achieved up to 2000 ps/nm. But after − 750 ps/nm residual dispersion 10^{-9} BER is no longer achieved.

6.4 Use of Bi-end Compensation Configuration in WDM System

For an 8-channel system with 0.8 nm channel spacing, the channels will have a total of approximately 550 ps/nm residual dispersion. We can choose −200 ps/nm to 350 ps/nm residual dispersion window as shown figure 6.11 where greater than 15 dBm input power can be applied to the system. For a 16-channel system, we need 1100 ps/nm window. We can select −600 ps/nm to 500 ps/nm residual dispersion window where input power is greater than 10 dBm. Even for a 32-channel where required residual dispersion window is 2200 ps/nm, we can use −700 ps/nm to 1500 ps/nm where input power can be applied greater than 8 dBm.

6.5 Comparison with Post- and Pre-Compensation Configuration

The performance of a compensation technique in presence of SPM mainly depends on the maximum threshold power that can be applied to the system and still achieve minimum required performance from the system. To compare post-, pre- and bi-end compensation configuration with one another, we present following two tables where the maximum threshold power limit is given against fiber length and for a WDM system.

Fiber Length	POCC	PRCC	BECC
1000 km	9 dBm	12.98 dBm	20.3 dBm
2000 km	6.2 dBm	5.45 dBm	18.3 dBm
3000 km	4.45 dBm	2.88 dBm	16.9 dBm
4000 km	3.23 dBm	1.13 dBm	12.1 dBm
5000 km	2.3 dBm	0.5 dBm	9.4 dBm

Table 4: Maximum threshold power at 3 dB eye opening penalty at 1000 km – 5000 km for POCC, PRCC and BECC

No. of channels	POCC	PRCC	BECC
8	11 dBm	12 dBm	15 dBm
16	8.5 dBm	8 dBm	10 dBm
32	8 dBm	4 dBm	8 dBm

Table 5: Maximum threshold power at 10^{-9} BER for WDM system for POCC, PRCC and BECC

Table 4 specifies maximum threshold power levels at 1000 km to 5000 km transmission link for POCC, PRCC and BECC. It is clear from the table that, at length 1000 km to 5000 km BECC always support highest maximum threshold power among the three compensation configuration. At longer length, both POCC and PRCC show huge degradation of threshold power due to SPM accumulation. On the other hand, even at 5000 km transmission fiber BECC allow 9.4 dBm. So, it is evident from the table that BECC is the suitable choice for a long-haul transmission system.

Table 5 specifies maximum threshold power levels determined at 10^{-9} BER at 1000 km for a WDM system for different number of channels. It is found that, for an 8-channel WDM system all three compensation schemes are capable of allowing high input power with BECC allowing the highest (i.e., 15 dBm). For 16 and 32 channels WDM system, maximum threshold power in PRCC decreases so much that it is not usable in a practical system for a high bit rated long haul WDM system. POCC and BECC are capable of allowing high input power levels with BECC allowing the higher.

So, from the above discussion it can be concluded that both for a long-haul single channel or multiple channel WDM system, BECC should be the best suitable compensation configuration.

6.6 Summary

In this chapter, we have discussed the performance of optical fiber transmission system with dispersion compensated by DCF connected at both end of the standard single-mode fiber. We have shown the effects of zero, positive and negative residual dispersions on the transmission performance. We put our emphasis especially on the self-phase modulation limited maximum threshold voltage that can be applied to the system and still achieving required performance (i.e., 10^{-9} BER). The most remarkable observation that can be made from the above analysis that in bi-end compensation scheme, zero residual dispersion exhibits highest maximum threshold than any other residual dispersion. We emphasize that our analysis shows that as in post- and pre-compensation bi-end compensation configuration exhibits better performance with positive residual dispersion than with negative residual dispersion.

For a long-haul transmission system bi-end compensation configuration shows better characteristics in comparison with both post- and pre-compensation configuration. It is found that at 1000 km to 5000 km transmission link in bi-end compensation configuration SPM effect is minimum. So, BECC gives the higher maximum threshold power at 3 dB eye opening penalty.

Moreover, we have discussed the feasibility of application of bi-end compensation configuration in a WDM system. With comparison to post- and pre-compensation configuration, it is found that bi-end compensation configuration allows higher threshold power for WDM system for all the channels. It is also found that, for an 8-channel WDM system, the region can be selected to contain both negative and positive residual dispersion. But for 16-channel and 32-channel WDM system we will have to extend the residual dispersion window toward the positive residual dispersion region.

Chapter 7

Conclusion

7.1 Conclusion of this Study

A detailed investigation has been carried to evaluate the performance of DCF compensating technique in presence of SPM at 10-Gb/s using standard single-mode fiber. The three compensating techniques, namely, POCC, PRCC and BECC perform differently under SPM.

NRZ optical transmission systems at 1000 km – 5000 km with complete/incomplete dispersion compensation are studied. The dispersion of transmission fiber is periodically compensated. For every compensation period, there exists a residual dispersion if GVD within SMF is under – or over compensated. During signal transmission, the pulse width may be compressed or broadened by the combined effect of SPM and dispersion when the residual dispersion is small. For the case of pulse compression, signal pulse cannot be further compressed when the compression is too much.

The interaction between the fiber dispersion and the SPM effect was shown to be a major factor that limits the amount of energy allowed to be launched into the dispersion compensated transmission link in our numerical study. This power limit will eventually provide an upper bound on the length of the transmission link due to the increasing loss for the longer link. Different noise constraint (shot and thermal noise of receiver, ASE noise of optical amplifier and inter-symbol interference) together with the power margins imposed by SPM, especially the maximum threshold, defines the region of suitable dispersion compensation. The maximum threshold also permits to identify the best performance region. Optimum residual dispersion is different for different compensation schemes means that the residual dispersion is not the fundamental figure of merit, but its optimum value depends on the compensation technique. Simulations carried out changing transmission length have shown little changes on the optimum residual dispersion. This means that the residual dispersion per amplifier spacing must decrease when the length increases.

Effects due to SPM are stronger for the post-compensated link in case of complete compensation. Both PRCC and BECC give higher maximum threshold power than POCC in case of complete compensation. But, in case of residual dispersion, PRCC shows inferior performance in comparison with both POCC and BECC. However, BECC shows best performance in case of both complete and incomplete compensation.

7.2 Proposal of a Design Rule for Long-Haul WDM System

The performance of a compensation technique in presence of SPM mainly depends on the maximum threshold power that can be applied to the system and still achieve minimum required performance from the system. From the discussion in section 6.5, BECC offers the highest maximum threshold power that can be launched to the transmission system. Moreover, there exists wide residual dispersion window for BECC at high maximum threshold power. It is found that BECC can support 8-channel, 16-channel and even 32-channel at considerable high maximum threshold power. So, we propose that BECC is the best suitable technique for standard single-mode fiber for a WDM system to be implemented.

7.3 Suggestion for Future Study

Throughout this analysis, FWM is considered negligible, as dispersion parameter of SMF is very high. But, at the length of the fiber where dispersion is completely compensated, FWM effects may be considerable. And as FWM is not compensated by any opposing effect, it will have an accumulated effect over the cascaded links. So, in future an investigation may be carried out to find out the pulse degradation due to FWM effects generation when dispersion is completely compensated in a transmission link using standard single-mode fiber with dispersion compensation.

References:

[1] G. J. Holzmann and B. Pehrson, *The Early History of Data Networks*, IEEE Computer Society Press, Los Alamitos, CA, 1995.

[2] D. Koenig, "Telegraphs and Telegrams in Revolutionary France," *Scientific Monthly*, pp. 431, 1944.

[3] A. Jones, *Historical Sketch of the Electrical Telegraph*, Putnam, New York, 1852.

[4] A. G. Bell, U.S. Patent No. 174,465, 1876

[5] T. H. Maiman, *Nature*, vol. 187, pp. 493, 1960.

[6] W. K. Pratt, *Laser Communication Systems*, Wiley, New York, 1969.

[7] S. E. Miller, *Sci. Am.* vol. 214, 1966.

[8] K. C. Kao and G. A. Hockham, *Proc. IEE*, vol. 113, pp. 1151, 1966.

[9] F. P. Kapron, D. B. Keck, and R. D. Maurer, *Appl. Phys. Lett.* vol. 17, pp. 423, 1970.

[10] A. E. Willner, Ed., *IEEE J. Sel. Topics Quantum Electron.*, vol. 6, pp. 827, 2000.

[11] D. Gloge, A. Albanese, C. A. Burrus, E. L. Chinnock, J. A. Copeland, A. G. Dentai, T. P. Lee, T. Li, and K. Ogawa, *Bell Syst. Tech. J.* vol. 59, pp. 1365, 1980.

[12] T. Miya, Y. Terunuma, T. Hosaka, and T. Miyoshita, *Electon. Lett.*, vol. 15, pp. 106, 1979.

[13] K. Nakagawa, *Trans. IECE Jpn. Pt. J*, vol. 78B, pp. 713, 1995.

[14] G. P. Agrawal, *Fiber-Optic Communication Systems*, 3rd Ed., Wiley, New York, 2002.

[15] G. A. Thomas, B. L. Shraiman, P. F. Glodis, and M. J. Stephan, *Nature*, vol. 404, pp. 262, 2000.

[16] J. Gower, *Optical Communication Systems*, 2nd Ed., New Delhi: Prentice Hall of India, 2001.

[17] N. Henmi, T. Saito and S. Nakaya, "An arrangement of transmission fiber dispersions for increasing the spacing between optical amplifiers in lumped repeater systems," *IEEE Photon. Technol. Lett.*, vol. 5, pp. 1337-1340, 1993.

[18] H. Taga, S. Yamamoto, N. Edagawa, Y. Yoshida, S. Akiba and H. Wakabayashi, "Performance evaluation of the different types of fiber chromatic-dispersion

equalization for IM-DD ultralong-distance optical communication systems with Er- doped fiber amplifiers," *J. Lightwave Technol.*, vol. 12, pp. 1616-1621,1994.

[19] F. Metera and M. Settembre, "Comparison of the performance of optically amplified transmission systems," *J. Lightwave Technol.*, vol. 14, pp. 1-12, 1996.

[20] J. M. Jacob, E. A. Golovchenko, A. N. Plilipetskii, G. M. Carter and C. R. Menyuk, "10-Gb/s transmission of NRZ over 10000 km and solitons over 13500 km error-free in the same dispersion-managed system," *IEEE Photon. Technol. Lett.* vol., 9, pp. 1412-1414, 1997.

[21] R. J. Nuyts, Y. K. Park and P. Gallion, "Dispersion equalization of a 10-Gb/s repeatered transmission system using dispersion compensating fibers," *J. Lightwave Technol.*, vol. 15, pp. 31-42, 1997.

[22] M. Z. Alam, "Analysis of FWM effect on an optical WDM system having unequal channel spacing and nonuniform chromatic dispersion," *MSc. Engg. Thesis*, Dept. of EEE, BUET, 2002.

[23] M. Faisal, "Analysis of Wavelength shift keying technique with dispersion management scheme to reduce four-wave mixing effect in optical WDM system," *MSc. Engg. Thesis*, Dept. of EEE, BUET, 2003.

[24] G. P. Agrawal, *Nonlinear Fiber Optics*, 3rd ed., Academic Press, San Diego, CA, 2001.

[25] S. Bigo and A. Bertaina, "WDM transmission experiments at 32×10 Gb/s over nonzero dispersion-shifted fiber and standard single-mode fiber," *IEEE Photon. Technol. Lett.*, vol. 11, pp. 1316-1318, 1999.

[26] A. H. Gnauck, J. M. Wiesenfeld, L. D. Garrett, M. Eiselt, F. Forghieri, L. Arcangeli, B. Agogliata, V. Gusmeroli and D. Scarano, "16×20 Gb/s, 400 km WDM transmission over NZDSF using a slope – compensating fiber – grating module," *IEEE Photon. Technol. Lett.*, vol. 12, pp. 437-439, 2000.

[27] R. W. Tkach, A. R. Chraplyvy, F. Forghieri, A. H. Gnauck and R. M. Derosier, "Four-photon mixing and high-speed WDM systems," *J. Lightwave Technol.*, vol. 13, pp.841-849, 1995.

[28] W. Zeiler, F. D. Pasquale, P. Bayvel and J. E. Midwinter, "Modeling of four-wave mixing and gain peaking in amplified WDM optical communication systems and networks," *J. Lightwave Technol.*, vol. 14, pp.1933-1942, 1996.

[29] G. Bellotti, A. Bertaina and S. Bigo, "Dependence of self-phase modulation impairments on residual dispersion in 10-Gb/s – based terrestrial transmissions using standard fiber," *IEEE Photon. Technol. Lett.*, vol. 11, pp. 824-826, 1999.

[30] S. Shen, C. – C. Chang, H. P. Sardesai, V. Binjrajka and A. M. Weiner, "Effects of self-phase modulation on sub-500 fs pulse transmission over dispersion compensated fiber links," *J. Lightwave Technol.*, vol. 17, pp. 452-461, 1999.

[31] S. Wen, "Bi-end dispersion compensation for ultralong optical communication system." *J. Lightwave Technol.*, vol.17, pp. 792-798, 1999.

[32] W. J. Tomlinson, R. H. Stolen, and C. V. Shank, "Compression of optical pulses chirped by self-phase modulation in fibers," *J. Opt. Soc. Amer. B*, vol. 1, pp. 139-149, 1984.

[33] J. P. Gordon, "Dispersive perturbations of solitons of the nonlinear Schrodinger equation," *J. Opt. Soc. Amer. B*, vol. 9, pp. 91-97, 1992.

[34] A. Gnauck and R. Jopson, in *Optical Fiber Telecommunications III*, vol. A, I. P. Kaminow and T. L. Koch, Eds., Academic Press, San Diego, CA, 1997, Ch. 7.

[35] L. Gruner-Nielsen, S. N. Knudsen, B. Edvold, T. Veng, D. Magnussen, C. C. Larsen and H. Damsgaard, *Opt. Fiber Technol.*, vol. 6, pp.164, 2000.

[36] S. Bigo, G. Bellotti and M. W. Chbat, "Investigation of cross-phase modulation limitation on 10-Gb/s transmission over various types of fiber infrastructures," presented at the OFC'99, paper ThC3.

[37] W. R. Bennett, *Electrical Noise*, McGraw-Hill, New York, 1960

[38] D. K. C. MacDonald, *Noise and Fluctuations: An Introduction*, Wiley, New York, 1962

[39] F. N. H. Robinson, *Noise and Fluctuations in Electronic Devices and Circuits*, Oxford University Press, Oxford, 1974

[40] P. P. Smyth, R. Wyatt, A. Fidler, P. Eardley, A. Sayles, and S. Graig-Ryan, *Electron. Lett.* 26, 1604 (1990)

[41] R.C. Steele and G. R. Walker, *IEEE Photon. Technol. Lett.* 2, 753 (1990)

[42] T. L. Blair and H. Nakano, *Electron. Lett.* 27, 835 (1991)

[43] T. Saito, Y. Sunohara, K. Fukagai, S. Ishikawa, N. Henmi, S. Fujita, and Y. Aoki, *IEEE Photon. Technol. Lett.* 3, 551 (1991)

[44] A. H. Gnauck and C. R. Giles, *IEEE Photon. Technol. Lett.* 4, 80 (1992)

[45] F. F. Röhl and R. W. Ayre, *IEEE Photon. Technol. Lett.* 5, 358 (1993)

[46] N. A. Olsson, "Lightwave systems with optical amplifiers," *J. Lightwave Technol.*, vol. 7, pp. 1071-1082, July 1989.